Evaluation of the Effects of Aging on Asphalt Rubber Pavements

by

Jordan Reed

A Thesis Presented in Partial Fulfillment
of the Requirements for the Degree
Master of Science

Approved November 2010 by the
Graduate Supervisory Committee:

Kamil Kaloush, Chair
Michael Mamlouk
Claudia Zapata

ARIZONA STATE UNIVERSITY

December 2010

ABSTRACT

Oxidative aging is an important factor in the long term performance of asphalt pavements. Oxidation and the associated stiffening can lead to cracking, which in turn can lead to the functional and structural failure of the pavement system. Therefore, a greater understanding of the nature of oxidative aging in asphalt pavements can potentially be of great importance in estimating the performance of a pavement before it is constructed. Of particular interest are the effects of aging on asphalt rubber pavements, due to the fact that, as a newer technology, few asphalt rubber pavement sections have been evaluated for their full service life. This study endeavors to shed some light on this topic.

This study includes three experimental programs on the aging of asphalt rubber binders and mixtures. The first phase addresses aging in asphalt rubber binders and their virgin bases. The binders were subjected to various aging conditions and then tested for viscosity. The change in viscosity was analyzed and it was found that asphalt rubber binders exhibited less long term aging. The second phase looks at aging in a laboratory environment, including both a comparison of accelerated oxidative aging techniques and aging effects that occur during long term storage. Dynamic modulus was used as a tool to assess the aging of the tested materials. It was found that aging materials in a compacted state is ideal, while aging in a loose state is unrealistic. Results not only showed a clear distinction in aged versus unaged material but also showed that the effects of aging on AR mixes is highly dependant on temperature; lower temperatures induce relatively minor stiffening while higher temperatures promote much more

significant aging effects. The third experimental program is a field study that builds upon a previous study of pavement test sections. Field pavement samples were taken and tested after being in service for 7 years and tested for dynamic modulus and beam fatigue. As with the laboratory aging, the dynamic modulus samples show less stiffening at low temperatures and more at higher temperatures. Beam fatigue testing showed not only stiffening but also a brittle behavior.

DEDICATION

To my family, who were there when I needed them.

ACKNOWLEDGEMENTS

I would first like to thank my advisor Dr. Kamil E. Kaloush, whose guidance and patience were essential to the success of this thesis project. His insights and support helped me meet my goals. I would also like to thank Dr. Michael Mamlouk and Dr. Claudia Zapata, who have been fixtures in my education at ASU. Their instruction has opened up my mind to new ideas and possibilities and for that I am grateful.

ADOT, especially George Way and Ali Zareh, supported this project by supplying samples and supporting ongoing research at ASU. Without them, none of this would have been possible.

Thank you to all my friends in the Advanced Pavements Research Group, for their friendship and help throughout this process. I would like to thank Dr. Krishna Biligiri in particular for imparting his knowledge of the intricacies of dynamic modulus testing to me in addition to acting as a sounding board for my ideas.

Lastly I would like to thank Kenneth Witczak and Peter Goguen for all their work in keeping the lab running smoothly. Their importance to this project cannot be understated.

TABLE OF CONTENTS

Page

LIST OF TABLES

LIST OF FIGURES

Figure Page

Figure Page

INTRODUCTION

Background

In the last quarter century, asphalt rubber hot mix has become a staple paving material. Asphalt rubber pavements offer several advantages, including an improved life cycle length. However, comparatively little is known about the aging characteristics of asphalt rubber when compared to more conventional Hot Mix Asphalt (HMA) paving materials. More importantly, a methodology for estimating the practical detrimental effects of oxidative aging on hot mix asphalt using asphalt rubber has not been fully developed. The experimental program undertaken as part of this thesis was designed to shed some light on the aging characteristics of these pavements and how such pavements can be rapidly aged and evaluated in the laboratory.

Asphalt rubber, or AR, is used in several states in a wide range of environmental conditions, despite being originally developed for cold weather conditions. The improved properties of an asphalt rubber binder allow for the use of gap and open graded pavement structures. In particular, relatively thin open graded friction courses have seen widespread use in Arizona as a top layer on predominately concrete pavements. The porous nature of Asphalt Rubber Friction Courses (ARFC) results in markedly less tire noise and vastly improved wet weather performance. Asphalt rubber pavements also exhibit improved fatigue resistance, resulting in increased pavement life compared to conventional HMA.

Two types of asphalt rubber pavements are commonly used in Arizona. The first, Asphalt Rubber Friction Course, or ARFC, is an open graded mixture commonly placed as the top friction layer in a pavement system. Typically this type of mixture has higher binder contents, generally above 8.5%. The air voids are also high at around 18%. The second type of asphalt rubber pavement is a gap graded mix known as ARAC, or asphalt rubber asphalt concrete. ARAC mixes have lower air voids between 5 and 11% and will likewise have lower binder contents between 6.5 and 8%. Both types of pavement contain crumb rubber reacted with the asphalt binder, with the crumb rubber being included at about 20% by weight of binder (Kaloush et. al., 2003).

Aging of asphalt pavements typically occurs through oxidation of the asphalt and evaporation of the lighter maltenes from the binder. This causes the pavement to stiffen, which inevitably results in cracking in the pavement structure. Asphalt rubber has been observed to be resistant to cracking and aging, perhaps due to the higher asphalt content or some property imparted by the reaction of crumb rubber with the virgin asphalt binder. For these reasons, AR has seen an increase in usage in recent years. An improved understanding and quantification of the aging characteristics of these pavements would be beneficial to the design process, allowing for improvement upon the current standards.

Objective

The primary objective of this study was to investigate the oxidative aging effects on asphalt rubber binders and mixtures. To this end, several tasks were identified. First, analysis was conducted on conventional and AR binders that were subjected to laboratory aging. The second was to identify an effective laboratory method for the rapid aging of AR mixes. Third, the properties of field samples were evaluated to identify the effects of aging as they occur during the service life of a pavement. Finally, the laboratory aging was compared to the field results in order to achieve a correlation between the two.

Scope of Work

The study undertaken as part of this thesis was divided into three parts. Phase one consisted of binder testing both asphalt rubber binders and their virgin base. The three binders used were a PG 58-22 from a project located in Flagstaff, I-40; and a PG 58-22 and PG 64-16 binders utilized on a test section in the Phoenix area on a frontage road for I-17. Testing consisted of penetration and softening point tests as well as a rotational viscosity temperature sweep. Binders were tested in their original states as well as the Rolling Thin Film Oven (RTFO) and Pressure Aging Vessel (PAV) conditions.

The second phase of the study was to rapidly age an AR material in the laboratory using different techniques and aging periods, then compare the results. The first method was to compact the AR material into testable samples, then subject these samples to high temperatures and convection air, rapidly oxidizing

them. The second method used the same aging conditions, except the AR material was aged in a loose state and then formed into samples. The effects of aging was evaluated by comparing the E* dynamic moduli between the test methods and known control values (AASHTO TP 62-07).

The last phase of the study involved the sampling and testing of field specimens. Specimens were taken from the I-17 frontage road test section laid out approximately 7 years before. Data was collected from this test section as part of previous projects so the original properties of the material were known (Sotil 2003, Kaloush et. al., 2003). Some samples were taken a year later and tested, giving information on how the pavement changed in the first year (Sotil 2003). In addition, an aging study was performed on the original material in the same fashion as the laboratory aging outlined above. The samples were tested for both E* dynamic modulus and beam fatigue according to AASHTO protocols (AASHTO TP-62-07 and AASHTO TP-8-94).

LITERATURE REVIEW

Prior to designing the research program for this project, necessary research was done on the subjects pertaining to the project. First, the research on asphalt binders focused on the aging and testing procedures for binders. After this, literature on the work of others in aging asphalt rubber was reviewed for pertinent information. A similar review was performed for asphalt rubber mixtures. Once again, testing and aging procedures were identified before investigating the literature for studies on the aging of asphalt rubber mixtures.

Binder Aging

Two aging procedures are used to age asphalt binders. The rolling thin film oven (RTFO) procedure, is designed to replicate the rapid short term aging that occurs during mixing and placement of a hot mix asphalt mixture (HMA). The pressure aging vessel (PAV) procedure, simulates the aging experienced after a long service life.

The RTFO procedure consists of adding 35g of binder to a glass bottle. The bottle is rolled on its side to pre-coat the inside. This bottle, along with 7 others, is placed in a vertically rotating carrousel inside of an oven set to 163°C. At the bottom of the carrousel a jet of air is blown into each bottle as they rotate past the nozzle. The carrousel rotates at a rate of 15 rpm, while the jet of air is set to 4000mL/min. This procedure continues for a total of 75 minutes. After the aging process, the binder is scraped from the bottles and tested (AASHTO T-240-09).

The PAV procedure takes 50g of RTFO treated binder in a 140mm diameter pan. This pan is then placed in a heated and pressurized vessel and subjected to 20 hours of aging. Pressure is set to 2.07 MPa and temperature held at 90°, 100°, or 110°C. After this process, the binder is scraped from the pan and tested.

Binder Testing

Conventional binder consistency tests traditionally included Brookfield rotational viscosity test, penetration, and softening point tests. Correlations are used to convert penetration and softening point data to viscosity data. Rotational viscosity testing utilizes a turning spindle submerged in asphalt to measure the viscosity of the asphalt. The spindle is turned at a constant rate while the required torque is measured. This is then related to viscosity mathematically. The first step to the procedure is to preheat the sample chamber and required spindle to the desired test temperature. Asphalt is then poured into the sample chamber and placed in a temperature control unit. The spindle is then lowered into the asphalt to the required depth and attached to the rotational viscometer. The temperature of the sample must be brought to the target temperature within 30 minutes and allowed to stabilize for 10 minutes. At this point, the viscometer is set to rotate the spindle at 20 rpm and is started. Once viscosity readings have stabilized, three measurements are taken at 1 minute intervals and averaged together (AASHTO T-316-06).

For the penetration test, binder is first poured into a container with a depth of at least 120% the expected penetration depth. This sample is cooled from 45 minutes to 2 hours, depending on sample size. It is then conditioned in a water bath at the target temperature for 45 minutes to 2 hours, again depending on the size of the sample. After this point, the sample is placed in a transfer dish filled with water of the appropriate temperature and placed under the penetrometer apparatus. This apparatus consists of a weighted needle attached to a measuring device and a timed release. The needle is 1mm in diameter with a truncated tip and weights approximately 50g. Additional weight is added to the needle, typically 50g for most tests. To conduct the test, the clean needle in placed flush with the surface of the binder sample and the position dial is zeroed. The needle is then released for either 5 or 60 seconds, depending on temperature. The amount of penetration is then measured, with the penetration number taken as 1pen = 0.1mm (AASHTO T-49-07). Penetration can then be converted to viscosity using the following equation (Witczak and Mirza, 1995):

$$\log(\eta) = 10.5012 - 2.2601 * \log(pen) + 0.00389 * \log(pen)^2$$

The third test is the softening point test. First, binder is poured into specially designed rings of approximately 23mm in diameter. Excess binder is then cut from the samples such that the binder is flush with the top and bottom of the ring. The rings are then placed in the test assembly and suspended in a water temperature bath, with ball guides placed around the rings. The bath will have a starting temperature of 5±1°C. The samples are then conditioned for 15 minutes,

along with steel balls with a diameter of 9.5mm and 3.50g. After the conditioning, the balls are placed in the ball guides such that they rest on the center of the binder in the rings. The temperature bath is then heated from below at a constant rate of 5°C/minute. The softening point is taken as the temperature where the asphalt sample falls from the rings and touches the assembly shelf below it (AASHTO T53-08).

Binder Aging Studies

The majority of research studies on HMA aging has been focused on the aging of asphalt binders. The negative effect that oxidative aging has on asphalt binders is critical in evaluating the binder's long term performance. In order to better understand the nature of this aging, a wide variety of testing procedures have been developed in various research projects.

Binder aging is primarily a result of the loss of lighter, volatile fractions of the asphalt binder, along with oxidation of the binder itself. This aging results in the overall hardening and stiffening of the binder. Several test procedures exist for rapidly aging asphalt binders, most utilizing thin films of asphalt subjected to extended heating and/or hot moving air. Some more exotic aging methods utilize microwave or ultraviolet/infrared radiation to achieve the same result (Airey, 2003).

Two of the most common test procedures are the rolling thin film oven test (RTFO) and pressure aging vessel test (PAV). In the RTFO, binder is placed in bottles which are then placed in a rotating carrousel inside of an oven set to

163°C. This rotation causes binder to coat the inside of the bottle, increasing the surface area exposed to oxidation while also decreasing the thickness of the binder film. At the lowest position hot air is blown into the bottles, further encouraging aging through oxidation and loss of volitiles. This method is utilized to simulate the short term aging that occurs during HMA production and placement. Different modified versions exist to better test different binder types. The PAV test is designed to simulate aging that will occur in the field by encouraging oxidation of asphalt binder over the loss of volatile components. It utilizes RTFOT-treated binders placed in pans at thin thicknesses. These pans are then placed in a sealed vessel and subjected to high pressures between 90°C and 110°C for 20 hours. However, there may be segregation of polymer additives in polymer modified binders (Airey, 2006).

Jung tested a number of aged binder properties from neat binder specimens and binder extracted from aged mixes (Jung, 2006). Binder oxidation was found to be similar in neat binder and binder extracted from mixtures. It was also found that oxidative aging decreases the capacity for HMA to self-heal and significantly reduces the strain-controlled fatigue life of an HMA pavement. Furthermore, while healing potential increases with higher binder content, at longer aging periods an increase in binder content does not significantly improve healing potential. This seems to suggest that there is a value at which a binder has fully oxidized and is not contributing to healing. Walubita tested similar mixes

and found that oxidative aging reduces an HMA mixture's fracture resistance in addition to its capacity to heal (Walubita, 2006).

Chipps et al performed a study into the aging characteristics of asphalt rubber binders (Chipps et. al., 2000). In order to rate the performance of the asphalt rubber, Chipps measured the hardening susceptibility, which is the relationship between oxidation and hardening. Oxidation converts the lighter polar aromatic components of an asphalt into asphaltenes, and this process results in the formation of carbonyls. Chipps evaluated carbonyl formation using Fourier transform infrared spectroscopy (FTIR) while also testing the complex viscosity using a dynamic shear rheometer on several binders. Various aging times and different blending procedures were used to prepare asphalt rubber binder samples.

Several blending procedures were used in Chipps' study, though two in particular stand out. The first used a 500rpm impeller to blend asphalt and crumb rubber for 1 hour at 177°C and was referred to as a "low cure". This type of blending is similar to procedures used in California and Arizona. The second "high cure" blends were made using a process seen in some terminal asphalt rubber blends. Crumb rubber was incorporated into asphalt at 230°C-260°C using a high shear mixer operating at between 4000 rpm and 8000 rpm. Total blend time was 6.5 hours for the high cure AR.

Chipps observed aging characteristics in both short and long term aging conditions. Short term aging refers to the period of rapid aging that asphalt cements exhibit before entering a less pronounced and constant long term aging

phase. The reason for this initial jump is that sulfur present in the asphalt reacts with other components of the binder to form carbonyls and thus asphaltenes. Once the sulfur is consumed, the asphalt then proceeds with its long term aging phase, where hardening susceptibility can be measured.

It was observed that the low cure samples, the crumb rubber would gel and expand but the individual crumb particles would stay intact. These samples showed both a lowered hardening rate and susceptibility, but it was difficult to mechanically determine the actual effect of adding the crumb rubber on the asphalt phase as the rubber crumbs came to dominate the aging process. On the other hand, in the high cure asphalt rubber the rubber particles dissolved into the asphalt. The high cure material showed improved aging characteristics over the virgin binder. In addition, since the crumb rubber dissolved it is known that this blending method will yield an improvement in the asphalt phase itself.

In another research study, it found that crumb rubber inclusions in an asphalt rubber binder also appear to absorb some of the maltenes of the binder (Lee, 2007). Lee observed this phenomenon by testing the percentile content of large molecular size (LMS) particles within an asphalt rubber binder utilizing gel permeation chromatography, with results displayed in FIGURE 1. The LMS values were seen to substantially increase as higher crumb rubber contents were used, indicating that the lighter, smaller maltenes were no longer loose in the binder. However, as aging progressed, the LMS values decreased with higher rubber contents. Lee took this as evidence to suggesting that the maltenes were at

first absorbed by the rubber particles and then released from the rubber particles during aging.

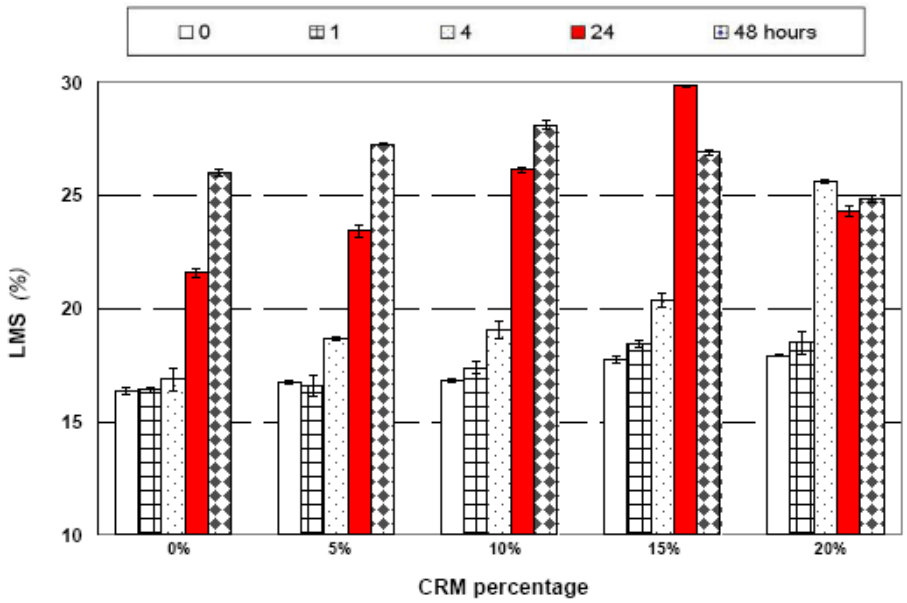

FIGURE 1. Large Molecular Size (LMS) of CRM Binders as a Function of Aging Period at 177°C *(*Lee, 2007*)*

However, the testing of binders from HMA mixtures aged in an oven in a loose state found that control and asphalt rubber mixtures did not show a significant difference in LMS content. The reasons Lee attributed to this lack of difference were that the binder film thickness was too thin and aging temperature was too low to facilitate a reaction.

Standard Laboratory Aging Protocol for Asphalt Mixtures

Currently, laboratory aging of asphalt mixtures is carried out under the SHRP-A-417 test protocol (SHRP-A-417). In this method, samples are placed in a forced draft oven at a constant temperature of 85 °C for a period of five days (120 hours). The protocol is intended to simulate the oxidative aging effects of about 7

to 10 years. This protocol has a provision that open graded mixtures should be aged in a low pressure oxygen chamber at 60 °C in order to mitigate sample degradation during aging.

E* Dynamic Modulus Testing Procedures

AASHTO TP 62-07 test protocol is followed for E* dynamic modulus testing (AASHTO TP-62-07). The protocol calls for testing three replicates for a mixture. For each specimen, E* tests are conducted at -10, 4.4, 21.1, 37.8 and 54.4 °C and 25, 10, 5, 1, 0.5 and 0.1 Hz loading frequencies. A 60 second rest period is used between each frequency to allow some specimen recovery before applying the new loading at a lower frequency. The E* tests are done using a controlled sinusoidal stress that produced strains smaller than 150 micro-strain. This ensured, to the best possible degree, that the response of the material is linear across the temperatures used. Generally, the dynamic stress levels are 69 to 690 kPa for colder temperatures (-10 to 21.1 °C) and 14 to 69 kPa for higher temperatures (37.8 to 54.4 °C). All E* tests are conducted in a temperature-controlled chamber capable of holding temperatures from –16 to 60 °C. A typical test specimen is shown in FIGURE 2.

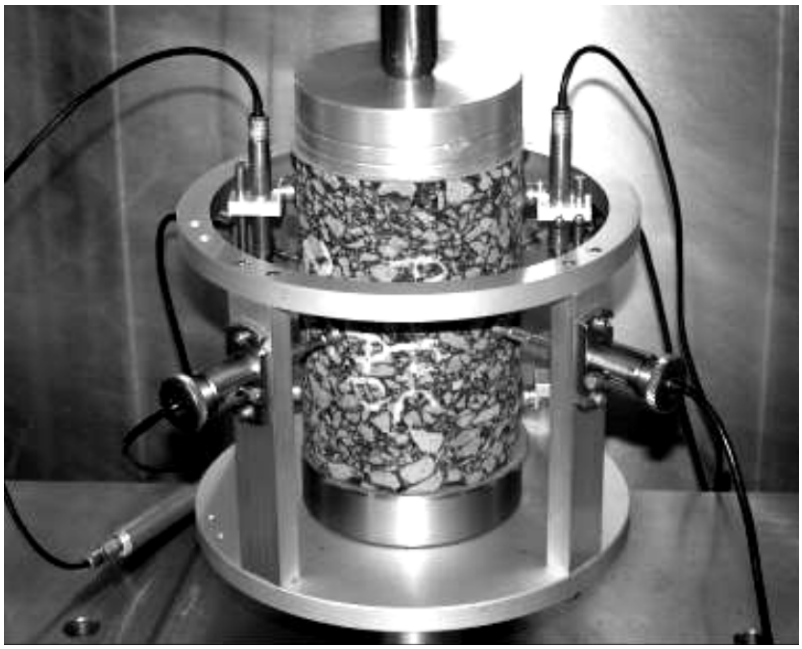

FIGURE 2. Typical E* Dynamic Modulus Test Sample

Beam Fatigue Testing Procedures

AASHTO TP-8 is commonly followed for beam fatigue testing (AASHTO TP-8-94). Specimen beams are manufactured with dimensions of 380mm in length, 50mm in height, and 63mm in width. These specimens are then subjected to a controlled haversine strain applied at a period of 10hz. Strain levels between 300 and 1000 microstrain are set for each specimen tested. There are no rest periods between loads. With the strain controlled test, peak strain remains constant during the test while the stress on the specimens decreases with number of cycles. A range of test temperatures are used to develop the general fatigue model equation. For comparative purposes, a test temperature of 21.1°C is

commonly utilized. FIGURE 3 below displays the conceptual loading case applied to beam specimens during testing.

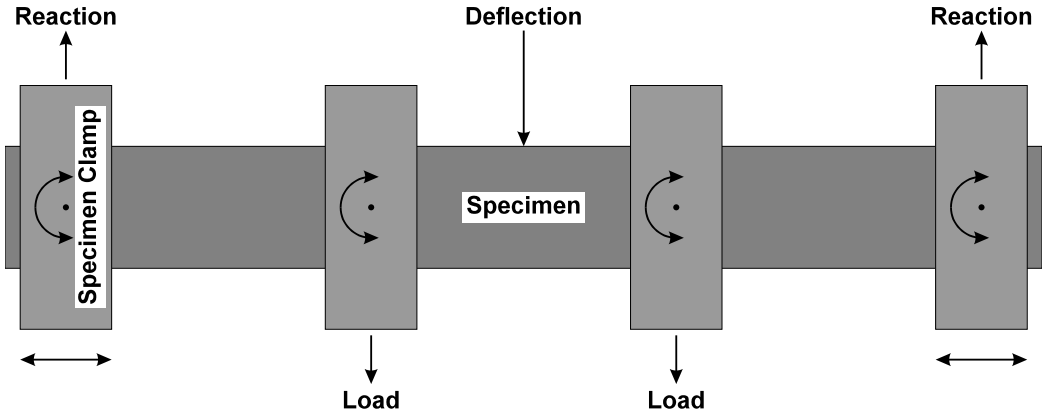

FIGURE 3. Conceptual Diagram of Beam Fatigue Test

The beam sample is restrained at four points along its length by clamps. The outside two clamps remain static vertically while the central two deflect to apply the desired strain to the sample. In order to mitigate moment effects from the sample restraints, each clamp is allowed to pivot. The outside two clamps are also allowed to shift horizontally as well, again to minimize undesired forces and moments applied to the test specimen. The device used in this study is an IPC Beam Fatigue Apparatus, displayed in FIGURE 4.

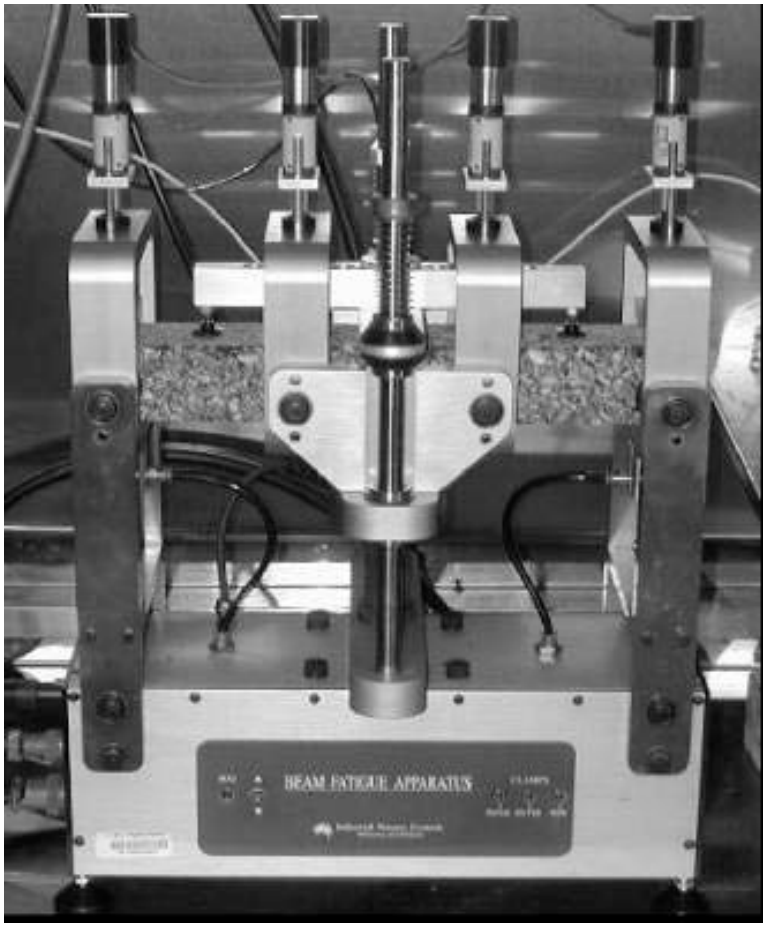

FIGURE 4. Beam Fatigue Testing Apparatus with Sample

Mixture Aging Studies

Raghavendra et al verified laboratory procedures to simulate the field-hardening of asphalt binders and mixes that were developed and adopted by American Association of State Highway and Transportation Officials (AASHTO) as Provisional Protocol PP2-99 (Raghavendra et al, 2006). This research study under the National Cooperative Highway Research Program (NCHRP) 9-23, was initiated to verify these protocols, identify their limitations, and make recommendations to enhance their predictive capabilities. Binders and field cores

were obtained from Long Term Pavement Performance (LTPP) and other sites across the United States. Plant-mix, laboratory-aged cores, and field-aged cores were characterized using E* dynamic modulus testing. Verification of the existing protocol was carried out using the data collected from testing. Warmer climates resulted in higher aging compared to cooler climates. Laboratory cores were found to have more uniform aging profiles than field cores. It was concluded that the existing protocol is insufficient to accurately predict the field aging of asphalt mixes. In addition, for pavements with air voids lower than 8% laboratory aging exposes the samples to harsher oxidation than they would experience in the field. Note that the findings were based on tests conducted on conventional asphalt mixes containing conventional, non-modified binders.

Othman performed a comparative study on cyclic thermal aging between a conventional and an asphalt rubber mixture utilizing the critical energy release rate, or J-Integral, as a metric for fracture resistance. In his study, samples were subjected to 0, 8, 28, and 56 temperature cycles. The temperature cycled between 20°C and 50°C over the course of a day, with equal times at the two temperature17s excepting a relatively short temperature transition time. Ultimately, Othman found that the asphalt rubber material exhibited superior fracture resistance to a conventional mix at all tested temperatures and aging conditions. He also compared unconfined compressive strengths and found that for both AR and conventional asphalt mixtures the strengths would decrease as the samples experienced more thermal cycles. At a low number of thermal cycles

the asphalt rubber showed an improvement in strength. However, as the number of cycles increased the unconfined compressive strength of the asphalt rubber mixture converged with that of the conventional material (Othman, 2006).

Saboundjian compared the beam fatigue life of field aged conventional and asphalt rubber mixtures. Both materials were from a California test section and were in service for 10 years before being removed to be tested. The samples were fashioned into 50mm by 50mm by 410mm beams and tested for beam fatigue, with strain-controlled loading times of 0.1 seconds at 60 cycles per minute. Test temperatures of -2°C and 22°C were utilized. The results of the study found that the aging experienced by the asphalt rubber samples resulted in a negligible effect on beam fatigue life at 22°C. At -2°C, there was a noticeable effect on fatigue life, but this was less than the effect seen in the conventional mixture (Saboundjian et. al., 2001).

EXPERIMENTAL TESTING PROGRAM

Program Summary

The testing program was divided into three distinct phases. The first phase was an analysis of the effects of aging on the viscosity of asphalt rubber binders and their virgin bases. The testing was performed and reported in previous studies and analyzed as part of this project (Kaloush et. al., 2002; Sotil, 2003). Two common aging techniques, RTFO and PAV aging, were utilized. The second phase was a short study comparing different accelerated aging techniques and durations in order to garner a basic understanding of the aging characteristics of asphalt rubber materials. The study consisted solely of dynamic modulus testing.

The next phase collected data and mixtures from previously constructed asphalt rubber pavements. This project was located on the I-17 frontage road between 16th Street and Pinnacle Peak Road in Phoenix, Arizona and constructed as a test section aimed at gauging the long term performance of asphalt rubber pavements. To this end, two mixtures were used. The first used over the majority of the site was an ARAC mixture utilizing a PG 64-16 binder as its base. The binder was mixed with approximately 22% crumb rubber by weight of asphalt. Maximum aggregate size for this gap graded mix was 3/4". Target binder content and air voids were 8% and 5.5% respectively. A second mix was also utilized on the test section to study the effect of binder type on long term performance. This mix was made utilizing a PG 58-22 binder and used the same percentage of crumb

rubber and same aggregate gradation. Air voids were increased to 8% while binder content was reduced to 7.5% (Kaloush et. al., 2002; Sotil, 2003).

As part of an earlier study, the original 64-16 mixture was subjected to laboratory aging identical to one of the methods used in phase 1 for four durations. This data was analyzed and compared to the data found from the field samples in an attempt to determine what duration of aging coincides with the amount of aging observed in the 7 year field samples.

Testing Program

The first phase of this project was the analysis of viscosity testing performed on various binders, aged and unaged, virgin and rubber modified, in order to evaluate their aging characteristics. Three binders were tested at three aging conditions and published as part of previous work (Kaloush et. al., 2002; Sotil, 2003). The next two phases of the project consisted of the testing of AR mixtures. These mixtures were tested from several different sites. Most were tested for dynamic modulus but some were also tested for beam fatigue. TABLE 1 below summarizes the mixture testing program of the project. Note that the testing on Original Lab and 1 Year field samples for the 58-22 and 64-16 ARAC mixtures were performed as part of Kaloush, et. al. 2002 and used for the analysis of aging in the 7 year field samples tested as part of this project. Likewise, the 64-16 ARAC laboratory aging study in this project was an analysis performed on the test results from a previous unpublished study.

TABLE 1. Summary of Mixture Testing Program

	Dynamic Modulus E*	Beam Fatigue
Initial Aging Study, 58-22		
ARFC Original	X	
ARFC 5 Day Pan	X	
ARFC 14 Day Pan	X	
ARFC 5 Day Core	X	
ARFC 14 Day Core	X	
Field Samples, 58-22		
58-22 7 Year	X	
58-22 Original Lab	X	
Field Samples, 64-16		
ARAC 7 Year Bucket	X	
ARAC 7 Year	X	X
ARAC 1 Year		X
ARAC Original Lab	X	X
Lab Aging, 64-16		
ARAC 1 Day Core	X	
ARAC 4 Day Core	X	
ARAC 7 Day Core	X	
ARAC 14 Day Core	X	

Binder Testing

Three asphalt rubber binders and their virgin bases from two projects were analyzed as part of this study. The virgin base for each binder was also analyzed. RTFO treatment was performed per specifications, while PAV was done at 100°C. After aging conditioning, viscosity testing was performed as part of a previous project (Kaloush et. al., 2002; Sotil, 2003). Testing consisted of a softening point test and two penetration tests at 15° and 25°C as well as a series of Brookfield rotational viscosity tests for various temperatures ranging between 60°

and 176.7°C. A summary of the test results analyzed from Sotil's work can be seen in TABLE 2, below.

TABLE 2. Summary of Binder Testing Program

Binder	Aging Condition	Number of Samples		
		Penetration	Softening Point	Brookfield
I-40 58-22 Virgin	Original	2	1	6
	RTFO	2	1	6
	PAV	2	1	6
I-40 58-22 AR	Original	2	1	4
	RTFO	2	1	4
	PAV	2	1	5
I-17 58-22 Virgin	Original	2	1	6
	RTFO	2	1	6
	PAV	2	1	6
I-17 58-22 AR	Original	2	1	5
	RTFO	2	1	6
	PAV	2	1	6
I-17 64-16 Virgin	Original	2	1	6
	RTFO	2	1	6
	PAV	2	1	5
I-17 64-16 AR	Original	2	1	6
	RTFO	2	1	6
	PAV	2	1	6

It was necessary to convert softening point and penetration values to viscosity in order to facilitate a unified analysis of the binder data. The viscosity of the softening point was approximated as 13,000 poises. This viscosity was used for all softening point temperatures. For penetration, the following equation was used:

$$\log(\eta) = 10.5012 - 2.2601 * \log(pen) + 0.00389 * \log(pen)^2$$

The variable η is the viscosity in centipoise and pen is units of penetration of 0.1mm. This equation was developed as part of a Strategic Highway Research

Program (SHRP) study and is accurate for penetrations between 3 and 300 (Witczak and Mirza, 1995). Once the viscosity for all test points was found, regression analysis was performed on the data using the form:

$$\log[\log(\eta)] = A_i + VTS_i * \log(T_R)$$

Once again η is in units of centipoises while T_R is temperature in degrees Rankine. The log[log(η)] values for the aging conditions were then compared to the original condition and a ratio calculated for various temperatures. This ratio was taken to be an indicator of the effect of aging.

Initial Aging Study

Artificial laboratory aging has the potential to unlock a great deal of understanding of the potential performance for HMA mixtures in general and asphalt rubber mixtures in particular. As part of the overall study, two separate experiments were performed. The first experiment compared two accelerated aging techniques and gaged their effectiveness at producing reasonable levels of oxidative aging in an ARFC mixture. Aging was evaluated using E* dynamic modulus along with compaction data.

The second experiment attempted to gage the amount of aging occurring during long term storage of an ARAC mixture. An ARAC mixture from the I-17 project was used to form E* specimens and tested (Kaloush et. al., 2002). Compaction effort and dynamic modulus were compared to gage aging. This experiment also attempted to compare compaction effort and dynamic modulus as effective means to measure oxidative aging.

The first experiment of the study included an ARFC mix with two aging durations (5 and 14 days) for each of the two aging procedures in addition to control samples not subjected to aging (unaged condition). Samples were prepared using field mixtures from the Arizona Department of Transportation (ADOT) Antelope Wash project to evaluate laboratory aging performance characteristics. The standard SHRP-A-417 aging protocol was followed but the study incorporated one additional level of aging (SHRP 1994). Therefore, the samples were aged for a period of 5 days conforming to the protocol. 14 days of aging was additionally used. Also, a confining mesh was used to prevent damage to the specimens, which is not a provision in the protocol but has been used successfully in other studies (Raghavendra et. al., 2006). In another method, the mix was aged in a loose state and the aged mix was used to prepare test specimens. The purpose of this method was to age the mix as homogeneously as possible.

The first procedure that was followed to subject samples to laboratory aging is described as follows. Laboratory samples that were subjected to the aging according to the current protocol are referred to as 'core aged' specimens. The sample cores for the mixtures were prepared after compaction using a gyratory compactor. Cores were then taken from the gyratory plugs and prepared into 150-mm high, 100-mm diameter cylindrical specimens. As a modification to the protocol, ARFC samples were wrapped in wire mesh secured by steel bands in order to control sample degradation during aging. As excess pressure would

deform the samples, care was taken to only tighten the bands just enough to secure the mesh cage. Mesh was also placed underneath the samples to minimize loss of material from the bottom of the samples. FIGURE 5 shows a typical ARFC sample wrapped in a mesh cage to be subjected to aging.

FIGURE 5. ARFC Sample Confined in Mesh Cage

The second methodology adopted to age ARFC mixes is described next. This methodology details the samples that were aged in a loose state in a pan. This procedure was termed ‘pan aging’. Pan aging was performed for the two aging durations: 5 and 14 days which were similar to the first procedure. Pan aging consisted of placing ARFC mix in large trays in a loose state with a depth of approximately 50-100 mm. The mix was then heated in a forced-draft oven at 85 °C for the aging duration. In order to uniformly age the specimens and avoid hardening in place, the samples were broken up and stirred throughout the aging process on a day-to-day basis. Location of the aging trays inside the oven was

also varied daily to minimize the effects of temperature variation inside the oven. After aging, specimens were compacted in a gyratory compactor and prepared into samples of 150-mm height and 100-mm diameter.

Air voids were obtained on all samples subjected to the two aging procedures described above and unaged specimens with a CoreLok device, which is accurate at measuring higher percent air voids. Three sample replicates were prepared for different aging conditions. Note that only two replicates of ARFC 14 day core and 14 day pan aged samples were available for testing because one sample from each set disintegrated during the aging process.

E* dynamic modulus tests were conducted on both unaged and aged samples per the standard protocol at five temperatures: -10, 4.4, 21.1, 37.8, and 54.4 °C and six loading frequencies: 25, 10, 5, 1, 0.5, and 0.1 Hz. TABLE 1 provides a summary of the experimental program.

Storage Aging

The second experiment attempted to gage if the properties of an asphalt rubber hot mix asphalt stored long term retained the properties it had when first manufactured. The mixture was reheated, compacted into gyratory plugs, and cut into E* dynamic modulus specimens. Compaction effort and E* were used as indicators for long term storage aging by comparing the results found in this study to the original tested values.

The mix used was a ¾" gap graded ARAC mix design utilizing PG 64-16 virgin asphalt binder modified with 20% crumb rubber per ADOT's Asphalt

Rubber specifications. The original mix was used on an ADOT test project on a frontage road along I-17 in 2002 (Kaloush et. al., 2002). It had been stored in sealed metal buckets for a period of 7 years prior to this experiment. This ARAC was reheated to compaction temperature and homogenized with care taken to minimize the exposure effects on aging from the reheating process. Three gyratory plugs were manufactured using the same mass of material originally used to yield 5.5% air voids. From these gyratory plugs, 150mm by 100mm cylindrical E* samples were cored. These three samples were then tested for dynamic modulus at a temperature of 21.1 °C with loading frequencies of 25, 10, 5, 1, 0.5, and 0.1 Hz. The results were then compared to those found when the mix was new in order to gauge the amount of aging that occurred during storage.

Field Testing

As part of the research project in the previous section, a pair of test sections were established in 2003 in order to evaluate the performance of ARAC pavements over time. Each of these sections utilized a different binder type. As part of this process several aluminum plates were placed between the existing pavement and the ARAC overlay to form a release layer, as shown in FIGURE 6. This was to allow for relatively large field samples to be recovered with minimal damage from the removal process. These samples were then tested for beam fatigue.

This project also manufactured laboratory specimens from the fresh loose mix for beam fatigue and dynamic modulus. Building upon this study, this thesis

project took additional field samples after 7 years and tested them for beam fatigue initial stiffness and dynamic modulus. These results were compared to those obtained in the original study.

FIGURE 6: Placement of Aluminum Plates Prior to ARAC Overlay

The two gap graded ARAC test sections utilized asphalt rubber binders with the base binders being PG 64-16 and PG 58-22. Cores and slabs were cut from each test section for dynamic modulus and beam fatigue specimen

respectively. The pavement depth was approximately 100mm, which required that additional steps be performed in the preparation of testable samples. Approximately twelve cores were taken from each test section, along with several slabs. However, difficulties in locating and cutting over the aluminum plates resulted in difficulties in the PG 58-22 section, resulting in an insufficient number of recoverable beam fatigue specimens.

A total of twelve cylindrical cores were taken from each test section for dynamic modulus. Cores were 100mm in width and approximately 100mm tall, though the height varied significantly. In addition, the ends of the specimens were neither even nor parallel, inhibiting the use of the cores in dynamic testing modulus. In order to remedy the issue, the cores were trimmed so that the faces were smooth and parallel and then stacked together to form 150mm tall samples. Three cores formed each sample, which were glued together with a thin film of the appropriate PG graded asphalt binder. In order to minimize the effect of the interfaces between cores on the dynamic modulus results, the LVDTs measuring sample deformation were only placed on the middle core. The middle core had a height of 70mm compared to 40mm for the either of the end cores. This increased height allowed for a greater gage length to be used with the samples that would have been possible using equal heights, improving the accuracy of the test. Sets of three cores were selected to be glued together into a sample based on how level and plumb the cores could be assembled together, with the best three sets being selected for testing. Stacking of cores had been previously validated as producing

representative samples (Witczak et. al., 2000). FIGURE 7 shows an assembled stacked core prior to instrumentation. Percent air voids was determined for each composite specimen using the saturated surface dry method. E* dynamic modulus tests were conducted per the standard protocol at five temperatures: -10, 4.4, 21.1, 37.8, and 54.4 °C and six loading frequencies: 25, 10, 5, 1, 0.5, and 0.1 Hz.

FIGURE 7. Stacked ARAC E* Specimens

Seven beam fatigue specimens were cut from the recovered slabs from the PG 64-16 section. Specimens were trimmed into 380mm long by 63mm wide by 50mm high beams, with care taken to retain the orientation the pavement sample had while in service in the roadway. Excess material was cut from all sides in order to ensure the beams were as close to specifications as possible while also avoiding any inconsistencies occurring at the top and bottom of the pavement section in order to achieve representative samples. The seven beams were tested at strain levels of 300, 400, 500, 600, 700, 800, and 1000 microstrain at a test temperature of 21.1°C and the initial stiffness was compared to those of the pavement compacted in the laboratory and recovered a year after placement. The number of samples used for each test can be found in TABLE 3.

TABLE 3. Field Sample Summary

	Dynamic Modulus E*	Beam Fatigue
Field Samples, 58-22		
58-22 7 Year	3	-
58-22 Original Lab	3	-
Field Samples, 64-16		
ARAC 7 Year Bucket	3	-
ARAC 7 Year	3	7
ARAC 1 Year	-	7
ARAC Original Lab	3	7
Lab Aging, 64-16		
ARAC 1 Day Core	1	-
ARAC 4 Day Core	2	-
ARAC 7 Day Core	1	-
ARAC 14 Day Core	2	-

TEST RESULTS AND ANALYSIS

Binder Testing

Three asphalt rubber binders and their virgin bases were tested for viscosity in their original condition as well as RTFO and PAV aged states. The various viscosity points were tabulated and converted to log[log(η)] viscosity and plotted versus the log value of the temperature in degrees Rankine. A regression line was then plotted through the data points, with the intercept being the A_i value and slope being the VTS_i value, also known as the temperature susceptibility. TABLE 4, below is an example of the tabulation while FIGURE 8 is an example of the plot and regression calculation.

TABLE 4. Example of Viscosity Versus Temperature Tabulation

I-40 58-22 Original Virgin						
Temp. °C	Temp. °R	Log Temp. °R	Pen. (0.1mm)	Viscosity cP	Log Log Visc. cP	Test
15	518.67	2.9905	34.2	-	0.8478	Penetration
25	536.67	2.9984	112.2	-	0.7697	Penetration
47	576.27	3.0153		1300000	0.7863	Soft. Point
60	599.67	3.0250		82000	0.6914	Brookfield
80	635.67	3.0396		9412.5	0.5992	Brookfield
100	671.67	3.0536		2250	0.5253	Brookfield
122	711.27	3.0685		587.5	0.4423	Brookfield
135	734.67	3.0771		287.5	0.3907	Brookfield
177	810.27	3.1038		62.5	0.2543	Brookfield

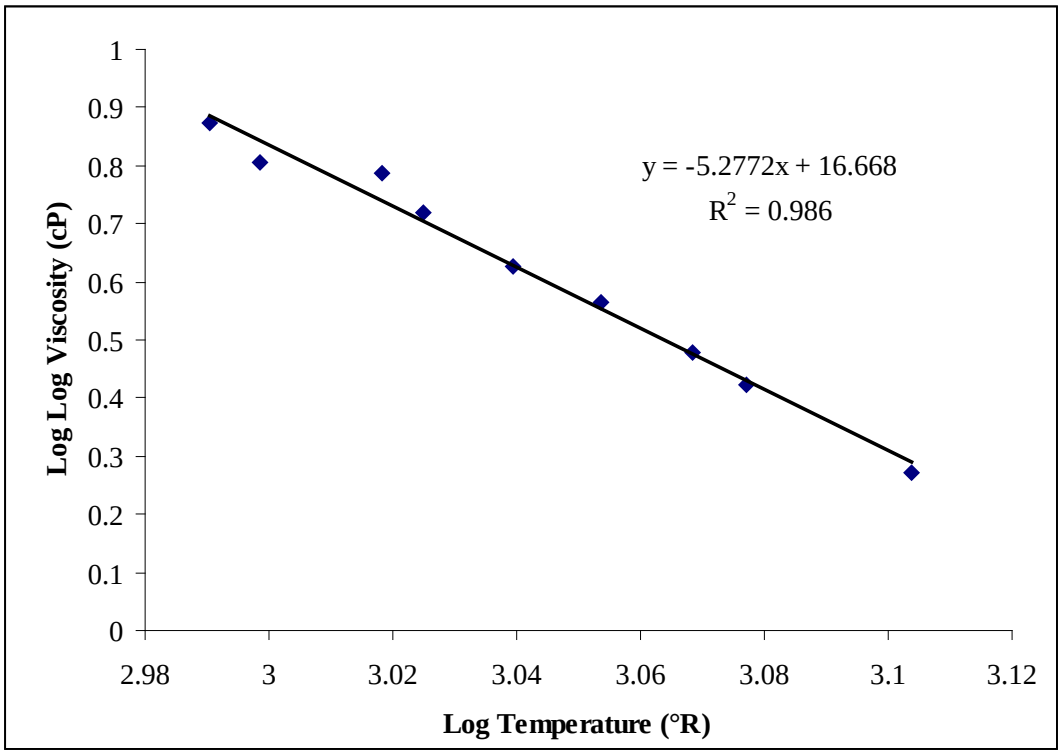

FIGURE 8. Temperature-Viscosity Regression Plot Example

Following the calculation, A_i and VTS_i values for the various binders were calculated. The results of these calculations can be seen in TABLE 5 on the next page.

TABLE 5. A_i and VTS_i Values

Binder	Aging Condition	Ai	VTSi
I40 58-22 Virgin	Original	10.875	-3.659
	RTFO	10.763	-3.608
	PAV	10.732	-3.583
I40 58-22 AR	Original	7.690	-2.480
	RTFO	7.287	-2.315
	PAV	7.147	-2.255
I17 58-22 Virgin	Original	11.453	-3.868
	RTFO	11.389	-3.836
	PAV	11.907	-4.007
I17 58-22 AR	Original	9.029	-2.972
	RTFO	8.808	-2.881
	PAV	8.644	-2.812
I17 64-16 Virgin	Original	11.163	-3.755
	RTFO	11.116	-3.728
	PAV	11.010	-3.678
I17 64-16 AR	Original	8.390	-2.738
	RTFO	8.543	-2.781
	PAV	8.544	-2.775

The regression equations were then used to calculate the log[log(η)] for all the binders. A ratio of the viscosity values was then taken for each of the aged binders and compared and plotted as a function of the log of the absolute temperature °R. A higher ratio indicates a greater increase in viscosity. Interestingly, for all binders tested, increased temperature results in an increase in this viscosity ratio. In all cases, as the aging condition increased in severity, the viscosity ratio increased as well. Therefore, an increased viscosity ratio at a given temperature is indicative of increased aging effects.

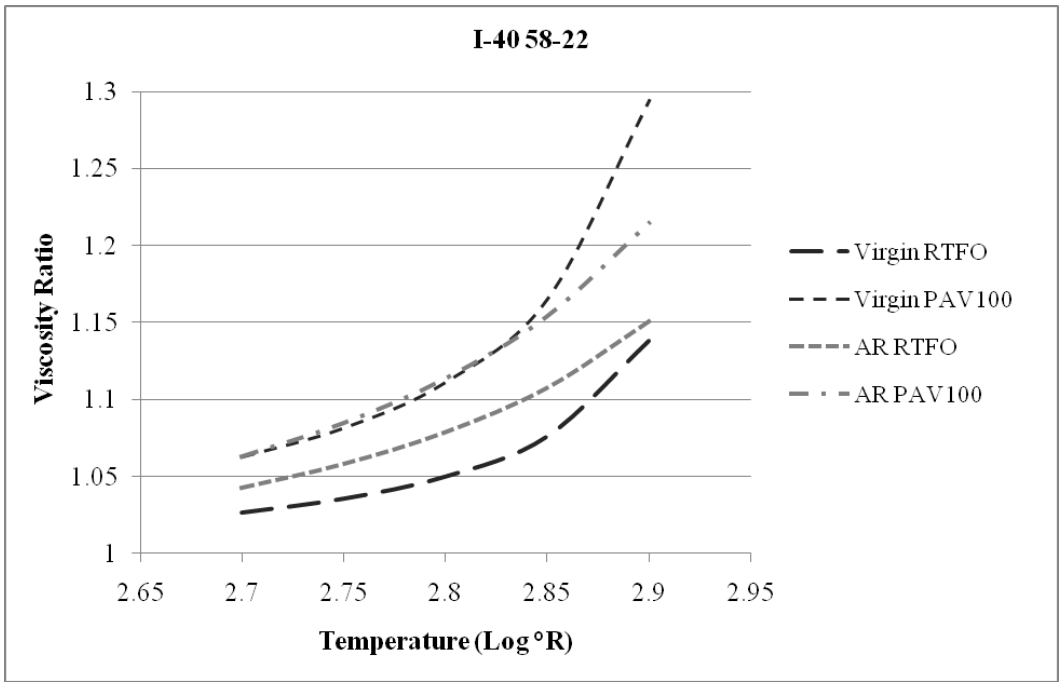

FIGURE 9. Viscosity Ratio Curves for I-40 PG 58-22 Binder

The I-40 58-22 binder viscosity ratio curves illustrate some of the traits that are seen in the other binders as well. Both the AR and virgin binders show an increase in the viscosity ratio as temperature increases. In the RTFO condition, the AR binder shows greater viscosity ratio and therefore more short term aging, though the rate of ratio increase is greater in the virgin binder. For the PAV condition, the AR binder and virgin binder have similar viscosity ratios, but again as temperature increases, the virgin binder exhibits a faster rate of ratio increase. It is interesting to note that the virgin binder shows a clear critical point where the slope of the viscosity ratio curve increases dramatically, while the AR binders show a smoother progression of increasing slope.

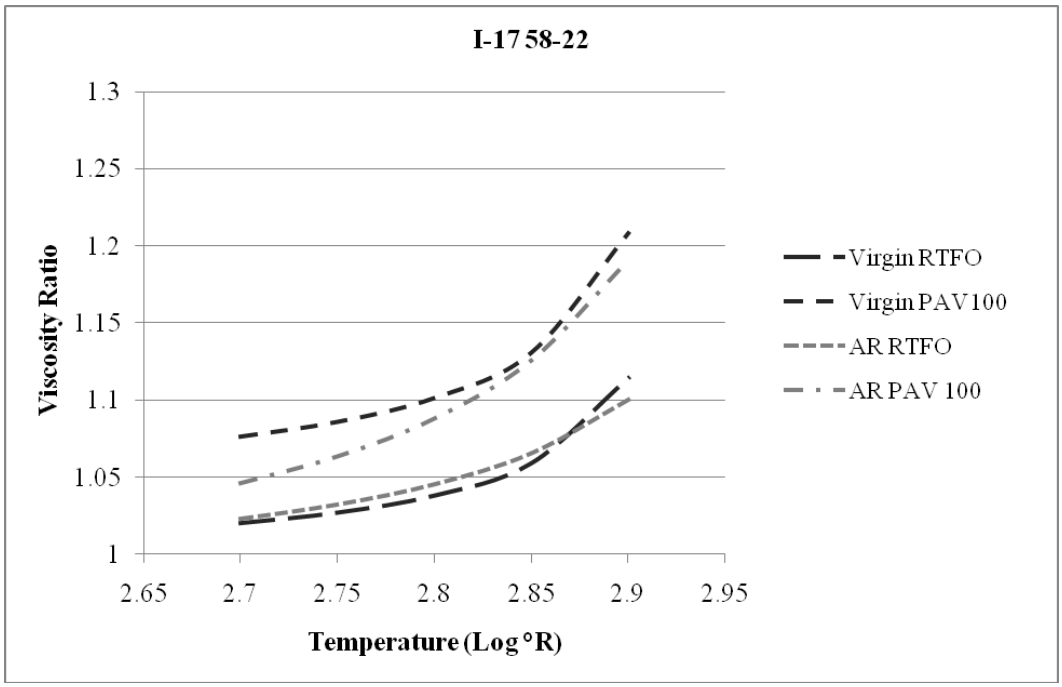

FIGURE 10. *Viscosity* Ratio Curves for I-17 PG 58-22 Binder

The I-17 PG 58-22 binder shows similar trends to the I-40, but the difference between AR and virgin binders in the RTFO condition is much less pronounced. Once again there is an critical point in the virgin RTFO curve where the effects of aging become more apparent. However, there appears to be a different behavior. This is most apparent in the in the PAV binders. Initially, the AR binder has a steeper slope but lower viscosity ratio. This causes it to approach the virgin binder curve. However, past the critical point the virgin curve once again begins to separate from the AR curve. This is also seen in the RTFO condition, though to a lesser degree.

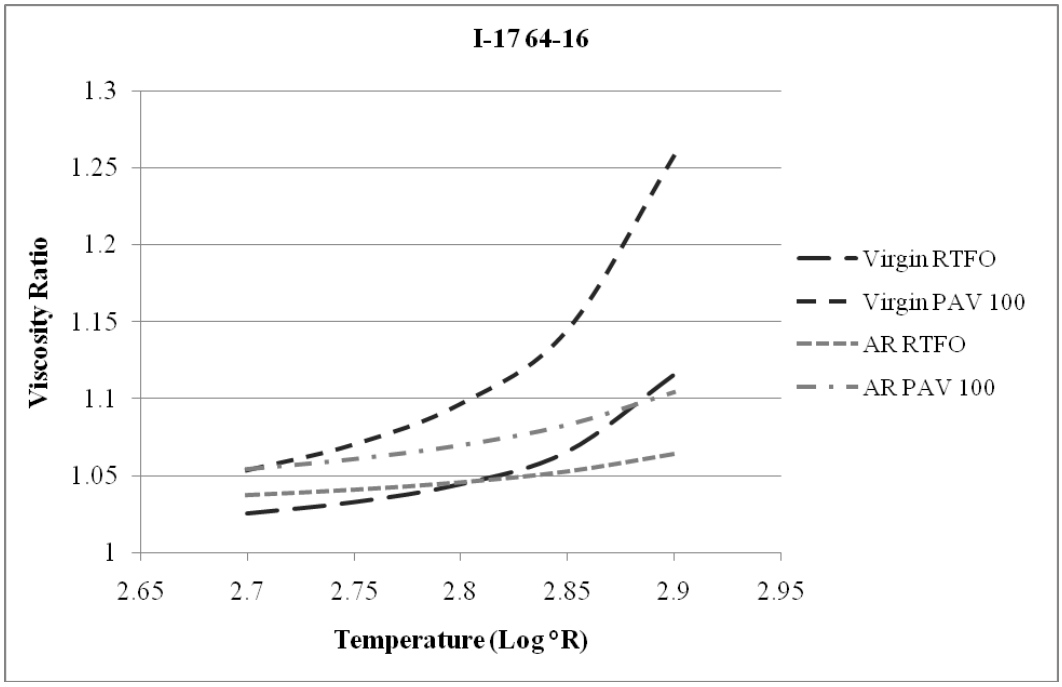

FIGURE 11. Viscosity Ratio Curves for I-17 PG 64-16 Binder

The behavior of the I-17 64-16 binder shows a significant difference from the previous two 58-22 binders. Once again the virgin binder curves show the same shape and critical point. However, the AR binders are significantly flatter, indicating a vastly decreased effect of aging on the binder viscosity at the higher temperatures. The virgin RTFO curve actually comes to cross the AR PAV curve at the higher temperatures.

This is likely due to the change in binder type. The softer lower PG graded asphalt binders will have a larger proportion of lighter maltenes and aromatics. Tire rubber reacts with and absorbs these lighter fractions, forming a sort of gel. It is possible that with the softer 58-22 binders there are still large

proportions of the lighter oils beyond that which reacted with the rubber. In this case, the unreacted lighter oils would be more exposed to the aging process and thus more likely to diffuse out of the binder, thereby coming to dominate the aging behavior of the binder. In the case of the stiffer 64-16, a larger proportion of the aromatics has reacted with the rubber and is therefore sequestered in the asphalt rubber gel. This results in a lowered apparent level of aging in the AR binder when compared to its virgin base.

Initial Aging Study

Comparison of gyratory compaction data between pan aged and un-aged mixes indicated that there is a significant increase in the force required to compact the pan aged specimens when compared to the un-aged ones suggesting that oxidation occurred in the aged samples. Furthermore, during the process of aging, it was observed that the loose mix exhibited a loss of characteristic adhesion of Crumb Rubber Modified (CRM) binder. Additionally, the mix's luster also changed from relatively smooth and shiny to a dull matte finish. This perhaps could be due to the oxidation of the mix. It is also interesting to note that the samples prepared after pan aging did not develop a CRM binder 'skin' which is typical of a freshly prepared asphalt rubber sample. The absence of this 'skin' suggested that the CRM binder had stiffened or changed in viscosity during aging. FIGURE 12 shows two typical samples, one of them being pan aged and the other core aged. As observed, the core aged specimen shows a 'skin' around the

circumference, which is typical of any freshly prepared ARFC sample, while the 'skin' on the pan aged sample was absent.

FIGURE 12. Pan Aged versus Core Aged Specimen

TABLE 7 provides a summary of compaction parameters and sample air voids before and after aging for both core and pan aging conditions. All the specimens were compacted to a height of 170 mm in a 150 mm diameter mold with a gyratory compactor. It was observed that the number of gyrations and shear stresses in the pan aged specimens were significantly greater than those of the core aged specimens, suggesting that the pan aged material was stiffer. Target air voids were 18% for all the specimens. Analysis of Variance (ANOVA) was performed on the sample air voids for each group. A confidence interval of 95% was assumed and ANOVA was performed assuming unequal variance. The statistical results indicate that there is no significant difference of average sample

air voids between ARFC specimens at different aging conditions as shown in TABLE 6.

TABLE 6. Comparison of Air Voids for Laboratory Aging of Asphalt Rubber Friction Course Mixtures

Aging Condition	Avg. Air Voids (%)	Variance of Air Voids (%)	Number of Samples
ARFC Control (Unaged)	17.72	0.004	3
ARFC 5-Day Core	19.77	11.912	3
ARFC 14-Day Core	18.83	0.594	2
ARFC 5-Day Pan	18.76	0.590	3
ARFC 14-Day Pan	18.7	0.010	2
P-Value		0.74	
F-statistic		0.49	
F-critical		3.84	

Post-aging, less variability with respect to sample air voids was observed with the pan aged samples, apparently due to the fact that the material was aged more uniformly and stirred prior to being formed into samples, promoting homogeneity. It should be noted that the initial air voids of the 5-day core aged specimens were obtained using a traditional bulk specific gravity test in a water bath. Note that air voids were re-estimated for 5-day core aged samples after aging to understand the change in air voids due to aging procedure which might eventually affect deformation in samples. Interestingly, air voids increased in core aged samples (about 7%).

TABLE 7. Compaction and Sample Air Voids for Core and Pan Aged Conditions

	Sample ID#	Gyrations	Shear Stress, Kpa	Pre-Aging AV, %	Post-Aging AV,%
5 Day Core	AW444	54	550	23.67	22.82
	AW445	64	550	18.53	20.85
	AW446	100	530	17.11	23.08
	Mean	72.67	543.33	19.77	22.25
	Standard Dev.	24.19	11.55	3.45	1.22
14 Day Core	AW442	48	545	18.28	23.73
	AW443	75	545	19.37	25.15
	Mean	62.55	467.84	17.17	19.87
	Std. Dev.	23.87	201.32	6.39	8.33
	Mean	68.20	544.00	19.39	
	Standard Dev.	74.84	527.23	18.39	
5 Day Pan	AW4A1	97	625	N/A	18.32
	AW4A2	95	620	N/A	18.32
	AW4A3	63	610	N/A	19.65
	Mean	85.00	618.33	N/A	18.76
	Std. Dev.	19.08	7.64	N/A	0.77
14 Day Pan	AW4A4	73	625	N/A	18.77
	AW4A5	93	625	N/A	18.63
	AW4A6	98	640	N/A	N/A
	Mean	88.00	630.00	N/A	18.70
	Std. Dev.	13.23	8.66	N/A	0.10

TABLE 8 provides changes in lateral dimensions of 5-day core aged samples before and after aging. It can be seen that the first sample experienced significant changes in height and width whereas the other two samples experienced minor

dimensional changes. During physical observation of the specimens, sample number 1 showed some slumping inside of its mesh cage. This was possibly due to its high initial air voids as seen in the table. Additionally, the other two samples showed similar increase in air voids despite a lack of deformation during aging. This can be attributed to the loss of lighter oils from the rubber particles in the asphalt. Generally, crumb rubber inclusions absorb and store the oils in the asphalt and transform the hard rubber into a relatively soft and fluffy material. Therefore, during the aging process, the asphalt binder film thickness decreases, indicating the evaporation of the lighter oils from the rubber inclusions, which increases sample air voids as shown in FIGURE 13. Similarly, the loss of lighter oils during aging also explains the absence of the 'skin' on the samples made out of pan aged mix, because the CRM binder revert to a hardened state. This eventually leads to a sample that looks dry on the outside (FIGURE 12).

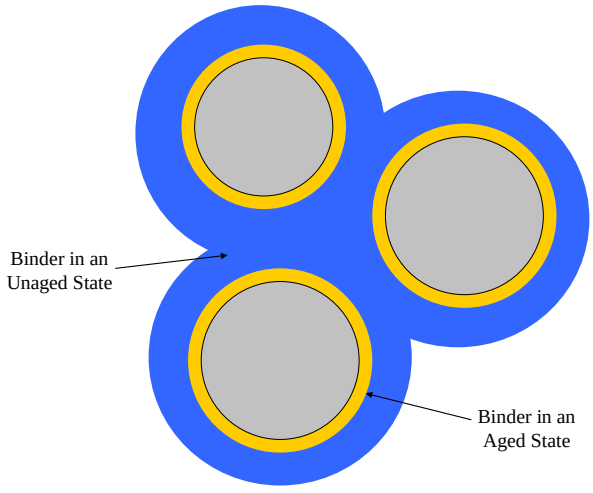

FIGURE 13. Increase of Air Voids Due to Aging and Decrease of Film Thickness

TABLE 8. Dimensional Changes due to Aging in 5-day Core Aged Specimens

Property	Sample	Pre-Aging	Post-Aging	% Change
Height (mm)	1	155.51	154.33	-0.76
	2	154.72	155.34	0.40
	3	155.97	156.79	0.52
Top-Width (mm)	1	102.27	103.4	1.09
	2	102.28	103.06	0.76
	3	102.61	102.33	-0.27
Bottom-Width (mm)	1	101.76	104.16	2.30
	2	103.06	103.04	-0.02
	3	102.74	102.63	-0.11
Air Voids (%)	1	23.67	22.78	-3.91
	2	18.53	21.06	12.01
	3	17.11	20.21	15.34

As mentioned previously, the ARFC mixtures were subjected to four aging levels: 5 and 14 day core aged and 5 and 14 day pan aged. E* tests were run on both the unaged and aged samples per AASHTO TP 62-03. Using the E* test results, a master curve was constructed at a reference temperature of 21.1 °C using the principle of time-temperature superposition. FIGURE 15 (a) and (b) show the average E* master curves for core and pan aged samples respectively. The figures also include a comparison of the E* values at unaged condition. The figure can be used for general comparison of the mixtures, but specific temperature-frequency combination values need to be evaluated separately. That is, one can not compare direct values on the vertical axis for a specific log reduced time values. Generally, the E* values decreased with increase in temperature for all the mixtures at different aging conditions. Core aged (5 and 14

day aged) samples exhibited highest E* values than the unaged mixtures at all temperatures and frequencies as observed in FIGURE 15.

On the other hand, an increase in aging duration decreased dynamic moduli for pan aged mixtures at all temperatures as illustrated in FIGURE 15 (b). This could have been due to harshness in the mix aging process in a loose state. Air was circulated thoroughly throughout the mix, leading to an increased rate of oxidization. Also, during the aging process with a loose mix (pan aging), the individual aggregates are coated with an oxidized binder whereas the samples aged in a compacted state (core aged) would not necessarily experience significant oxidation between the aggregates, illustrated in FIGURE 14. Essentially, aging in a loose mix vastly reduced the effects of the binder on the dynamic modulus of the mixture, leaving only the aggregate interlock to govern the stiffness of the mix.

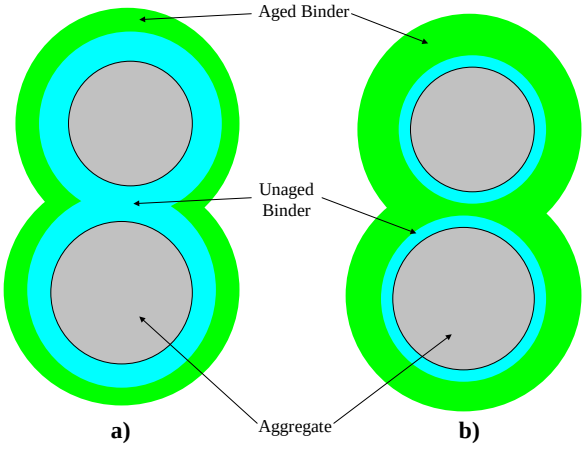

FIGURE 14. Schematic of Binder Coating on Aggregates at (a) Core (b) Pan Aged Conditions

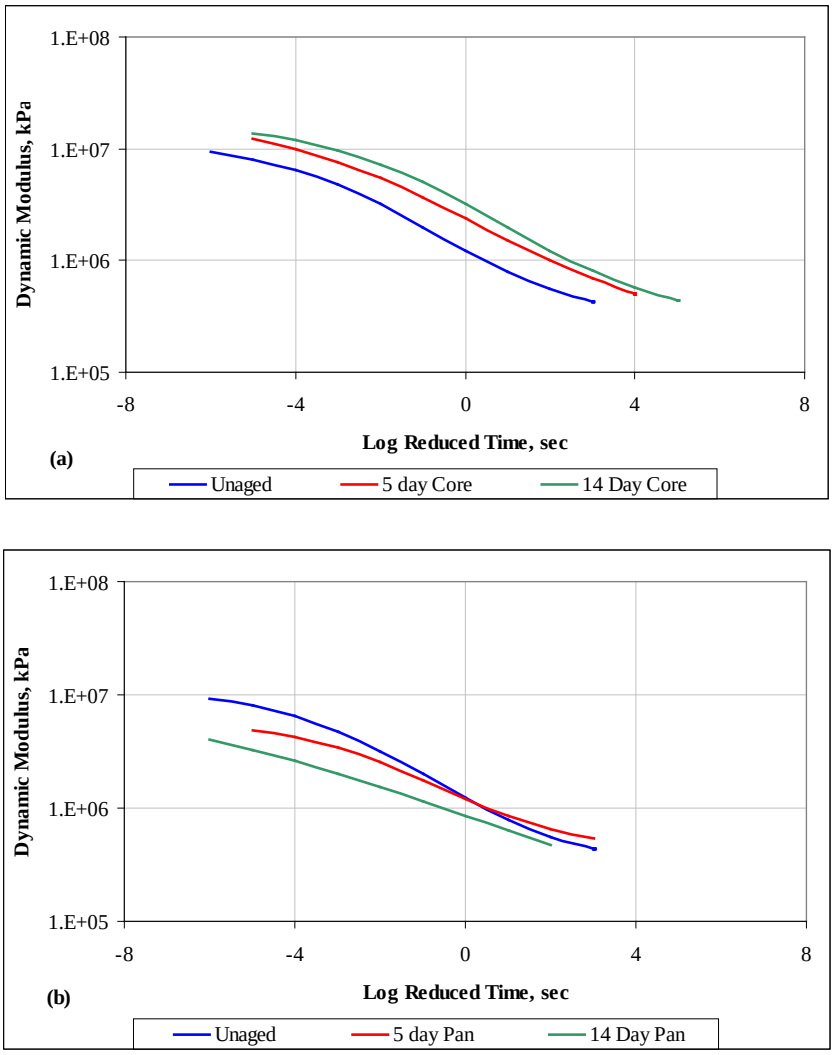

FIGURE 15. Dynamic Modulus Master Curves for ARFC Mixtures at (a) Core Aged (b) Pan Aged Condition

As mentioned previously, one of the objectives of this research study was to establish relationships between unaged and aged mixtures through the development of modular aging ratios. Modular aging ratio aids in understanding the effects of aging on the mixtures' stiffness (here E* dynamic moduli) with respect to stiffness of a control (unaged) mix. Modular aging ratio (MAR) is given by the following equation:

$$MAR = \frac{E^*_{AGED}}{E^*_{CONTROL}}$$

Where:

MAR = Modular Aging Ratio

E^*_{AGED} = E* Dynamic Modulus for the aged mixture

$E^*_{CONTROL}$ = E* Dynamic Modulus for the unaged mixture

MAR for core aged samples at both 5 and 14 day aging conditions were calculated for each E* test temperature and frequency. FIGURE 16 presents the relationship between temperature and MAR for each aging condition for ARFC mixture. As observed from the figure, MAR increased with increase in temperature. A higher MAR would indicate an increase in aging effects, especially at higher temperatures. One would desire to have a higher modulus value at high temperatures to avoid rutting, and at the same time, a lower modulus value at low temperatures to counter cracking potential. Along with an increase in E* values at all temperatures for different aging durations, a greater increase in MAR also was observed at higher temperatures relative to lower temperatures. This is indicative of mixture's significant resistance to rutting. An increase in MAR (about 30-50%) at low temperatures indicates the stiffening of the mixture due to aging. Nevertheless, with limited data and analyses undertaken in this study, one may expect a considerable significant decrease in thermal cracking resistance of ARFC mixtures with aging. Note that the sensitivity of the change in MAR continues to change as temperature increases.

TABLE 9. Average Dynamic Modulus and MAR Values for ARFC, Core Aged

Temperature, °C	E*, kPa			MAR	
	Original	5-Day	14-Day	5-Day	14-Day
-10	8,505,827	11,071,965	13,075,678	1.30	1.54
4.4	4,438,446	6,957,951	9,154,107	1.57	2.06
21.1	2,271,685	3,763,269	4,640,133	1.66	2.04
37.8	1,025,256	1,749,730	2,572,966	1.71	2.51
54.4	938,985	1,035,582	1,093,290	1.10	1.16

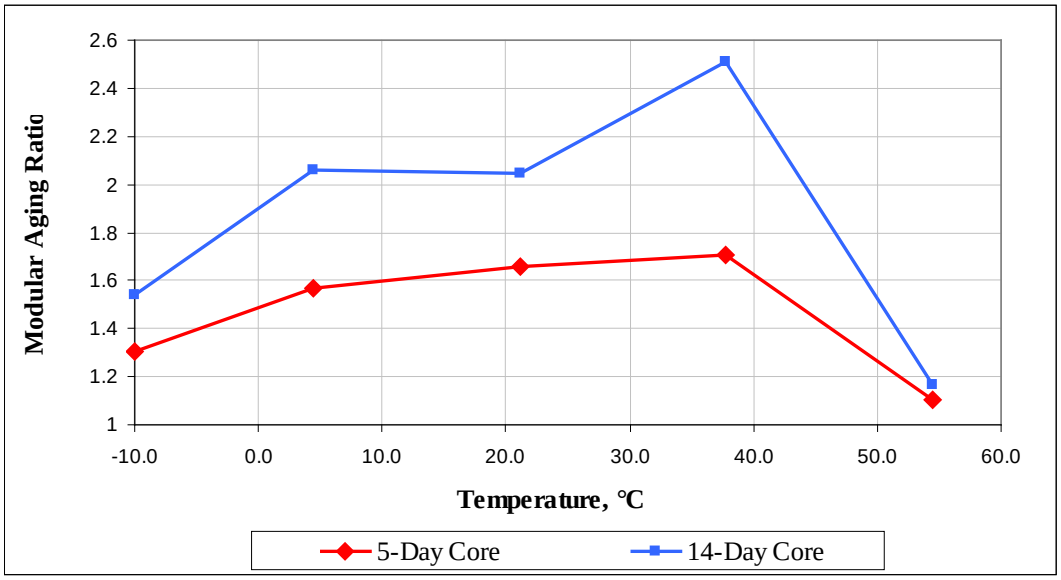

FIGURE 16. Modular Aging Ratio for ARFC, Core Aged

Testing on the ARAC mixture indicated that minor though significant aging occurred over seven years of storage. Compaction effort did not seem to indicate any aging occurred, though subsequent analysis of air content and dynamic modulus results indicate that enough aging occurred as to make the stored material no longer representative of the original mix. Compaction

parameters, such as the mass of mix compacted and the final specimen dimensions, were the same as used with the original ARAC. Compared to the historic data, the number of gyrations required for compaction was statistically identical for the stored mixture, shown in TABLE 10. Shear stress, another indicator of compaction effort, was likewise identical. However, a comparison of air voids noticed a minor increase in the long term storage samples. It is interesting to note that the increase in air voids also occurred in the accelerated laboratory aging, supporting the theory that oxidative aging causes AR binders to contract. Also note that %AV was taken after the specimens had been cut into suitable dimensions for dynamic modulus.

TABLE 10. Comparison of Compaction Effort and Air Voids

Aging Condition	Gyrations	Shear Stress, Kpa	A.V., %
Original (40 Samples)	87.20	550	5.5
Long Term Storage			
JA601	90	550	6.11
JA602	86	550	6.21
JA603	81	550	6.03
JA604	106	550	6.29
Average	90.75	550	6.20
P-Statistic	0.29		
T-Statistic	-0.61		
T Critical	2.13		

Once the gyratory compaction was completed and the plugs cut into E* dynamic modulus samples, dynamic modulus testing was performed for the full range of temperatures and loading frequencies. During testing, it was found that

the specimens exceeded maximum permanent deformation at the 130°C test temperature, so these results were thrown out. From the remaining results, master curves and MAR values were generated, displayed in FIGURE 17 and FIGURE 18.

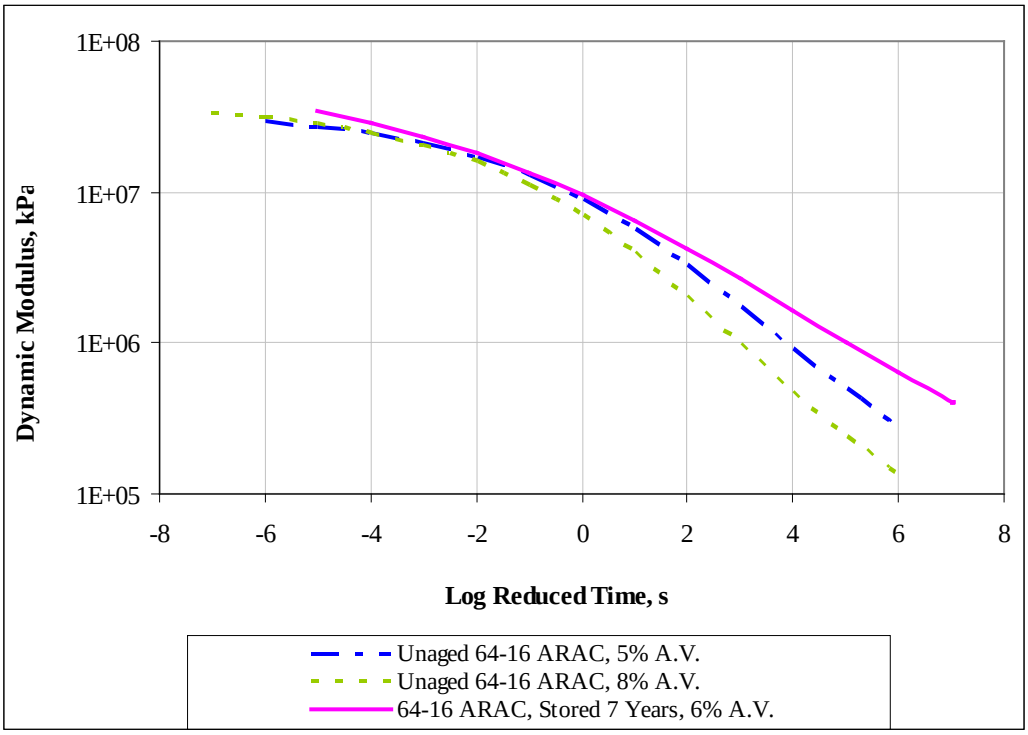

FIGURE 17. Comparison of Master Curves Between Unaged and Storage Aged 64-16 ARAC

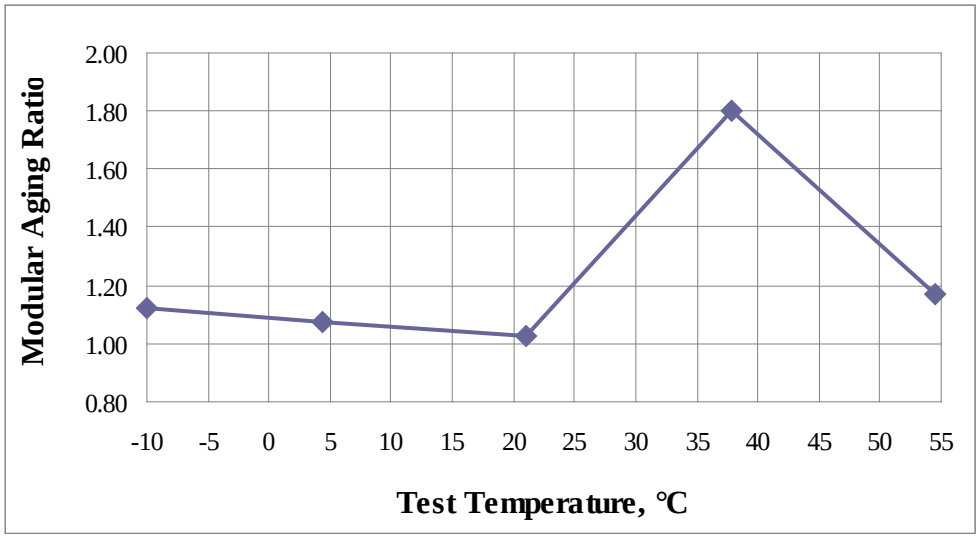

FIGURE 18. MAR of 64-16 ARAC After 7 Years of Storage

TABLE 11. MAR Results, 64-16 ARAC After 7 Years of Storage

Temperature, °C	Original	Storage Aged	
	|E*|, ksi	|E*|, ksi	MAR
-10.0	3767	4238	1.13
4.4	2557	2740	1.07
21.1	1494	1530	1.02
37.8	349	628	1.80
54.4	103	121	1.17

Dynamic modulus was similar or greater throughout the test temperatures, which is consistent with the results for core aged asphalt rubber specimens from the previous study. This indicates that the oxidative aging in this does not penetrate sufficiently into the binder as to cause it to behave as the pan aged mix, despite both being essentially aged in a loose state. Also, the MAR profile is fairly consistent as well, with the greatest differences in modular aging ratios occurring as test temperatures are increased. However, at very cold temperatures MAR is higher than at moderate temperatures, indicating that the effects are more

pronounced in such situations. While having a higher modulus at high temperatures is actually a benefit that decreases susceptibility to permanent deformation, the increased modulus at lower temperatures indicates a decreased resistance to thermal cracking.

E* Field Results

Dynamic modulus testing on the PG 64-16 and PG 58-22 ARAC field samples revealed that the aging patterns in the field are consistent with what was found in the accelerated laboratory aging of pavement cores as well as the aging occurring during long term storage. Dynamic modulus values for both mixes increased relative to the original values, with MAR values once again showing the greatest increase at higher test temperatures. In addition to comparing the results to the original test data, MAR values were compared to those generated through accelerated laboratory aging of the original mixtures. Using these MAR values, it is possible to correlate the age of a pavement to the amount of time a sample is subjected to the core aging method. This allows for the creation of laboratory aged specimens that are representative of a future pavement condition.

FIGURE 19, below, shows the MAR values for the field cores extracted from the test section. The MAR curves exhibit a peak at the 37.8°C test temperature while remaining relatively stable at the lower temperatures and exhibiting a reduction in MAR at 54.4°C. This pattern was typical of many ARAC mixes tested as part of this project. Also interesting to note is that MAR values are significantly higher for the samples made with 58-22 binder. A greater

MAR value indicates a higher level of oxidative aging, possibly stemming from the air voids of the section or the amount of lighter oils in the asphalt. This binder is also softer than the binder used in the other test section, which may influence the rate of aging in the field.

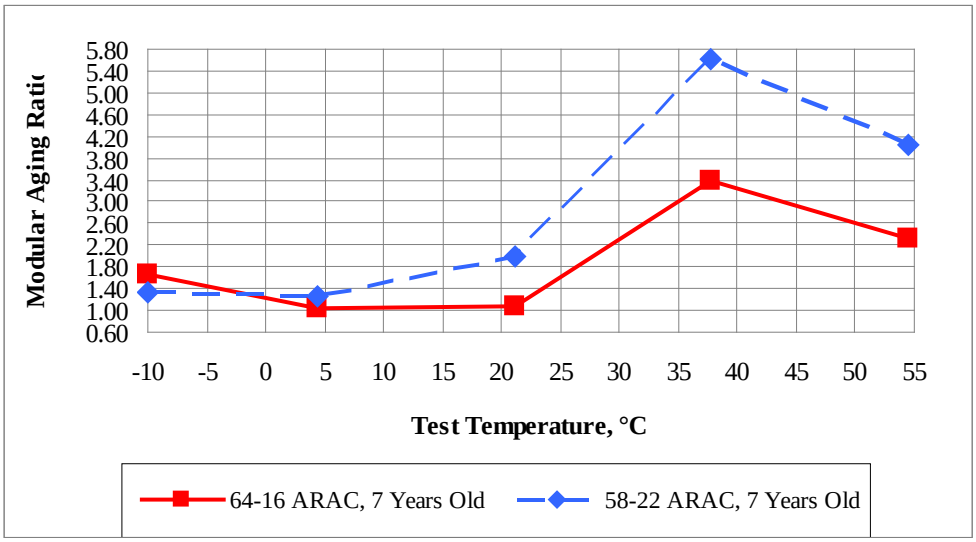

FIGURE 19. Comparison of MAR Values of Field Samples

TABLE 12. Dynamic Modulus and MAR Values of Field Samples

Temp, °C	Virgin 64-16 ARAC	64-16 ARAC, 7 Years		Virgin 58-22 ARAC	58-22 ARAC, 7 Years	
	|E*|, ksi	|E*|, ksi	MAR	|E*|, ksi	|E*|, ksi	MAR
-10.0	3767	6303	1.67	2968	3908	1.32
4.4	2557	2677	1.05	2032	2540	1.25
21.1	1494	1603	1.07	808	1605	1.99
37.8	349	1183	3.39	211	1182	5.61
54.4	103	240	2.32	64	259	4.03

Comparing the dynamic moduli of the field samples to those of some laboratory aged samples yielded some interesting results. Note that the lab aged

samples were prepared and tested as part of an older project and utilized the same original mix as the field samples. These laboratory aged specimens were wrapped in wire mesh and placed in a forced draft oven at 85°C for durations of 1, 4, 7, and 14 days.

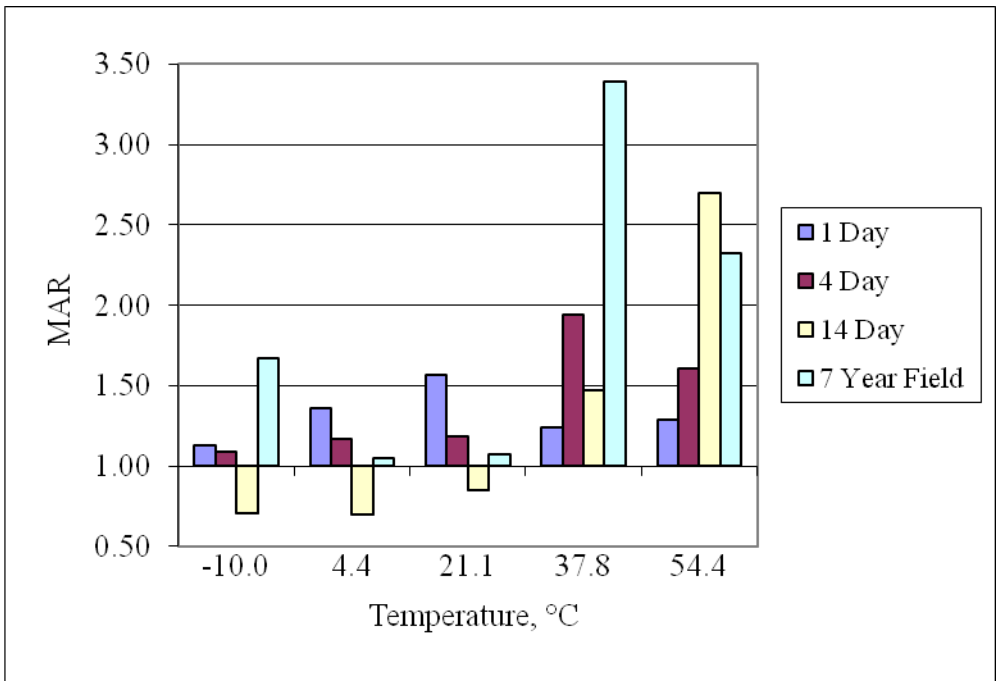

FIGURE 20. Comparison of MAR of Field Samples to Laboratory Aged Samples

TABLE 13. MAR of Field and Laboratory Aged Samples

Temp, °C	Original	1 Day Lab		4 Day Lab		7 Day Lab	
	|E*|, ksi	|E*|, ksi	MAR	|E*|, ksi	MAR	|E*|, ksi	MAR
-10.0	3767	4238	1.13	4115	1.09	4355	1.16
4.4	2557	3480	1.36	2988	1.17	3120	1.22
21.1	1494	2342	1.57	1768	1.18	2216	1.48
37.8	349	433	1.24	677	1.94	438	1.26
54.4	103	133	1.29	166	1.61	143	1.39

14 Day Lab		7 Year Field	
|E*|, ksi	MAR	|E*|, ksi	MAR
2652	0.70	6303	1.67
1781	0.70	2677	1.05
1267	0.85	1603	1.07
512	1.47	1183	3.39
279	2.70	240	2.32

There are several interesting trends seen in the laboratory aged samples seen above. First, none of the specimens exhibit the higher MAR at the lowest test temperature. The 1 day condition shows a flat MAR across the temperatures very close to 1.00, indicating minimal aging is occurring over the first day. The 4 day aging shows a similar pattern to the field aging with a peak at the 37.8°C temperature, although the MAR values are significantly lower overall. The 7 day aging condition is inconsistent with the other three conditions, mirroring the 1 day closely despite the steady increases seen in the 4 day and 14 day conditions. Finally, the 14 day condition shows a steadily increasing curve with no peak at 37.8°C. However, the lower temperature MAR values are below 1, indicating a

decrease in E* for these temperatures. This decrease is most likely due to degradation in the specimens similar to what occurred with the pan aging specimens during the initial laboratory aging study. Unfortunately, none of these laboratory aging conditions match those observed field when comparing E* and MAR. The closest match is the 4 day condition, though the questionable nature of the 7 day condition and the spread between 4 and 14 days. Additional testing conditions in this range would have allowed for increased resolution of the progression of aging in the HMA mixture and allowed for a better pinpointing of the laboratory aging time most indicative of the condition.

Beam Field Results

Test results for beam fatigue clearly indicate the effects of oxidative aging on the asphalt rubber field specimens. A comparison of initial stiffness conducted between laboratory specimens, 1 year field specimens, and 7 year field specimens shows an increase in initial stiffness as aging increases. More interesting, the initial stiffness is relatively insensitive to strain level in the laboratory and 1 year conditions, but the 7 year field condition shows a relatively extreme sensitivity in addition to a greater stiffness for all measured cases. This can be seen in TABLE 14 where the 7 year field samples have a much higher average initial stiffness and again in TABLE 15 where there is a high degree of sensitivity to of stiffness to the strain level. In effect, it shows that with aging the pavement has become far more brittle and thus more susceptible to damage resulting from large strains.

TABLE 14. Average Initial Stiffness

Aging Condition	Average Initial Stiffness, Mpa
Original	215
1 Year, Field	266
7 Years, Field	3958

TABLE 15. Initial Stiffness and Strain Level for 7 Year Field Specimens

Strain Level, Microstrain	Initial Stiffness, Mpa
300	4946
400	5270
500	3630
600	5175
700	2626
800	4036
1000	2021

Testing the field samples until failure indicated a loss of fatigue life when compared to the original mixture. The year field material in all tested cases failed at a lower strain level for a given number of test cycles. This is due to the loss of flexibility and increase in stiffness caused by aging and the loss of the lighter maltenes from the asphalt binder. Drawing a trend line through both sets of data, it is apparent that the number of cycles until failure for the aged material is less dependent on strain level as the virgin material, as indicated by the flatter slope of the trendline shown in FIGURE 21. Also worth noting is that there is a higher level of variability in the field samples. This is understandable due to the less

controlled aging and preparation of samples when compared to the laboratory manufactured specimens used to evaluate the virgin condition.

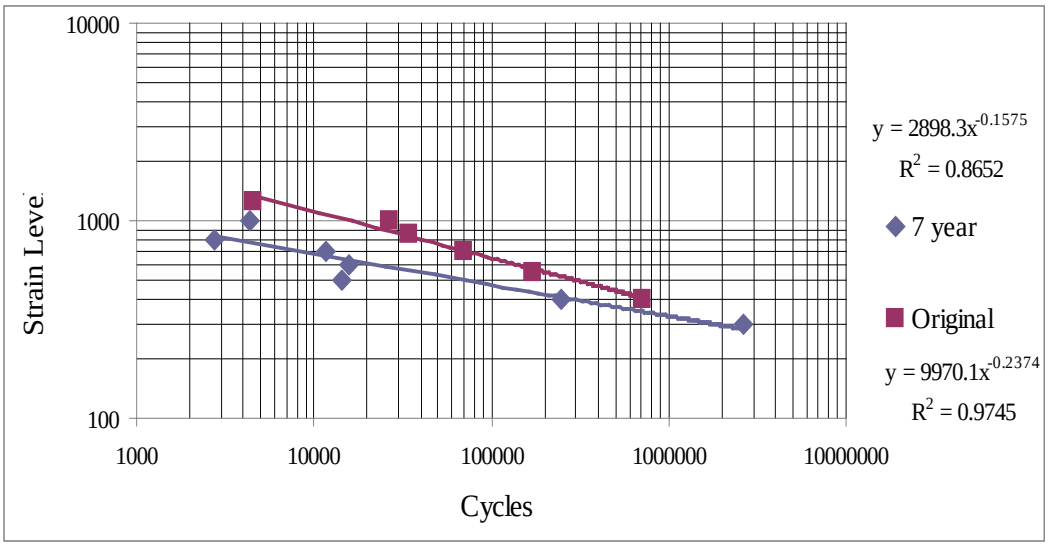

FIGURE 21. Fatigue Relationship Between Original and Field Samples

TABLE 16. Fatigue Data for Original and Field Samples

Source	Strain Level, Microstrain	Initial Stiffness, Mpa	Cycles at 50% Stiffness
Original	400	2148	704560
	550	2050	171960
	700	2386	70230
	850	2255	34700
	1000	2843	26530
	1250	2774	4580
7 Year Field	300	4946	2657320
	400	5270	248310
	500	3630	14410
	600	5175	15680
	700	2626	11560
	800	4036	2720
	1000	2021	4340

SUMMARY AND CONCLUSIONS

The three phases of the project yielded significant insight into the nature of aging in asphalt rubber pavements. The first phase consisted of comparing the viscosities of rubber modified and virgin binders at various aging conditions. The second phase consisted of aging an asphalt mixture utilizing two different aging procedures in order to determine the effectiveness of two different mixture aging procedures. In addition, aging effects on a stored mixture were evaluated. The final phase investigated the aging effects seen in the field. Samples were taken from the field and tested. These test results were then compared to those found for the original pavement mix. All the phases undertaken as part of this study yielded valuable insights as to the nature of asphalt rubber aging.

The binder testing showed several interesting behaviors of asphalt rubber binders. First, for both asphalt rubber and the virgin bases showed increasing ratios of unaged viscosity to aged viscosity with temperature. In addition, more intensive aging showed an increase in viscosity ratio. The AR binders showed a lesser increase in this viscosity ratio with temperature. For the softer 58-22 binders, the ratio for AR binders was similar to the virgin asphalt. For the 64-16 binders, asphalt rubber showed substantially less aging than the virgin bases. It is thought that this is a result of the proportion of aromatics and maltenes in the binders and the amount reacted with the rubber particles. As the amount of aromatics decreases, a larger proportion is saved in the rubber particles. This sequestering of the lighter fractions results in a lower rate of loss of these particles

and therefore causes the asphalt rubber binders to be more resistant to aging effects.

The various mixture aging processes tested in the laboratory indicated that the core aging process of a compacted specimen was superior to the pan aging of loose mix. The behavior observed in the loose mix indicated that the cohesion between aggregates had been negatively affected to a degree that was unrealistic for field aging. It is believed that the cause of this was the essentially uniform aging of asphalt around each aggregate particle while in the field and core aging process less aging occurs between aggregate particles.

Aging behavior in the core aged samples was characterized using the ratio between aged and unaged E* dynamic modulus values. This ratio was termed the modular aging ratio or MAR. MAR exhibits a pattern whereby the MAR value is low at lower temperatures and increases with temperature, eventually peaking at approximately 37.8°C and then exhibiting a downward trend. The cause of this downward trend is unknown but it is possibly due to lessening of the influence of asphalt binder at higher temperatures. This trend in the MAR value was also observed in nearly all other aged asphalt rubber specimens, indicating that the greatest effect of aging occurs at this critical temperature. Therefore, the best temperature to test at to measure aging is 37.8°C. It is unknown if it also occurs in conventional asphalt mixtures. Dimensional and air void information for the core aged specimens were taken before and after aging. Significant changes in air void content were observed while dimensional changes were miniscule. This

seems to indicate that the AR binder contracted as a result of aging, perhaps due to the loss of volatile elements stored in the asphalt rubber.

Samples taken from a test section were tested for dynamic modulus beam fatigue after being in service for approximately 7 years. Using data collected as part of an earlier study, the MAR values for dynamic modulus were calculated. Once again, a similar pattern in the MAR versus temperature curve was observed, with the MAR value peaking at around 37.8°C. This seems to indicate that the core aging process is a reasonable method for the aging of asphalt mixtures. MAR values were higher for the 58-22 mixture, most likely due to the larger proportions of maltenes in the binder resulting in a greater percentile loss of those lighter fractions. This is consistent with the observations in the binder analysis. Beam fatigue testing indicated that the aged asphalt rubber pavement was significantly stiffer after field aging, but that it also exhibited decreased fatigue life as well. The reduced fatigue life makes sense, as an increased stiffness would result in more cracking along with reduced healing in the beams.

The earlier study on the I-17 test section mixes used aging procedures identical to the core aging method on the new mix. It was hoped that the data from this study could be analyzed and compared to the MAR values obtained from the field. Unfortunately, there were too few data to form a correlation and too little resolution between 5 and 14 days. The MAR pattern observed for all other portions of the aging study was not readily apparent in this early study. However, there is a slight peaking in some curves indicating that the trend might

be forming in the MAR curves for 4 and 5 days of aging. The single data point for 7 days of aging does not fall into this pattern, but it does not follow the trend of the other aging conditions performed as part of this study and is thus a likely outlier. The next aging condition is 14 days and while it does not follow the pattern observed earlier this could be the result of substantial aging resulting in damage to the samples. In addition, stored original mix was evaluated and found to have aged significantly despite being contained in a bucket for 7 years. Aging conforming to the typical MAR pattern was observed, indicating that the mix was no longer representative of its original state.

Overall, the asphalt rubber binder appears to have performed in a superior manner in regards to aging than its virgin base. This effect is most apparent in the stiffer 64-16 binder. It is assumed that this is a result of a higher proportion of the maltenes in the asphalt reacting with and becoming stored by the rubber. Storage of the lighter fractions also seems to be indicated in the volumetric changes observed in the core aging of compacted mixtures. The observed modular aging ratio of asphalt rubber appears to follow a well defined pattern where MAR is low at lower temperatures but becomes more apparent at higher temperatures due to the reduced temperature susceptibility and increased stiffening of the material post-aging. Similar MAR patterns were observed in the core aged, storage aged, and field aged asphalt rubber HMA. This indicates that the core aging method is likely an effective procedure for rapidly inducing aging effects in lab samples indicative of the aging that would occur in the field. The peak MAR occurs at

37.8°C and therefore this temperature is the best to test at in order to gauge aging. Stiffening was also observed in the beam fatigue tests, though the stiffening also resulted in a lowered fatigue life.

RECOMMENDATIONS FOR FUTURE RESEARCH

The results obtained from this project provided a wealth of useful insights and observations as to the nature of aging in asphalt rubber specimens. An observable trend in the MAR curve has been identified, but the exact specifics as to the rate at which the MAR forms have not. A broader range of testing periods and mixtures would allow for a better understanding of how asphalt rubber pavements age. It is essential that spacing between different temperatures is fairly consistent in order to provide the resolution necessary in order to clearly identify the rate at which the established MAR pattern forms. A larger number of mixtures will verify that the pattern occurs in all asphalt rubber mixtures. Additional aging temperatures will allow for an ideal temperature to be found, improving the accuracy of laboratory aging. Similar testing on conventional mixtures should be performed to evaluate if asphalt rubber pavements perform better when aged.

The development of effective laboratory aging procedures has the potential to better indicate the long term performance of an HMA mixture. However, the establishment of additional test sections will be necessary in order to accurately relate laboratory aging to field aging. In the absence of additional test sections, similar mixes to those in the field could be made, aged, and tested before being compared to tested field cores.

The mechanics of how crumb rubber reacts with asphalt, specifically the lighter fractions, is not well understood. Isolating the reacted rubber and then

exposing this rubber gel to aging while evaluating its volumetric properties would not only verify the capacity of the crumb rubber to act as a reservoir for maltenes, but also provide insight into how these maltenes are then released back into the binder. An alternative would be to age virgin and asphalt rubber binders and compare the mass loss that occurs as a result.

REFERENCES

AASHTO Designation T-49-07. Standard Method of Test for Penetration of Bituminous Materials, 2007

AASHTO Designation T-240-09. Effect of Heat and Air on a Moving Film of Asphalt Binder (Rolling Thin-Film Oven Test), 2009

AASHTO Designation T-316-06. Standard Method of Test for Viscosity Determination of Asphalt Binder Using Rotational Viscometer, 2006

AASHTO Designation TP-8-94. Determining the Fatigue Life of Compacted Hot-Mix Asphalt (HMA) Subjected to Repeated Flexural Bending, 1994

AASHTO Designation TP-64-07. Standard Method of Test for Determining Dynamic Modulus of Hot-Mix Asphalt (HMA), 2007

Airey, G. D., *State of the Art Report on the Ageing Test Methods for Bituminous Pavement Materials*, The International Journal of Pavement Engineering, Vol. 4, 2003

Chipps, G. D., Davison, R., and Glover, C., *A Model for Oxidative Aging of Rubber-Modified Asphalts and Implications to Performance Analysis*, Energy & Fuels, Vol. 15, 2001

Jung, Sung Hoon, *The Effects of Asphalt Binder Oxidation on Hot Mix Asphalt Concrete Mixture Rheology and Fatigue Performance*, Texas A&M University, 2006

Kaloush, K.E., Witczak, M.W., Way, G.B., Zborowski, A., Abojaradeh, M., Sotil, A., *Performance Evaluation of Arizona Asphalt Rubber Mixes Using Advanced Dynamic Material Characterization Tests*, Final Report, Arizona State University, 2002

Kaloush, K.E., Zborowski, A., Sotil, A., Way, G.B., *Material Characteristics of Asphalt Rubber Mixtures*, Proceedings of the Asphalt Rubber 2003 Conference, p.129-145, December 2003

Lee, Soon-Jae, *Characterization of Recycled Aged CRM Binders*, Clemson University, 2007

Othman, Ayman M., *Fracture Resistance of Rubber-Modified Asphaltic Mixes Exposed to High-Temperature Cyclic Aging*, Journal of Elastomers and Plastics, Volume 38, January 2006

Raghavendra, S., Zapata, C., Mirza, M., Houston, W., Witczak, M., *Verification of the Rate of Asphalt Mix Aging Simulated by AASHTO PP2-99 Protocol*, Transportation Research Board Annual Meeting, 2006

SHRP 1994, Accellerated Performance-Related Tests for Asphlat-Aggregate Mixes and Their Use in Mix Design and Analysis Systems, Report No. SHRP-A-417, Strategic Highway Research Program, National Research Council, Washington DC., 1994

Saboudjian, S., Minassian, G., Raad, L., "Field Aging Effects on Fatigue of Asphalt Concrete and Asphalt-Rubber Concrete", *Transportation Research Record*, Issue 1767, Transportation Research Board, 2001

Sotil, A., *Material Characterization of Asphalt Rubber Mixtures Using the Dynamic Modulus Test*, Arizona State University, 2003

Walubita, Lubinda F., *Comparison of Fatigue Analysis Approaches for Predicting Fatigue Lives of Hot-Mix Asphalt Concrete (HMAC) Mixtures*, Texas A&M University, 2006

Witczak, M.W., Bonaquist, R., Von Quintus, H., and Kaloush, K., *Specimen Geometry and Aggregate Size Effects in Uniaxial Compression and Constant Height Shear Tests*, Journal of the Association of Asphalt Paving, Vol. 69, 2000

Witczak, M.W. and Mirza, M.W., *Development of a Global Aging System for Short and Long Term Aging of Asphalt Cements*, Journal of the Association of the Asphalt Paving Technologists, Vol. 64, 1995

APPENDIX A

BINDER RESULTS

I-40 58-22 Original Virgin						
Temp. °C	Temp. °R	Log Temp. °R	Penetration .1mm	Viscosity cP	Log Log Visc. cP	Test
15	518.67	2.715	34.2	1.105E+09	0.956	Penetration
25	536.67	2.730	112.2	7.662E+07	0.897	Penetration
47	576.27	2.761		1.300E+06	0.786	Soft. Point
60	599.67	2.778		82000	0.691	Brookfield
80	635.67	2.803		9412.5	0.599	Brookfield
100	671.67	2.827		2250	0.525	Brookfield
122	711.27	2.852		587.5	0.442	Brookfield
135	734.67	2.866		287.5	0.391	Brookfield
177	810.27	2.909		62.5	0.254	Brookfield

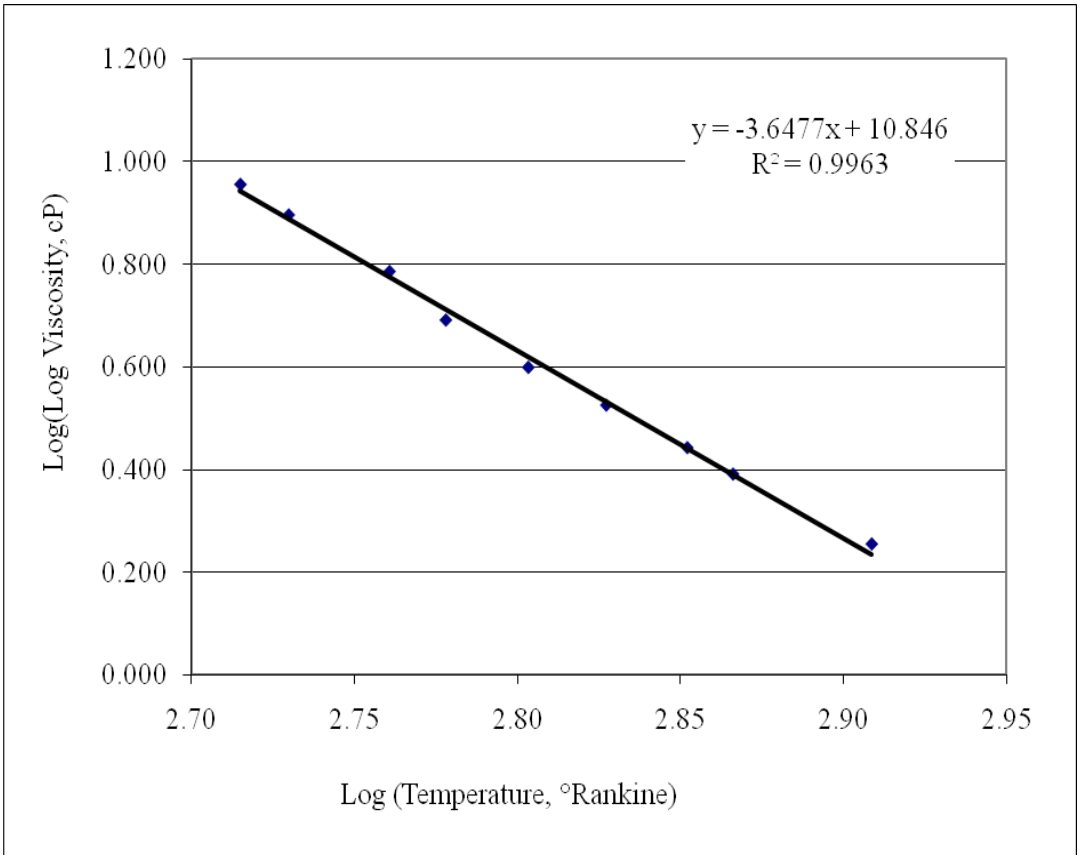

I-40 58-22 RTFO Virgin						
Temp. °C	Temp. °R	Log Temp. °R	Penetration .1mm	Viscosity cP	Log Log Visc. cP	Test
15	518.67	2.715	21.8	3.042E+09	0.977	Penetration
25	536.67	2.730	66.2	2.505E+08	0.924	Penetration
51	583.47	2.766		1.300E+06	0.786	Soft. Point
60	599.67	2.778		175750	0.720	Brookfield
80	635.67	2.803		17142	0.627	Brookfield
100	671.67	2.827		4588	0.564	Brookfield
122	711.27	2.852		1013	0.478	Brookfield
135	734.67	2.866		450	0.424	Brookfield
177	810.27	2.909		75	0.273	Brookfield

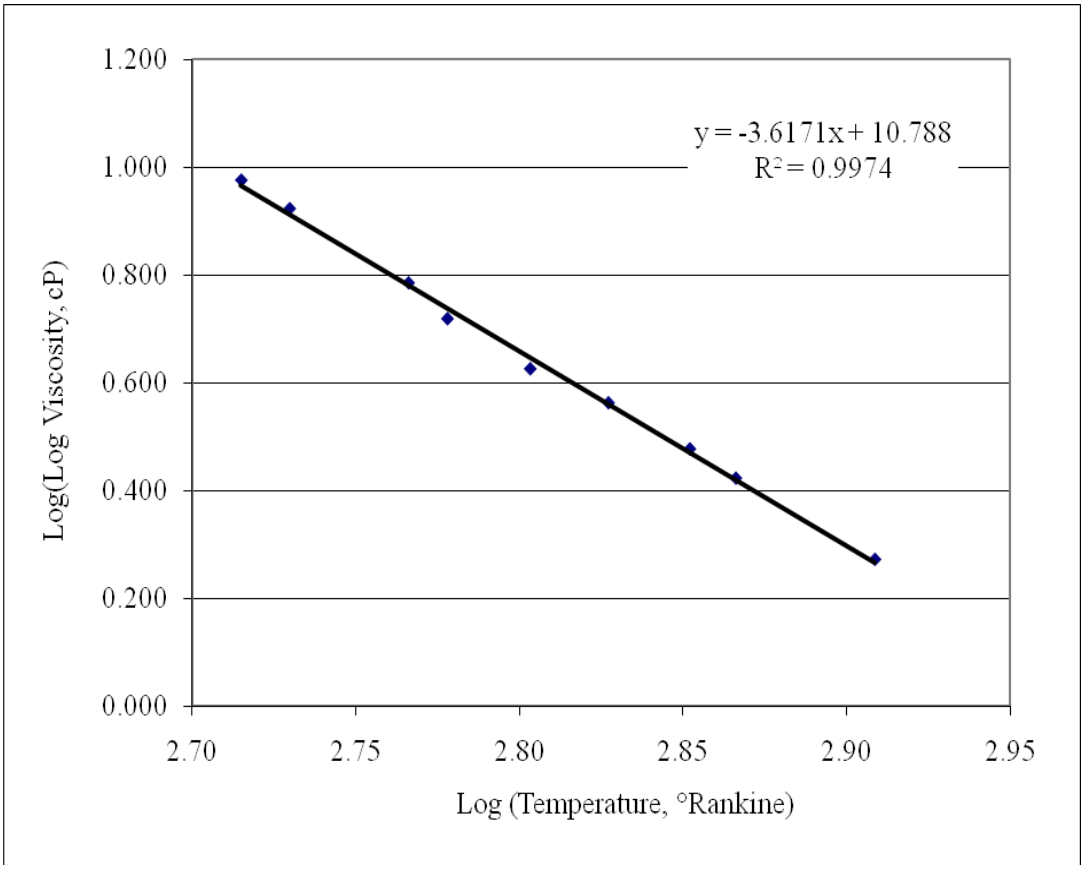

I-40 58-22 PAV Virgin						
Temp. °C	Temp. °R	Log Temp. °R	Penetration .1mm	Viscosity cP	Log Log Visc. cP	Test
15	518.67	2.715	10.2	1.681E+10	1.010	Penetration
25	536.67	2.730	30.0	1.483E+09	0.962	Penetration
58	596.07	2.775		1.300E+06	0.786	Soft. Point
60	599.67	2.778		285933	0.737	Brookfield
80	635.67	2.803		79000	0.690	Brookfield
100	671.67	2.827		10854	0.606	Brookfield
122	711.27	2.852		2098	0.521	Brookfield
135	734.67	2.866		923	0.472	Brookfield
177	810.27	2.909		103	0.304	Brookfield

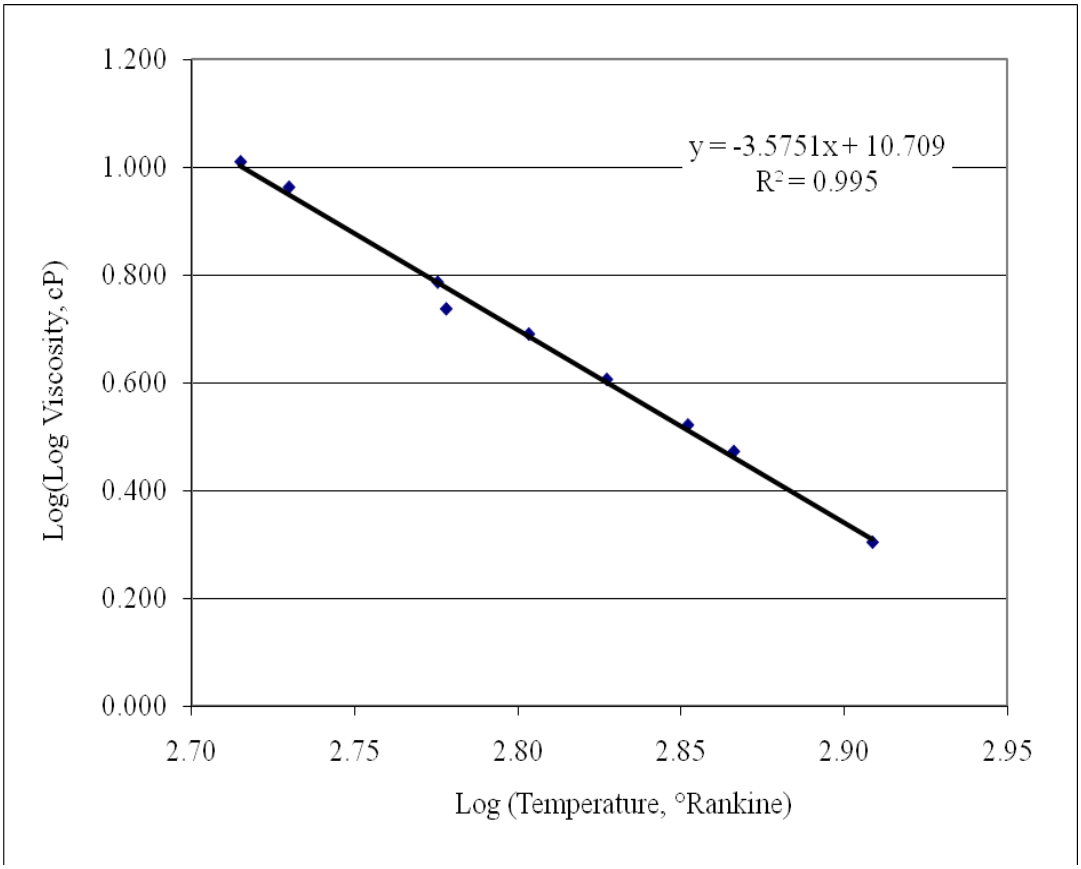

I-40 58-22 Original AR						
Temp. °C	Temp. °R	Log Temp. °R	Penetration .1mm	Viscosity cP	Log Log Visc. cP	Test
15	518.67	2.715	28.7	1.639E+09	0.964	Penetration
25	536.67	2.730	46.7	5.486E+08	0.941	Penetration
59.5	598.77	2.777		1.300E+06	0.786	Soft. Point
100	671.67	2.827		47000	0.670	Brookfield
121.1	709.65	2.851		10500	0.604	Brookfield
135	734.67	2.866		5600	0.574	Brookfield
176.7	809.73	2.908		1700	0.509	Brookfield

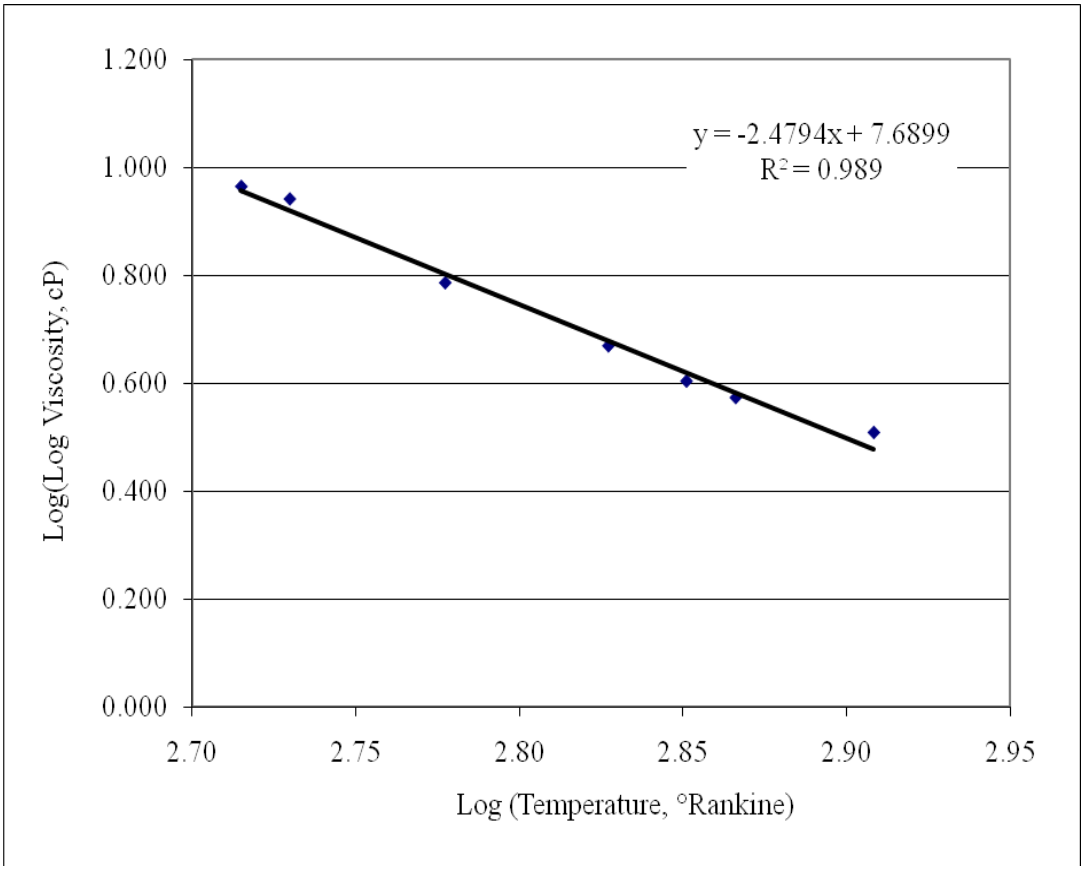

I-40 58-22 RTFO AR						
Temp. °C	Temp. °R	Log Temp. °R	Penetration .1mm	Viscosity cP	Log Log Visc. cP	Test
15	518.67	2.715	11.7	1.234E+10	1.004	Penetration
25	536.67	2.730	30.3	1.451E+09	0.962	Penetration
79.5	634.77	2.803		1.300E+06	0.786	Soft. Point
100	671.67	2.827		2267000	0.803	Brookfield
121.1	709.65	2.851		44250	0.667	Brookfield
135	734.67	2.866		18833	0.631	Brookfield
176.7	809.73	2.908		4333	0.561	Brookfield

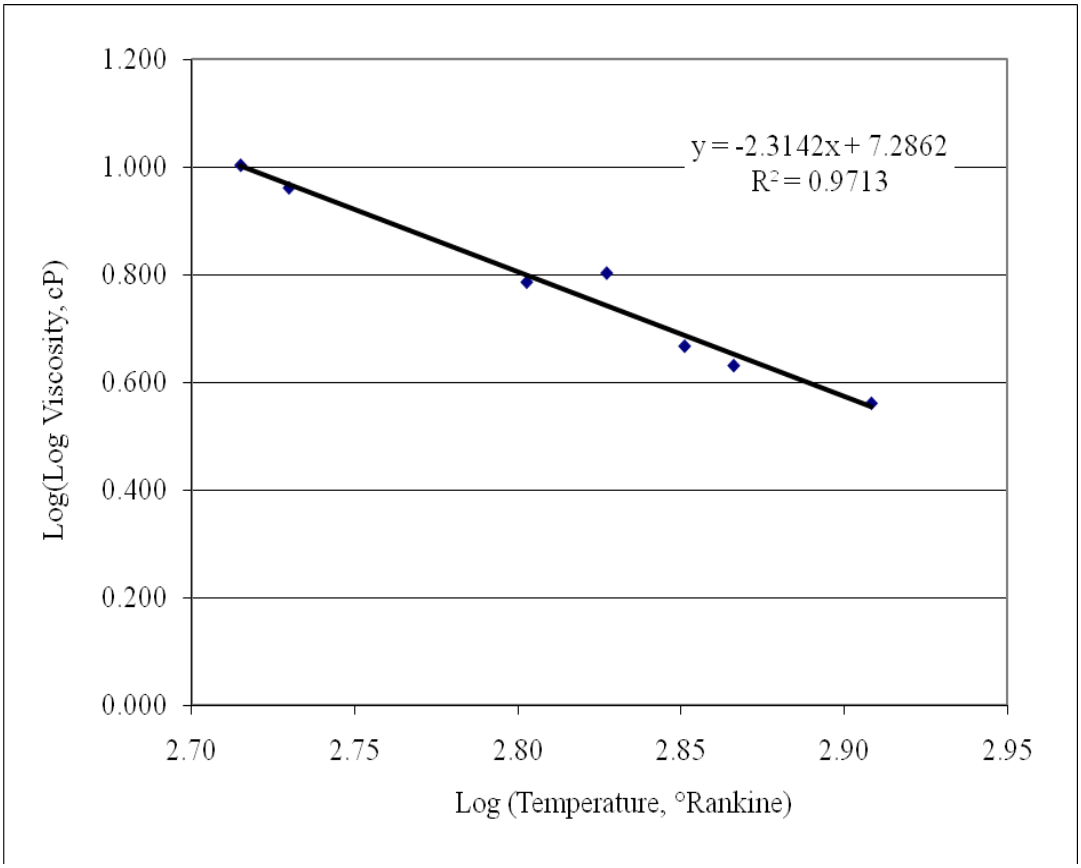

I-40 58-22 PAV AR						
Temp. °C	Temp. °R	Log Temp. °R	Penetration .1mm	Viscosity cP	Log Log Visc. cP	Test
15	518.67	2.715	7.3	3.539E+10	1.023	Penetration
25	536.67	2.730	14.3	7.819E+09	0.995	Penetration
99.75	671.22	2.827		1.300E+06	0.786	Soft. Point
100	671.67	2.827		302000	0.739	Brookfield
121.1	709.65	2.851		235000	0.730	Brookfield
135	734.67	2.866		78000	0.689	Brookfield
150	761.67	2.882		29000	0.650	Brookfield
176.7	809.73	2.908		6900	0.584	Brookfield

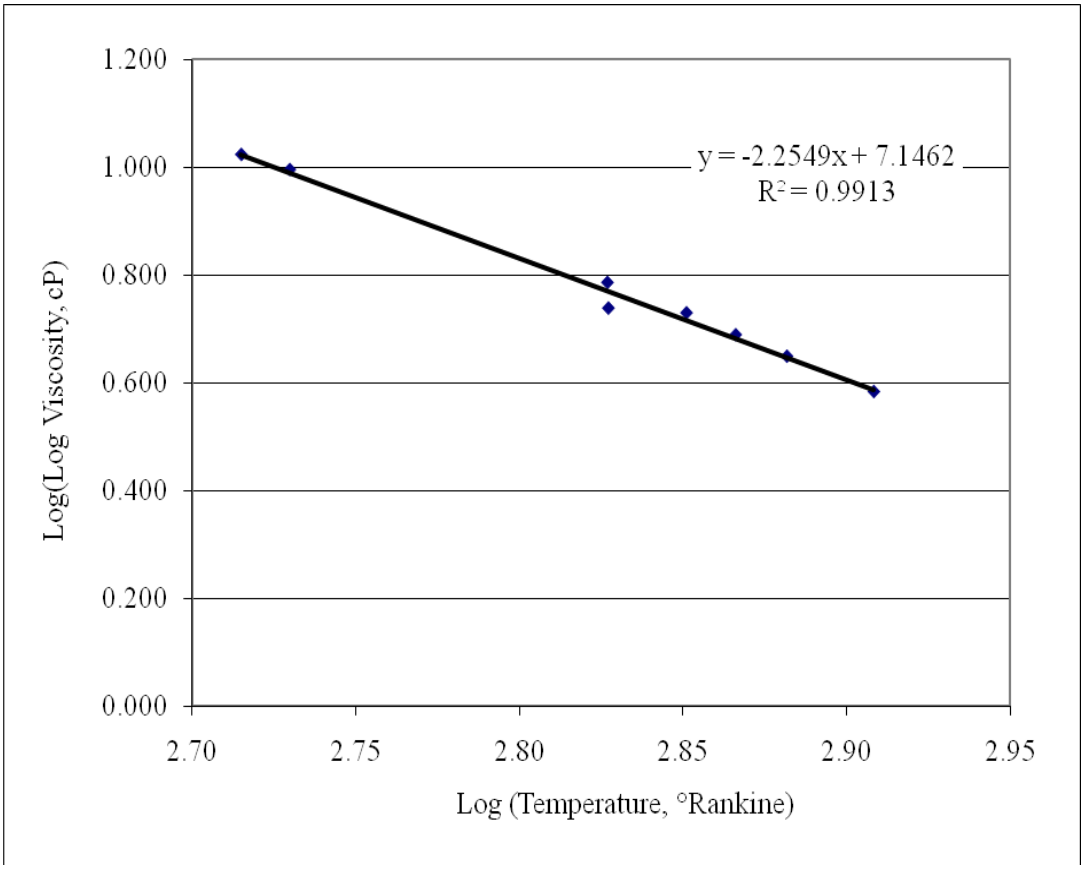

I-17 58-22 Original Virgin						
Temp. °C	Temp. °R	Log Temp. °R	Penetration .1mm	Viscosity cP	Log Log Visc. cP	Test
15	518.67	2.715	22.0	2.980E+09	0.977	Penetration
25	536.67	2.730	104.5	8.988E+07	0.901	Penetration
46	574.47	2.759		1.300E+06	0.786	Soft. Point
60	599.67	2.778		69000	0.685	Brookfield
80	635.67	2.803		8400	0.594	Brookfield
100	671.67	2.827		1700	0.509	Brookfield
121.1	709.65	2.851		450	0.424	Brookfield
135	734.67	2.866		205	0.364	Brookfield
176.7	809.73	2.908		50	0.230	Brookfield

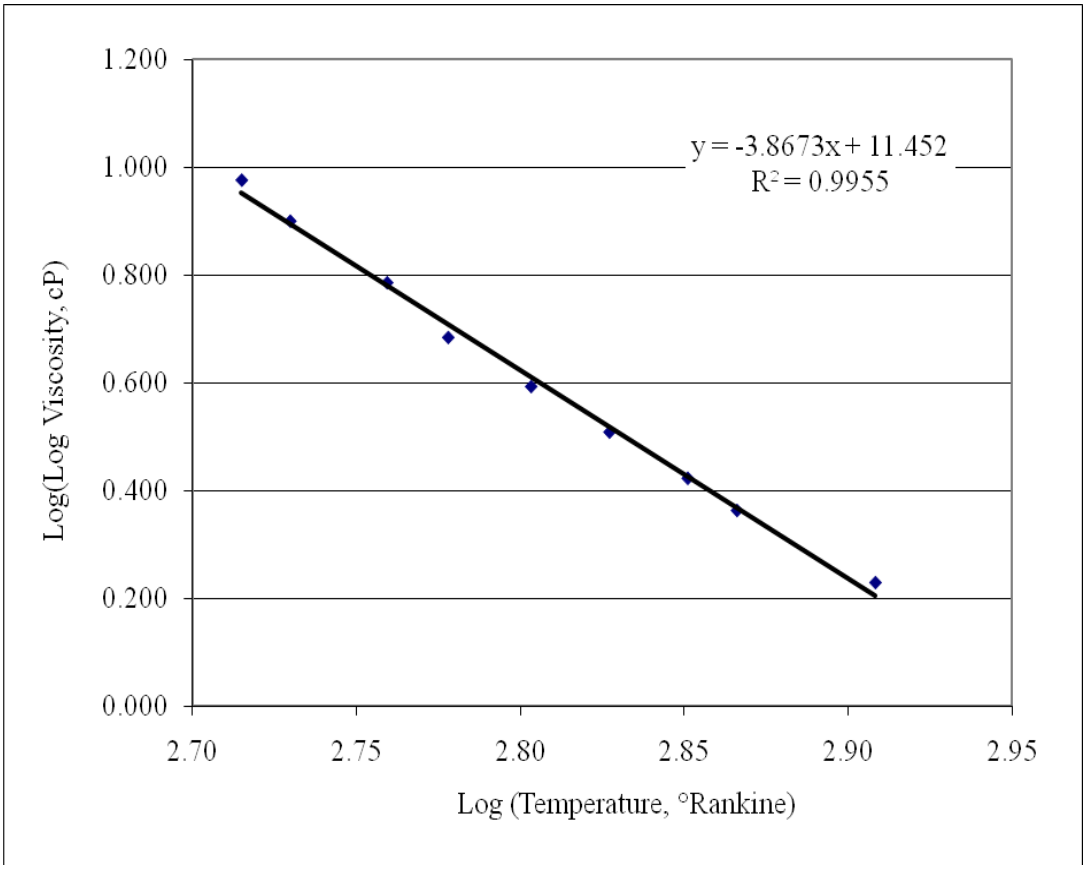

I-17 58-22 RTFO Virgin						
Temp. °C	Temp. °R	Log Temp. °R	Penetration .1mm	Viscosity cP	Log Log Visc. cP	Test
15	518.67	2.715	20.0	3.693E+09	0.981	Penetration
25	536.67	2.730	48.6	5.015E+08	0.940	Penetration
52	585.27	2.767		1.300E+06	0.786	Soft. Point
60	599.67	2.778		130000	0.709	Brookfield
80	635.67	2.803		12700	0.613	Brookfield
100	671.67	2.827		2300	0.527	Brookfield
121.1	709.65	2.851		700	0.454	Brookfield
135	734.67	2.866		306	0.395	Brookfield
176.7	809.73	2.908		62.5	0.254	Brookfield

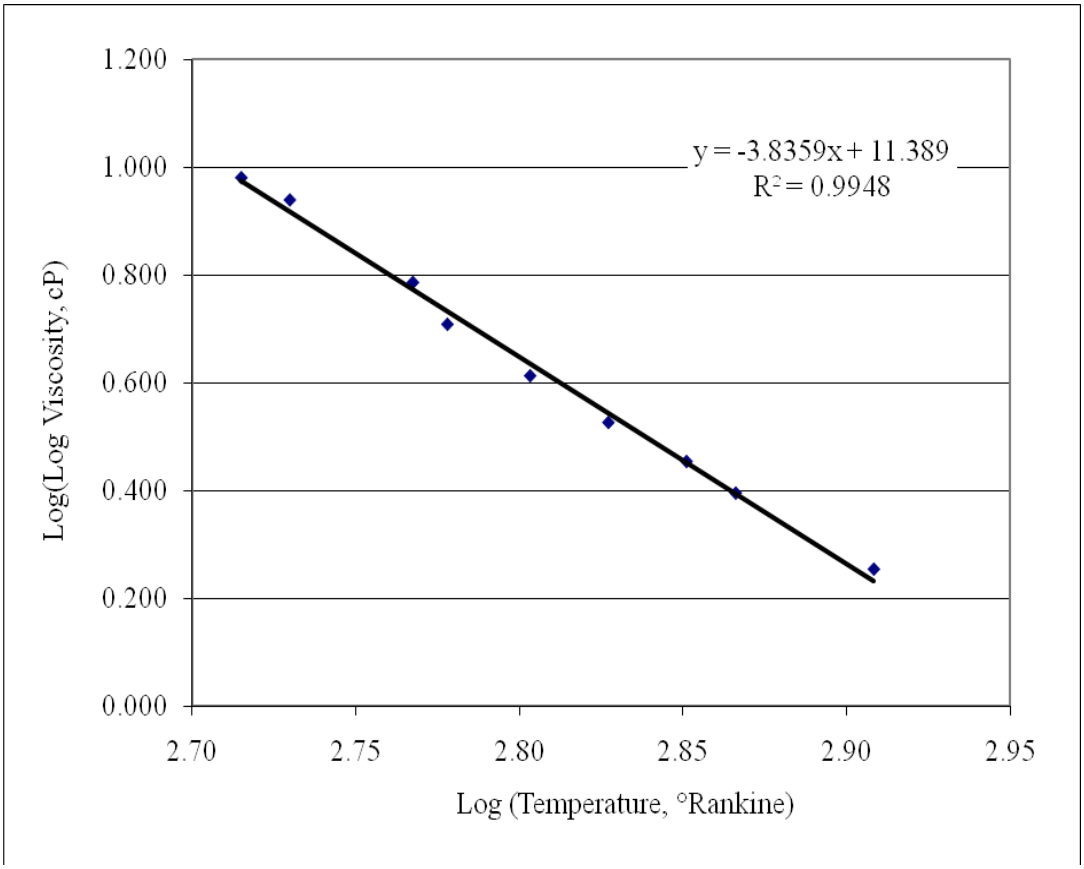

I-17 58-22 PAV Virgin						
Temp. °C	Temp. °R	Log Temp. °R	Penetration .1mm	Viscosity cP	Log Log Visc. cP	Test
15	518.67	2.715	9.7	1.883E+10	1.012	Penetration
25	536.67	2.730	23.0	2.696E+09	0.975	Penetration
60	599.67	2.778		1.300E+06	0.786	Soft. Point
60	599.67	2.778		5000000	0.826	Brookfield
80	635.67	2.803		27150	0.647	Brookfield
100	671.67	2.827		3850	0.555	Brookfield
121.1	709.65	2.851		890	0.470	Brookfield
135	734.67	2.866		405	0.416	Brookfield
176.7	809.73	2.908		75	0.273	Brookfield

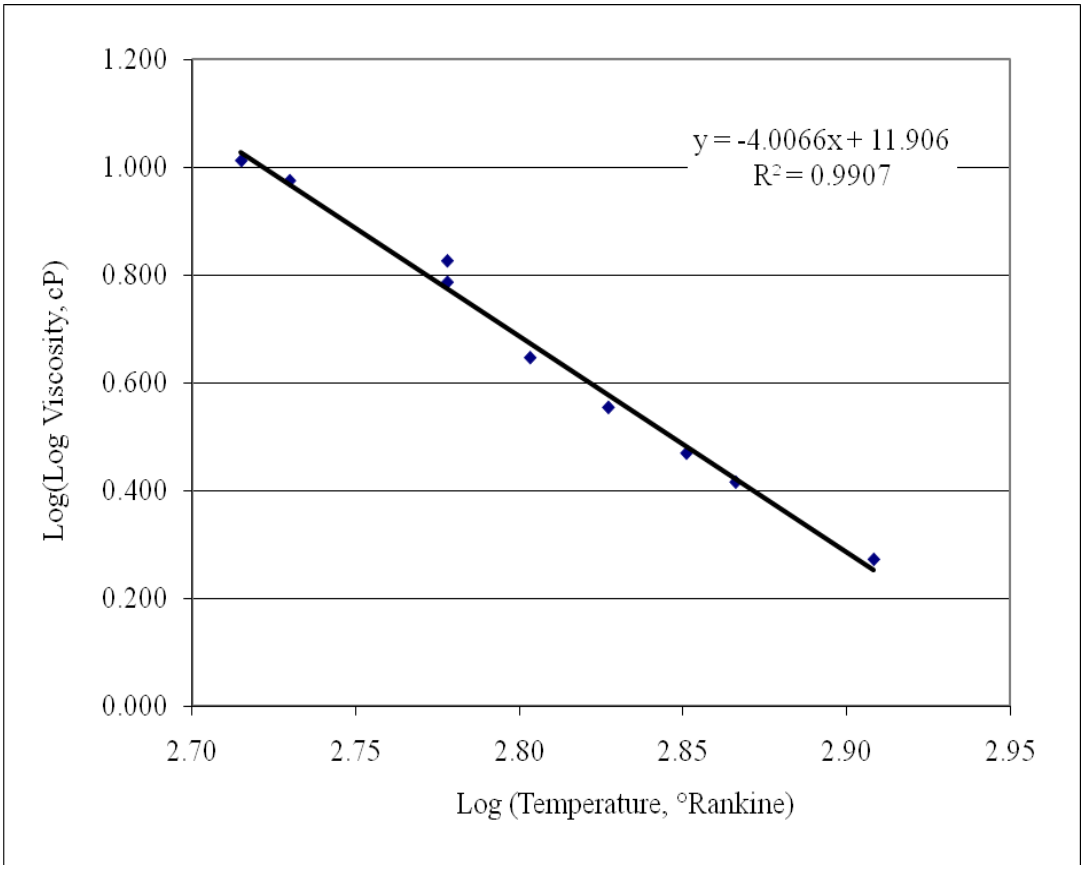

I-17 58-22 Original AR						
Temp. °C	Temp. °R	Log Temp. °R	Penetration .1mm	Viscosity cP	Log Log Visc. cP	Test
15	518.67	2.715	17.0	5.323E+09	0.988	Penetration
25	536.67	2.730	56.3	3.604E+08	0.932	Penetration
54.5	589.77	2.771		1.300E+06	0.786	Soft. Point
80	635.67	2.803		42500	0.665	Brookfield
100	671.67	2.827		9216	0.598	Brookfield
121.1	709.65	2.851		3328	0.547	Brookfield
135	734.67	2.866		1536	0.503	Brookfield
176.7	809.73	2.908		512	0.433	Brookfield

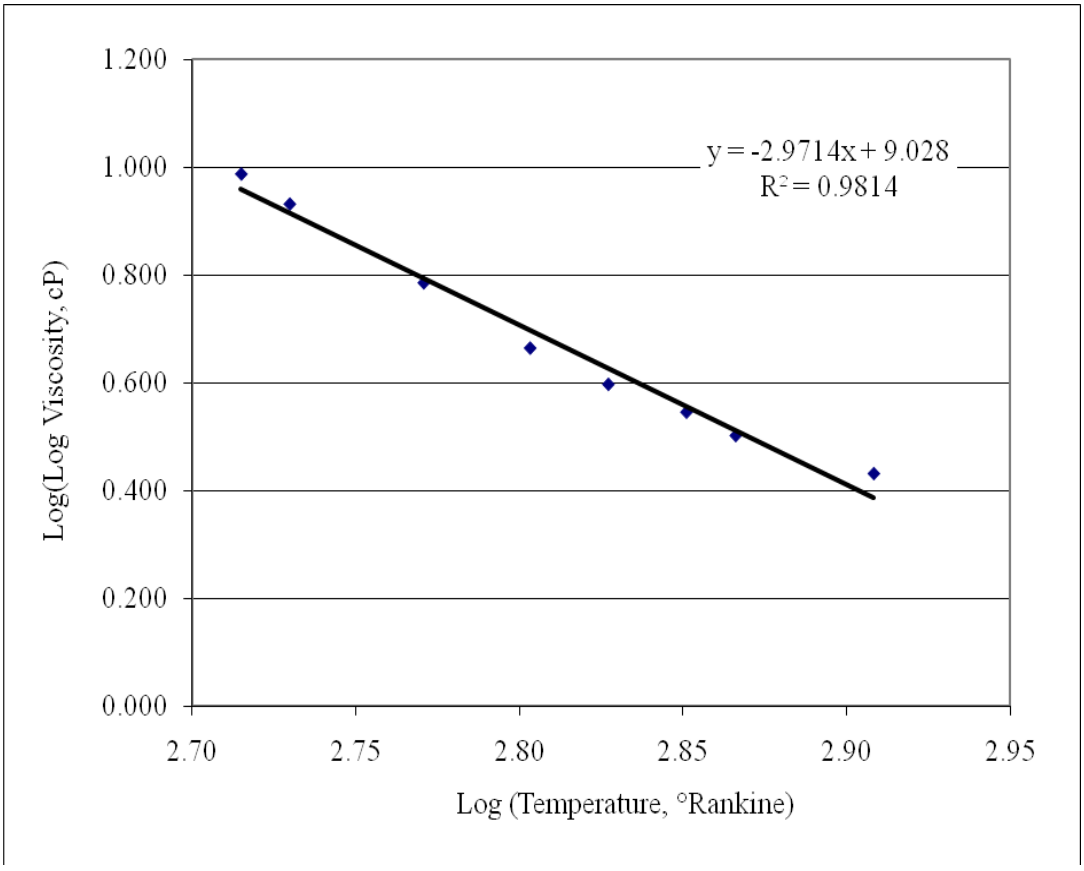

I-17 58-22 RTFO AR						
Temp. °C	Temp. °R	Log Temp. °R	Penetration .1mm	Viscosity cP	Log Log Visc. cP	Test
15	518.67	2.715	13.0	9.737E+09	0.999	Penetration
25	536.67	2.730	34.0	1.120E+09	0.957	Penetration
66	610.47	2.786		1.300E+06	0.786	Soft. Point
60	599.67	2.778		3000000	0.811	Brookfield
80	635.67	2.803		119000	0.705	Brookfield
100	671.67	2.827		22000	0.638	Brookfield
121.1	709.65	2.851		5632	0.574	Brookfield
135	734.67	2.866		2425	0.530	Brookfield
176.7	809.73	2.908		1024	0.479	Brookfield

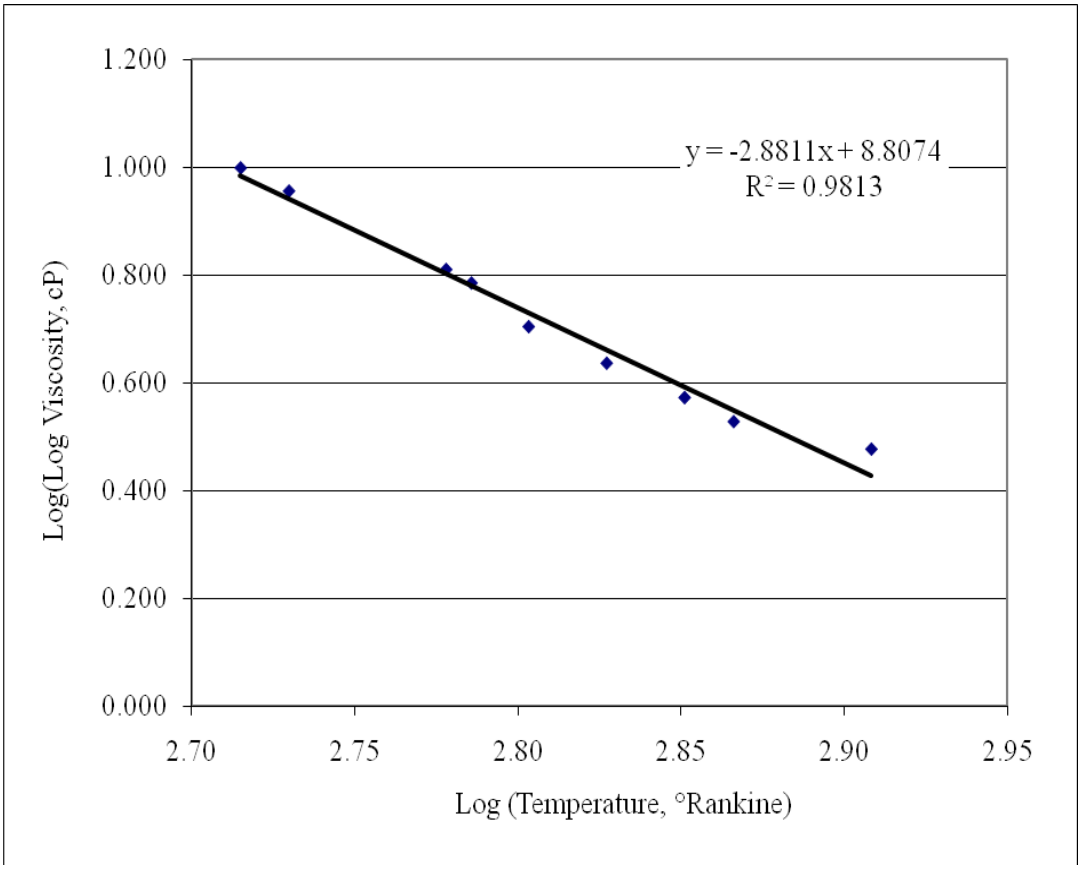

I-17 58-22 PAV AR						
Temp. °C	Temp. °R	Log Temp. °R	Penetration .1mm	Viscosity cP	Log Log Visc. cP	Test
15	518.67	2.715	9.2	2.121E+10	1.014	Penetration
25	536.67	2.730	20.0	3.693E+09	0.981	Penetration
74.5	625.77	2.796		1.300E+06	0.786	Soft. Point
60	599.67	2.778		7403760	0.837	Brookfield
80	635.67	2.803		431000	0.751	Brookfield
100	671.67	2.827		55800	0.676	Brookfield
121.1	709.65	2.851		11264	0.608	Brookfield
135	734.67	2.866		4864	0.567	Brookfield
176.7	809.73	2.908		1536	0.503	Brookfield

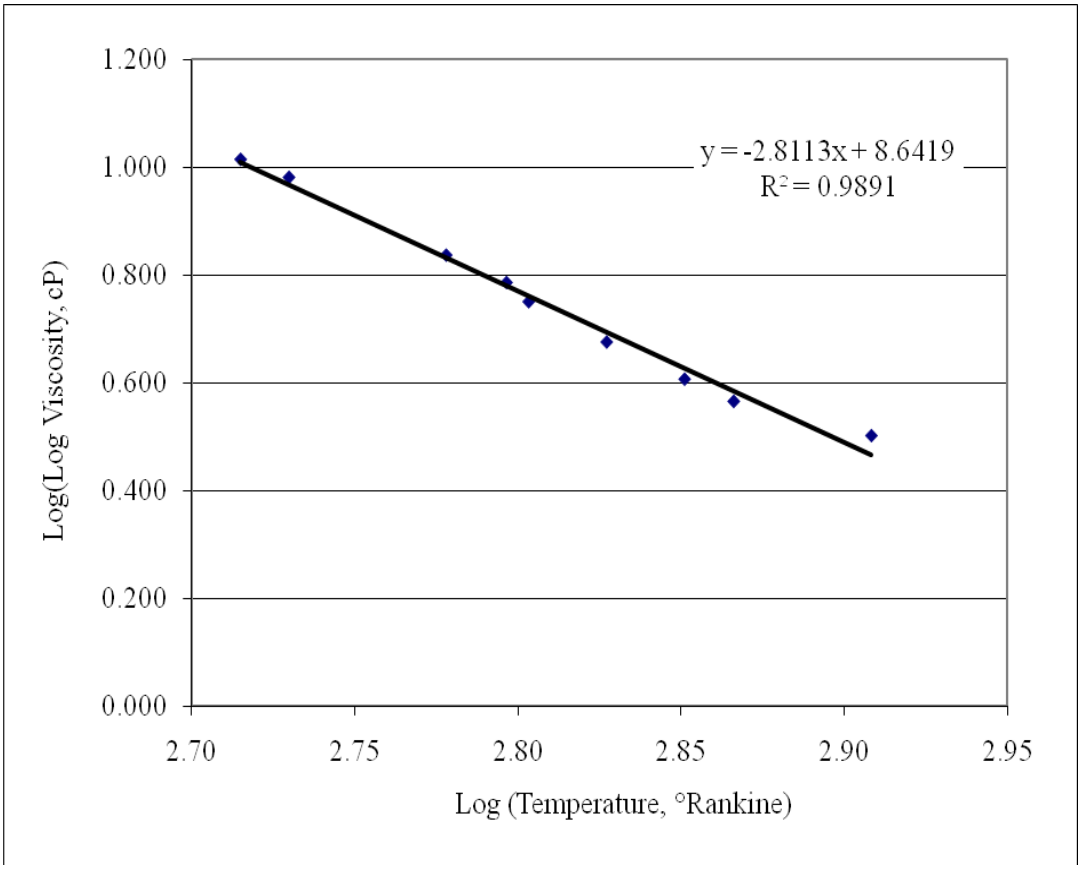

I-17 64-22 Original Virgin						
Temp. °C	Temp. °R	Log Temp. °R	Penetration .1mm	Viscosity cP	Log Log Visc. cP	Test
15	518.67	2.715	18.5	4.401E+09	0.984	Penetration
25	536.67	2.730	60.4	3.078E+08	0.929	Penetration
47	576.27	2.761		1.300E+06	0.786	Soft. Point
60	599.67	2.778		169500	0.718	Brookfield
80	635.67	2.803		16600	0.625	Brookfield
100	671.67	2.827		2925	0.540	Brookfield
121.1	709.65	2.851		762.5	0.460	Brookfield
135	734.67	2.866		362.5	0.408	Brookfield
176.7	809.73	2.908		62.5	0.254	Brookfield

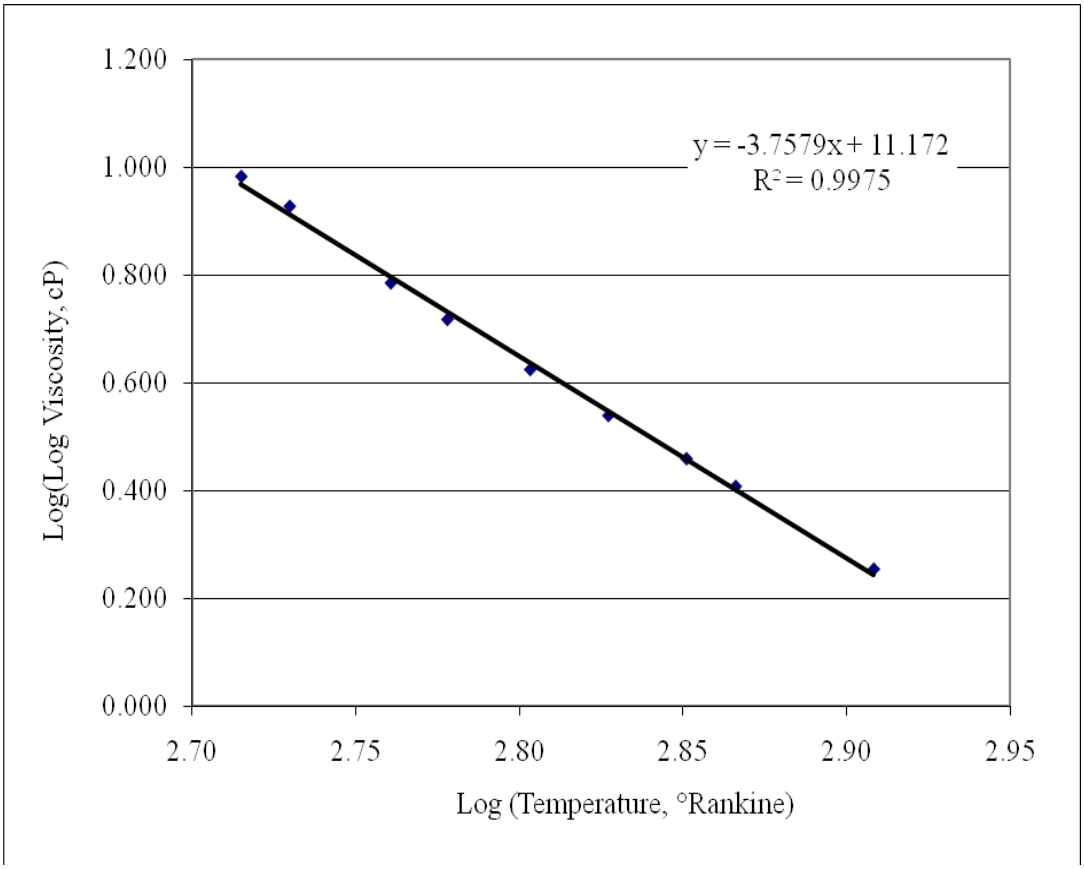

I-17 64-22 RTFO Virgin						
Temp. °C	Temp. °R	Log Temp. °R	Penetration .1mm	Viscosity cP	Log Log Visc. cP	Test
15	518.67	2.715	11.0	1.418E+10	1.007	Penetration
25	536.67	2.730	34.0	1.120E+09	0.957	Penetration
52	585.27	2.767		1.300E+06	0.786	Soft. Point
60	599.67	2.778		432000	0.751	Brookfield
80	635.67	2.803		34000	0.656	Brookfield
100	671.67	2.827		5100	0.569	Brookfield
121.1	709.65	2.851		1150	0.486	Brookfield
135	734.67	2.866		525	0.435	Brookfield
176.7	809.73	2.908		87.5	0.288	Brookfield

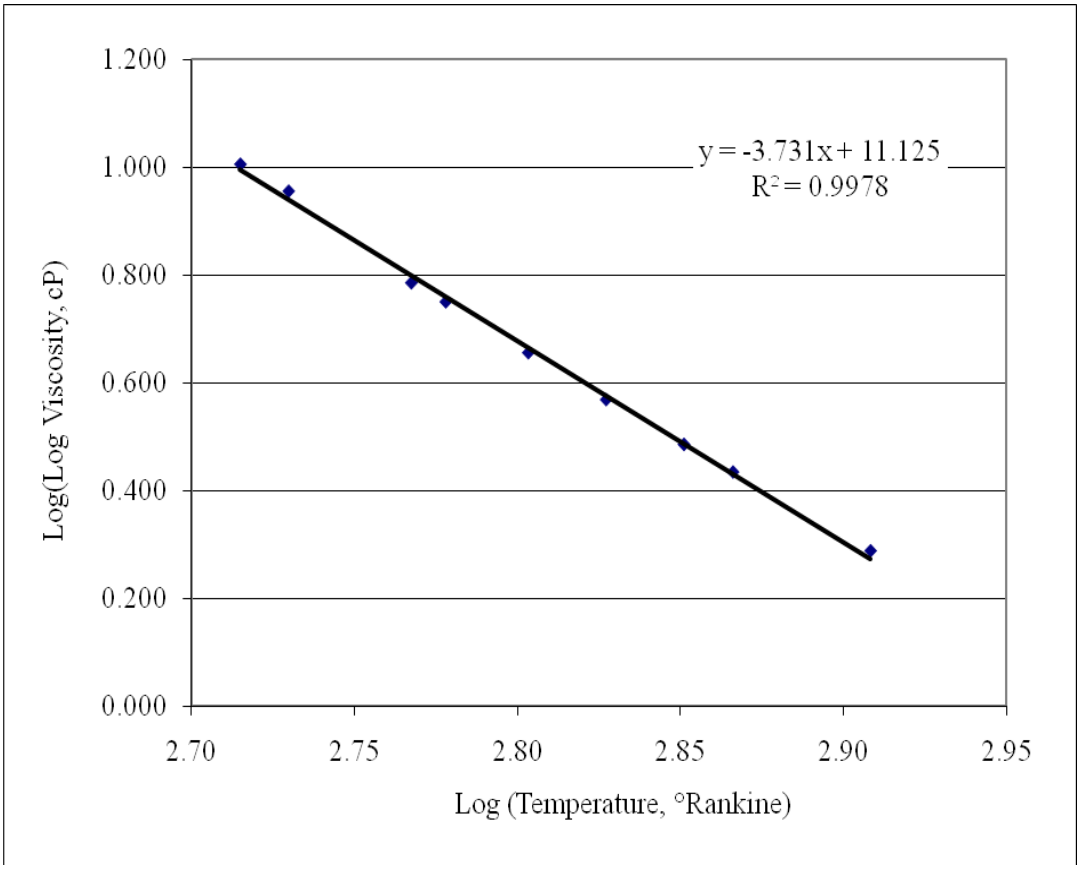

I-17 64-22 PAV Virgin						
Temp. °C	Temp. °R	Log Temp. °R	Penetration .1mm	Viscosity cP	Log Log Visc. cP	Test
15	518.67	2.715	8.0	2.906E+10	1.020	Penetration
25	536.67	2.730	21.5	3.138E+09	0.978	Penetration
62.75	604.62	2.781		1.300E+06	0.786	Soft. Point
80	635.67	2.803		105000	0.701	Brookfield
100	671.67	2.827		11250	0.608	Brookfield
121.1	709.65	2.851		2000	0.519	Brookfield
135	734.67	2.866		825	0.465	Brookfield
176.7	809.73	2.908		125	0.322	Brookfield

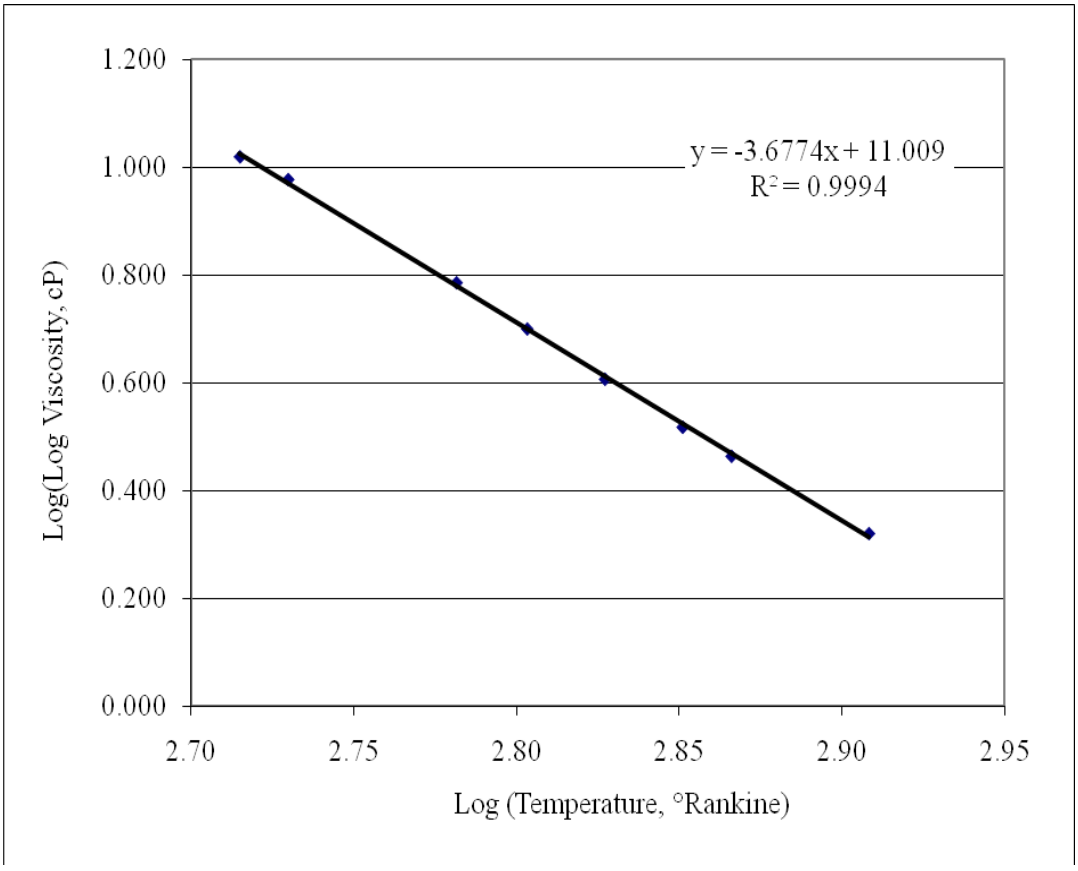

I-17 64-22 Original AR						
Temp. °C	Temp. °R	Log Temp. °R	Penetration .1mm	Viscosity cP	Log Log Visc. cP	Test
15	518.67	2.715	20.0	3.693E+09	0.981	Penetration
25	536.67	2.730	51.7	4.365E+08	0.937	Penetration
60	599.67	2.778		1.300E+06	0.786	Soft. Point
60	599.67	2.778		830000	0.772	Brookfield
80	635.67	2.803		69000	0.685	Brookfield
100	671.67	2.827		11700	0.609	Brookfield
121.1	709.65	2.851		4352	0.561	Brookfield
135	734.67	2.866		3072	0.543	Brookfield
176.7	809.73	2.908		1024	0.479	Brookfield

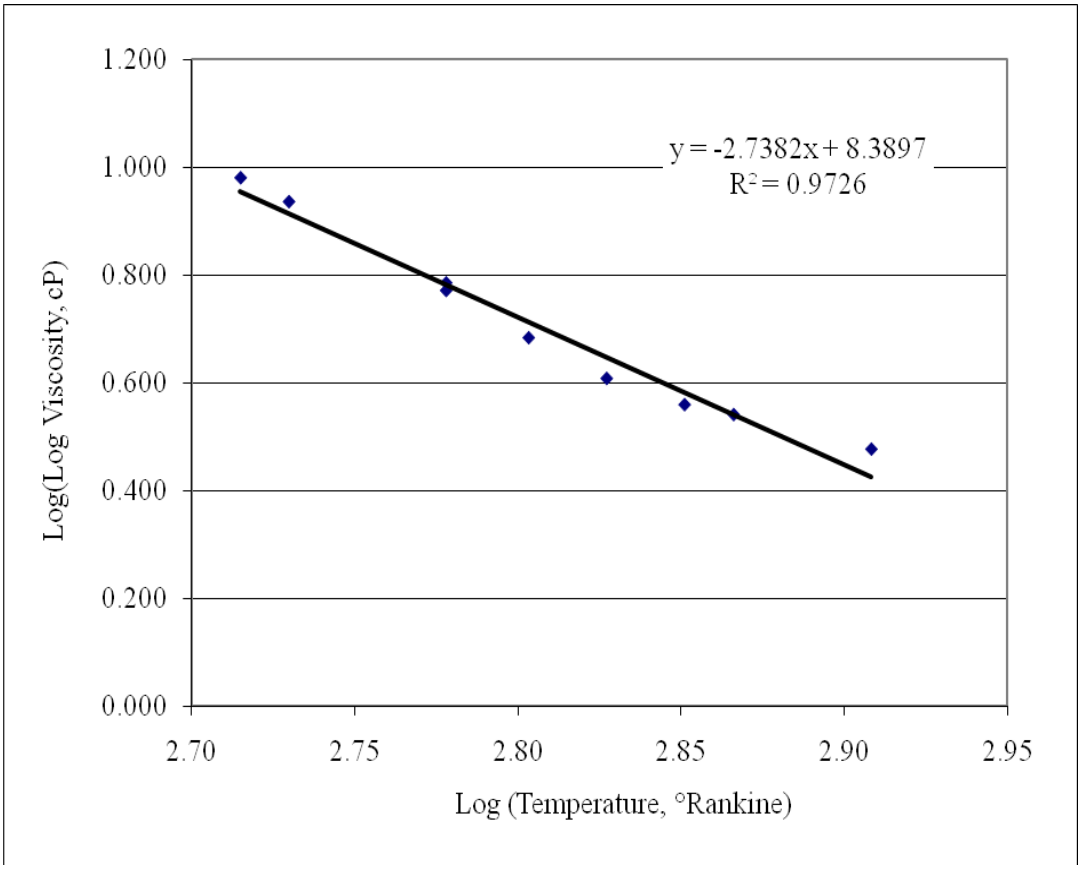

I-17 64-22 RTFO AR						
Temp. °C	Temp. °R	Log Temp. °R	Penetration .1mm	Viscosity cP	Log Log Visc. cP	Test
15	518.67	2.715	10.0	1.758E+10	1.011	Penetration
25	536.67	2.730	29.5	1.540E+09	0.963	Penetration
50.8	583.11	2.766		1.300E+06	0.786	Soft. Point
60	599.67	2.778		3620000	0.817	Brookfield
80	635.67	2.803		297000	0.738	Brookfield
100	671.67	2.827		42000	0.665	Brookfield
121.1	709.65	2.851		8100	0.592	Brookfield
135	734.67	2.866		3500	0.550	Brookfield
176.7	809.73	2.908		1536	0.503	Brookfield

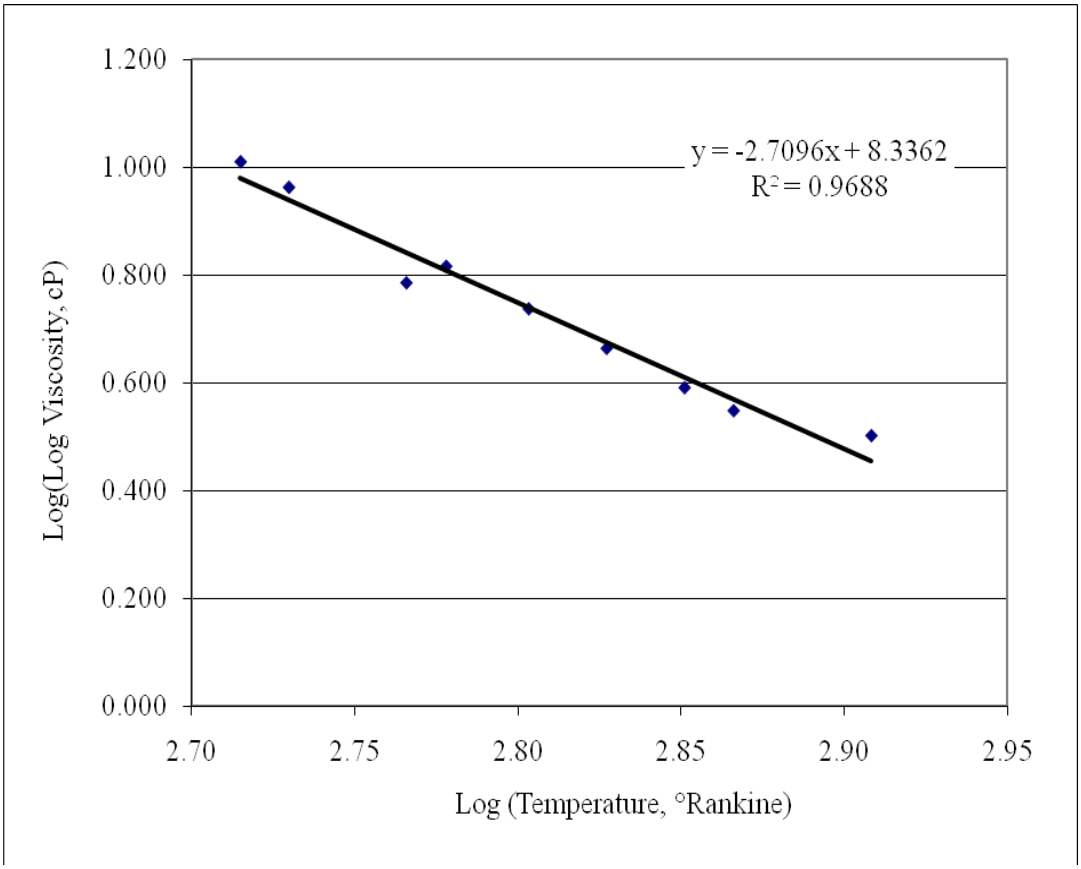

I-17 64-22 PAV AR						
Temp. °C	Temp. °R	Log Temp. °R	Penetration .1mm	Viscosity cP	Log Log Visc. cP	Test
15	518.67	2.715	8.7	2.406E+10	1.016	Penetration
25	536.67	2.730	17.7	4.861E+09	0.986	Penetration
71	619.47	2.792		1.300E+06	0.786	Soft. Point
60	599.67	2.778		8800000	0.842	Brookfield
80	635.67	2.803		548000	0.759	Brookfield
100	671.67	2.827		59300	0.679	Brookfield
121.1	709.65	2.851		11700	0.609	Brookfield
135	734.67	2.866		4864	0.567	Brookfield
176.7	809.73	2.908		2048	0.520	Brookfield

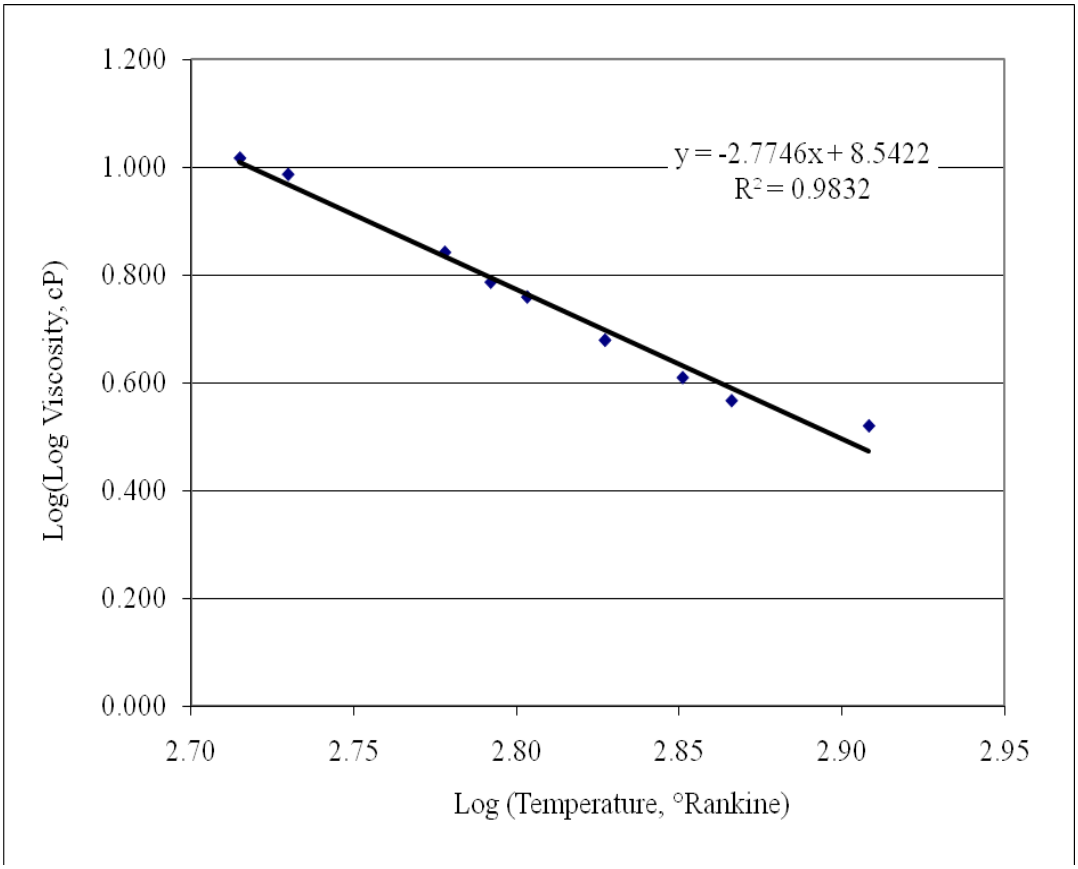

APPENDIX B

DYNAMIC MODULUS RESULTS

Antelope Wash Original																
Air Voids, %Va				Temp.	Shift	Freq.	Dynamic Modulus, |E*| (ksi)					Phase Angle, Φ (degree)				
Rep1	Rep2	Rep3	Avg.	°F	Factor	Hz	Rep1	Rep2	Rep3	Avg. |E*|	St. Dev.	Rep1	Rep2	Rep3	Avg. Φ	St. Dev.
17.66	17.72	17.79	17.72	14	3.9750	25	1547	1053	1374	1325	251	12	14	11	12.1	1.5
						10	1443	960	1301	1235	248	15	13	13	13.8	0.9
						5	1356	880	1216	1151	244	15	14	13	14.1	1.3
						1	1096	732	1018	949	192	18	15	14	15.4	2.0
						0.5	988	668	931	862	171	18	16	15	16.2	2.0
						0.1	768	537	749	685	128	21	16	16	17.5	2.7
				40	1.8523	25	782	571	862	738	150	17	15	16	16.0	0.9
						10	688	501	743	644	127	18	16	17	16.7	1.0
						5	618	447	662	576	114	18	17	18	17.7	0.8
						1	470	342	496	436	83	20	19	20	19.8	1.1
						0.5	415	302	437	385	72	22	20	21	20.8	0.8
						0.1	305	220	320	282	54	26	23	24	24.3	1.9
				70	0.0000	25	512	273	391	392	119	22	21	22	21.5	0.6
						10	434	230	324	330	102	22	21	23	22.2	0.7
						5	380	199	281	287	91	24	22	22	22.6	0.9
						1	279	142	199	207	69	31	26	26	27.7	2.9
						0.5	244	121	172	179	62	34	27	27	29.3	3.7
						0.1	179	86	119	128	47	44	32	32	36.0	6.7
				100	-1.1978	25	241	122	189	184	60	28	29	26	27.9	1.7
						10	192	101	153	149	46	31	28	26	28.7	2.4
						5	169	88	131	130	41	36	30	28	31.1	4.0
						1	126	63	91	93	31	48	35	34	39.2	7.9
						0.5	117	56	81	85	30	53	38	37	42.9	8.5
						0.1	109	46	64	73	32	62	47	46	51.8	9.0
				130	-1.7398	25	250	118	127	165	74	26	37	27	29.9	6.2
						10	217	90	102	136	70	31	31	25	29.1	3.6
						5	208	77	89	125	72	32	30	26	29.3	3.3
						1	165	57	69	97	59	53	37	33	41.2	10.6
						0.5	158	54	65	92	57	59	41	39	46.5	11.3
						0.1	146	47	63	86	53	84	52	61	65.5	16.4

Parameter	Temp. (°F)	All Data	Average	Rep. #1	Rep. #2	Rep. #3
δ	-	4.585	4.677	4.663	4.280	4.565
α	-	1.649	1.545	1.822	1.853	1.672
β	-	0.384	0.491	0.443	0.206	0.295
γ	-	0.512	0.552	0.381	0.467	0.548
Log a(14°F)	14	4.053	3.975	4.109	4.398	3.952
Log a(40°F)	40	1.895	1.851	1.850	2.035	1.908
Log a(70°F)	70	0.000	0.000	0.000	0.000	0.000
Log a(100°F)	100	-1.243	-1.195	-1.022	-1.278	-1.412
Log a(130°F)	130	-1.831	-1.731	-1.217	-1.799	-2.323
	Se/Sy	0.306	0.075	0.103	0.078	0.039
	R^2	0.958	0.998	0.996	0.998	0.999
	Σe2	1.482	0.043	0.101	0.028	0.010

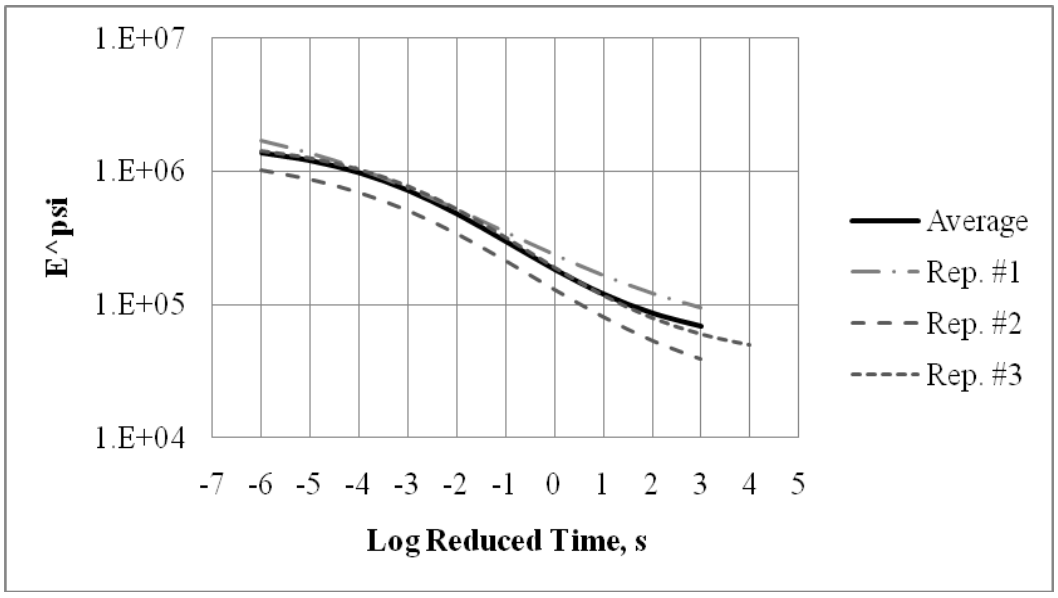

Antelope Wash 5-Day Core																
Air Voids, %Va				Temp.	Shift Factor	Freq.	Dynamic Modulus, |E*| (ksi)					Phase Angle, Φ (degree)				
Rep1	Rep2	Rep3	Avg.	°F		Hz	Rep1	Rep2	Rep3	Avg. |E*|	St. Dev.	Rep1	Rep2	Rep3	Avg. Φ	St. Dev.
23.67	18.53	17.11	19.77	14	3.1409	25	1465	1803	2142	1803	338	7	9	12	9.3	2.5
						10	1202	1607	2012	1607	405	11	11	12	11.3	0.6
						5	1070	1483	1896	1483	413	11	12	12	11.6	0.3
						1	886	1244	1602	1244	358	11	11	11	11.1	0.2
						0.5	806	1139	1472	1139	333	10	11	12	11.3	0.8
						0.1	649	906	1163	906	257	13	13	13	12.7	0.1
				40	1.7531	25	672	1193	1409	1092	379	13	13	12	12.5	0.9
						10	645	1095	1290	1010	331	14	15	12	13.6	1.9
						5	585	989	1204	926	314	14	17	13	14.6	1.9
						1	466	726	972	721	253	15	22	14	17.1	4.7
						0.5	424	630	885	647	231	16	21	14	17.2	3.5
						0.1	335	458	688	494	179	17	23	16	18.8	3.7
				70	0.0000	25	515	712	736	654	121	19	14	16	16.4	2.5
						10	413	620	606	546	116	19	17	19	18.4	1.5
						5	371	530	526	476	91	19	20	19	19.4	0.9
						1	284	375	384	348	55	21	23	19	21.0	1.7
						0.5	246	324	335	302	48	22	23	20	21.7	1.5
						0.1	173	239	242	218	39	25	24	22	23.6	1.3
				100	-1.5711	25	258	356	293	302	49	23	20	21	21.3	1.6
						10	213	306	242	254	47	24	22	20	21.9	2.2
						5	209	275	217	233	36	25	22	19	21.9	2.8
						1	153	198	158	169	25	29	22	22	24.3	3.8
						0.5	137	173	139	150	20	29	25	23	25.6	3.3
						0.1	115	126	105	116	11	33	24	25	27.5	5.0
				130	-2.9525	25	187	147	198	177	27	33	24	22	26.5	6.2
						10	159	129	163	150	19	26	22	21	23.1	2.7
						5	142	118	143	135	14	29	20	20	23.1	5.5
						1	105	92	105	101	7	30	22	22	24.7	4.7
						0.5	91	85	94	90	4	29	22	23	24.4	4.0
						0.1	75	73	75	74	1	34	25	26	28.2	4.7

Parameter	Temp. (°F)	All Data	Average	Rep. #1	Rep. #2	Rep. #3
δ	-	4.414	4.452	2.457	4.454	4.543
α	-	2.105	2.038	5.246	2.164	1.848
β	-	-0.117	-0.127	-0.264	-0.099	-0.227
γ	-	0.361	0.379	0.125	0.359	0.460
Log a(14°F)	14	3.390	3.442	3.314	2.787	4.537
Log a(40°F)	40	1.743	1.766	1.654	1.550	2.208
Log a(70°F)	70	0.000	0.000	0.000	0.000	0.000
Log a(100°F)	100	-1.563	-1.574	-1.361	-1.673	-1.678
Log a(130°F)	130	-2.939	-2.948	-2.425	-3.459	-2.822
	Se/Sy	0.402	0.046	0.117	0.064	0.110
	R^2	0.926	0.999	0.995	0.998	0.995
	Σe2	0.650	0.003	0.021	0.020	0.019

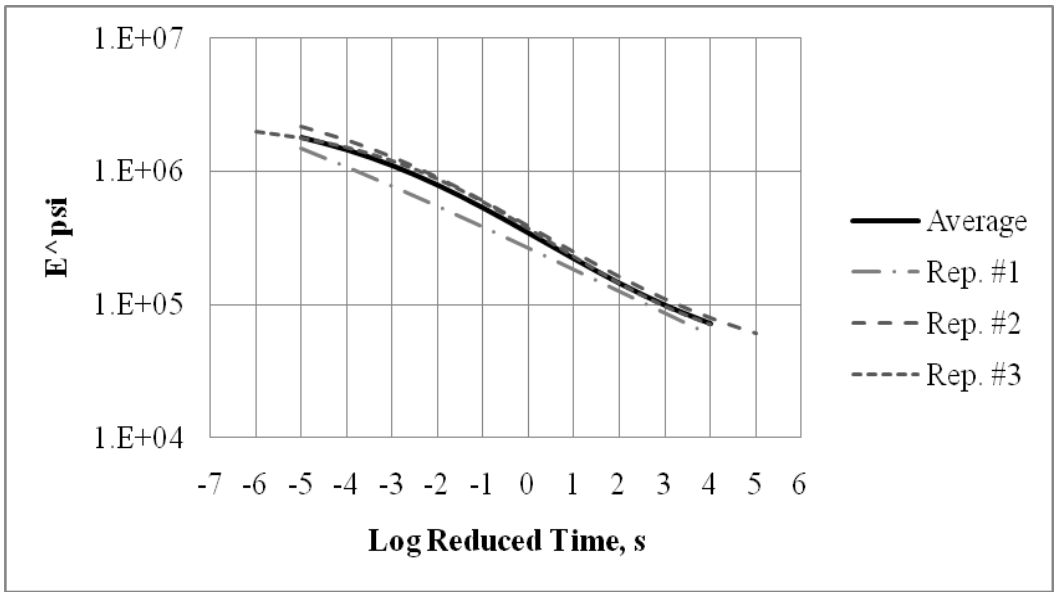

Antelope Wash 14-Day Core																
Air Voids, %Va				Temp.	Shift Factor	Freq.	Dynamic Modulus, |E*| (ksi)					Phase Angle, Φ (degree)				
Rep1	Rep2	Rep3	Avg.	°F		Hz	Rep1	Rep2	Rep3	Avg. |E*|	St. Dev.	Rep1	Rep2	Rep3	Avg. Φ	St. Dev.
18.23	19.37	N/A	18.80	14	3.2008	25	2001	1612	N/A	1806	275	8	8	N/A	7.9	0.3
						10	1967	1553	N/A	1760	293	11	11	N/A	10.6	0.1
						5	1829	1449	N/A	1639	269	12	12	N/A	12.0	0.5
						1	1510	1215	N/A	1363	209	13	12	N/A	12.8	0.4
						0.5	1367	1108	N/A	1238	183	13	13	N/A	13.1	0.4
						0.1	1107	903	N/A	1005	144	13	13	N/A	13.4	0.1
				40	1.6975	25	1363	959	N/A	1161	286	10	12	N/A	11.1	1.7
						10	1400	972	N/A	1186	302	12	12	N/A	11.8	0.0
						5	1296	899	N/A	1097	280	13	14	N/A	13.4	0.5
						1	1041	728	N/A	884	221	15	16	N/A	15.6	1.0
						0.5	939	663	N/A	801	195	15	14	N/A	14.8	0.7
						0.1	695	513	N/A	604	129	18	18	N/A	18.0	0.1
				70	0.0000	25	804	563	N/A	684	170	19	16	N/A	17.3	2.2
						10	709	498	N/A	603	149	14	14	N/A	14.2	0.1
						5	631	446	N/A	538	130	17	16	N/A	16.5	0.7
						1	489	352	N/A	420	97	19	18	N/A	18.8	0.6
						0.5	427	318	N/A	373	77	21	20	N/A	20.7	1.1
						0.1	311	241	N/A	276	50	24	22	N/A	23.2	1.0
				100	-1.6481	25	506	349	N/A	428	111	16	18	N/A	17.3	1.5
						10	390	293	N/A	341	68	22	21	N/A	21.5	0.1
						5	326	249	N/A	287	54	23	22	N/A	22.5	0.2
						1	217	171	N/A	194	32	26	26	N/A	26.0	0.4
						0.5	179	144	N/A	161	24	27	27	N/A	27.1	0.2
						0.1	124	102	N/A	113	15	30	30	N/A	30.1	0.0
				130	-3.2374	25	182	183	N/A	182	1	23	26	N/A	24.6	1.8
						10	160	151	N/A	156	6	23	25	N/A	23.9	1.3
						5	141	131	N/A	136	7	21	23	N/A	22.2	1.5
						1	106	98	N/A	102	6	28	28	N/A	28.1	0.6
						0.5	97	90	N/A	93	5	30	30	N/A	30.2	0.2
						0.1	83	75	N/A	79	6	37	38	N/A	37.5	0.4

Parameter	Temp. (°F)	All Data	Average	Rep. #1	Rep. #2	Rep. #3
δ	-	4.553	4.546	4.587	4.335	4.590
α	-	1.867	1.879	1.839	2.116	1.841
β	-	-0.396	-0.397	-0.409	-0.441	-0.397
γ	-	0.458	0.452	0.473	0.381	0.472
Log a(14°F)	14	3.176	3.202	3.109	3.430	3.109
Log a(40°F)	40	1.685	1.699	1.664	1.780	1.664
Log a(70°F)	70	0.000	0.000	0.000	0.000	0.000
Log a(100°F)	100	-1.638	-1.651	-1.652	-1.637	-1.653
Log a(130°F)	130	-3.219	-3.244	-3.283	-3.122	-3.286
	Se/Sy	0.198	0.094	0.099	0.082	0.097
	R^2	0.983	0.997	0.996	0.997	0.996
	Σe2	0.117	0.020	0.021	0.018	0.021

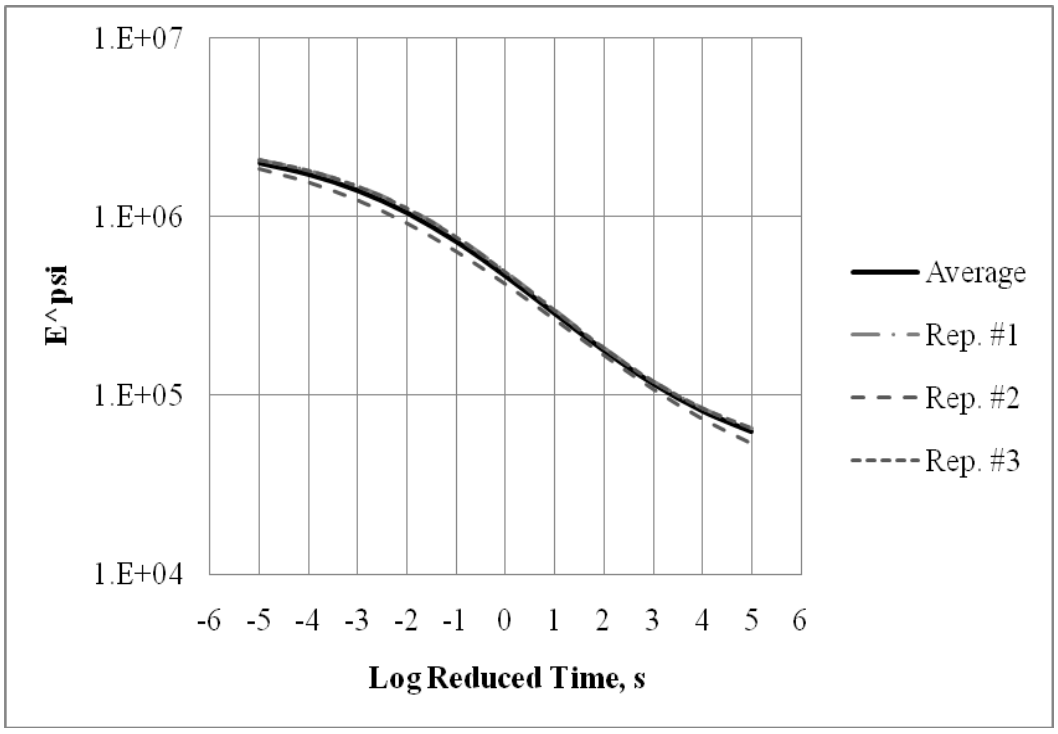

Antelope Wash 5-Day Pan																
Air Voids, %Va				Temp.	Shift Factor	Freq.	Dynamic Modulus, |E*| (ksi)					Phase Angle, Φ (degree)				
Rep1	Rep2	Rep3	Avg.	°F		Hz	Rep1	Rep2	Rep3	Avg. |E*|	St. Dev.	Rep1	Rep2	Rep3	Avg. Φ	St. Dev.
18.32	18.32	19.65	18.76	14	3.3555	25	610	836	613	686	130	9	12	13	11.4	1.7
						10	595	773	559	642	115	12	13	13	12.8	0.7
						5	561	711	519	597	101	13	13	15	13.5	0.9
						1	474	583	405	487	90	14	14	18	15.2	2.4
						0.5	444	535	364	448	86	15	14	19	16.1	2.6
						0.1	369	444	287	366	78	17	16	21	17.7	2.5
				40	1.6022	25	418	832	397	549	245	16	14	15	15.1	0.7
						10	392	742	361	498	211	15	16	16	15.7	0.8
						5	364	667	334	455	184	16	16	17	16.6	0.2
						1	292	448	264	335	100	17	23	18	19.5	3.4
						0.5	267	394	240	300	82	17	24	20	20.2	3.3
						0.1	216	305	193	238	59	18	25	21	21.6	3.5
				70	0.0000	25	235	447	196	293	135	21	24	18	21.0	2.8
						10	201	408	180	263	126	20	26	16	20.5	4.8
						5	181	352	164	232	104	19	25	15	19.8	5.0
						1	141	230	135	169	53	19	28	18	21.4	5.3
						0.5	133	201	124	152	43	20	28	17	21.5	5.3
						0.1	109	160	103	124	31	19	28	19	21.8	5.2
				100	-1.1391	25	164	193	178	179	15	28	26	23	25.4	2.3
						10	147	181	154	161	18	23	19	20	20.7	1.8
						5	131	165	140	145	17	21	19	18	19.4	1.4
						1	95	125	110	110	15	21	19	21	20.5	1.0
						0.5	87	113	103	101	13	21	20	21	20.6	0.5
						0.1	72	93	91	85	12	21	21	24	22.1	1.6
				130	-1.8126	25	150	174	119	148	28	21	24	20	21.7	2.3
						10	140	157	110	136	23	18	20	15	17.7	2.3
						5	128	142	103	124	20	14	18	15	15.7	1.8
						1	107	113	86	102	14	16	19	18	17.6	1.4
						0.5	101	105	83	96	12	16	18	19	17.7	1.5
						0.1	93	92	76	87	10	19	21	22	20.8	1.9

Parameter	Temp. (°F)	All Data	Average	Rep. #1	Rep. #2	Rep. #3
δ	-	4.659	4.774	4.135	4.972	4.470
α	-	1.283	1.161	1.802	0.973	2.113
β	-	0.208	0.394	-0.301	0.409	0.688
γ	-	0.490	0.579	0.318	0.948	0.272
Log a(14°F)	14	3.610	3.357	4.955	2.494	3.106
Log a(40°F)	40	1.698	1.605	2.182	1.308	1.520
Log a(70°F)	70	0.000	0.000	0.000	0.000	0.000
Log a(100°F)	100	-1.140	-1.145	-1.072	-1.235	-1.177
Log a(130°F)	130	-1.721	-1.828	-1.038	-2.390	-2.006
	Se/Sy	0.574	0.153	0.122	0.216	0.120
	R^2	0.842	0.991	0.994	0.982	0.995
	Σe2	0.776	0.023	0.024	0.071	0.032

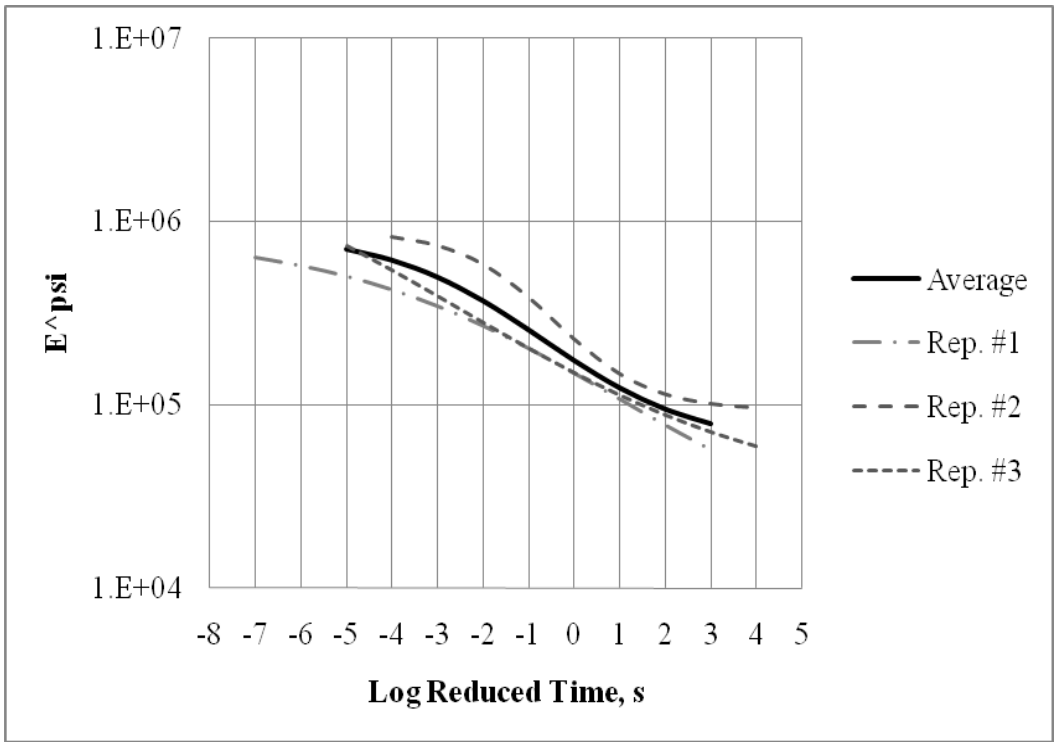

Antelope Wash 14-Day Pan																
Air Voids, %Va				Temp.	Shift Factor	Freq.	Dynamic Modulus, |E*| (ksi)					Phase Angle, Φ (degree)				
Rep1	Rep2	Rep3	Avg.	°F		Hz	Rep1	Rep2	Rep3	Avg. |E*|	St. Dev.	Rep1	Rep2	Rep3	Avg. Φ	St. Dev.
18.77	18.63	N/A	18.70	14	3.7122	25	473	407	N/A	440	47	11	3	N/A	6.6	5.8
						10	435	394	N/A	414	29	10	13	N/A	11.8	2.0
						5	430	373	N/A	401	40	11	16	N/A	13.7	3.2
						1	372	307	N/A	340	47	13	16	N/A	14.8	2.0
						0.5	351	285	N/A	318	47	13	16	N/A	14.8	2.2
						0.1	306	240	N/A	273	46	14	16	N/A	15.1	1.9
				40	1.6381	25	366	255	N/A	311	79	18	15	N/A	16.7	1.8
						10	374	241	N/A	308	93	14	15	N/A	14.6	0.3
						5	358	225	N/A	292	94	18	15	N/A	16.4	2.5
						1	280	185	N/A	233	67	21	16	N/A	18.6	3.7
						0.5	251	172	N/A	212	56	22	17	N/A	19.5	3.8
						0.1	191	146	N/A	168	32	22	17	N/A	19.8	3.7
				70	0.0000	25	157	150	N/A	153	5	18	20	N/A	18.7	1.3
						10	144	142	N/A	143	1	19	19	N/A	19.0	0.3
						5	128	131	N/A	130	2	22	18	N/A	20.0	2.5
						1	94	105	N/A	100	7	22	19	N/A	20.5	2.3
						0.5	84	97	N/A	91	9	21	19	N/A	20.0	1.3
						0.1	68	81	N/A	74	9	20	20	N/A	19.9	0.5
				100	-0.8141	25	148	211	N/A	179	45	29	18	N/A	23.5	8.4
						10	119	195	N/A	157	54	24	15	N/A	19.3	6.1
						5	103	178	N/A	141	53	22	16	N/A	18.8	4.5
						1	79	141	N/A	110	44	20	17	N/A	18.6	1.6
						0.5	73	129	N/A	101	40	19	17	N/A	18.0	1.4
						0.1	62	109	N/A	86	34	19	18	N/A	18.4	0.9
				130	-0.8066	25	137	138	N/A	138	1	23	21	N/A	21.9	1.2
						10	117	134	N/A	125	12	22	18	N/A	19.9	2.4
						5	100	125	N/A	112	17	21	17	N/A	19.4	2.9
						1	72	105	N/A	89	23	20	18	N/A	19.4	1.3
						0.5	64	102	N/A	83	26	21	17	N/A	19.0	2.6
						0.1	52	97	N/A	75	32	21	20	N/A	20.9	0.6

Parameter	Temp. (°F)	All Data	Average	Rep. #1	Rep. #2
δ	-	4.573	4.227	4.734	4.663
α	-	1.004	1.486	0.886	1.851
β	-	0.460	-0.116	0.895	1.133
γ	-	0.699	0.403	1.038	0.275
Log a(14°F)	14	3.738	3.848	4.826	3.185
Log a(40°F)	40	1.644	1.697	2.084	1.384
Log a(70°F)	70	0.000	0.000	0.000	0.000
Log a(100°F)	100	-0.800	-0.841	-0.909	-0.626
Log a(130°F)	130	-0.759	-0.828	-0.646	-0.498
	Se/Sy	0.666	0.206	0.219	0.301
	R^2	0.780	0.984	0.982	0.965
	Σe2	2.458	0.092	0.065	0.134

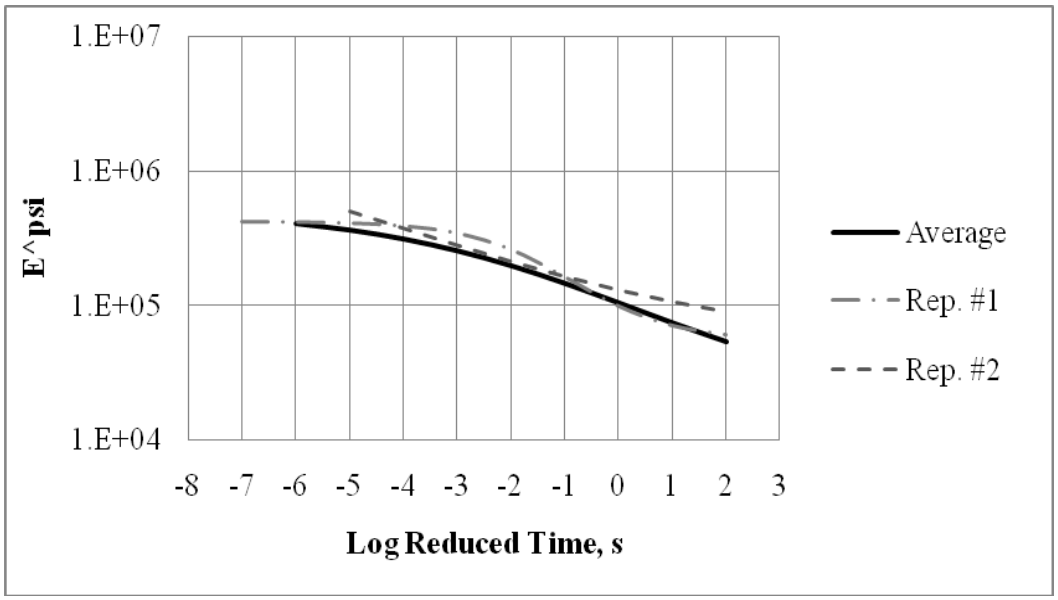

I-17 58-22 Original																
Air Voids, %Va				Temp.	Shift Factor	Freq.	Dynamic Modulus, |E*| (ksi)					Phase Angle, Φ (degree)				
Rep1	Rep2	Rep3	Avg.	°F		Hz	Rep1	Rep2	Rep3	Avg. |E*|	St. Dev.	Rep1	Rep2	Rep3	Avg. Φ	St. Dev.
N/A	N/A	N/A	8.00	14	3.5924	25	4107	4224	2946	3759	707	6	9	12	9.2	3.1
						10	3942	3784	2701	3475	675	8	8	13	9.7	2.7
						5	3703	3347	2726	3259	495	8	9	14	10.4	3.0
						1	3175	2857	2271	2768	459	9	10	15	11.4	3.0
						0.5	2969	2557	2100	2542	435	9	11	15	11.8	3.1
						0.1	2351	1975	1697	2008	328	11	12	17	13.2	3.4
				40	2.2069	25	2951	2843	2186	2660	414	12	11	10	10.7	1.1
						10	2736	2580	1984	2433	397	12	9	11	10.9	1.5
						5	2538	2374	1862	2258	352	12	11	13	11.8	1.1
						1	2079	1954	1512	1849	298	14	13	14	13.7	0.7
						0.5	1892	1772	1387	1684	264	15	14	16	15.0	1.3
						0.1	1466	1374	1080	1307	202	18	16	17	17.0	0.8
				70	0.0000	25	1505	1258	1026	1263	239	17	18	19	18.1	0.8
						10	1296	1073	877	1082	210	20	20	22	20.8	1.4
						5	1113	926	766	935	174	21	21	23	21.5	1.0
						1	792	640	539	657	127	26	27	29	27.3	1.4
						0.5	657	528	468	551	97	28	30	32	29.8	1.8
						0.1	423	336	324	361	54	36	36	38	36.7	1.3
				100	-2.2602	25	421	308	495	408	94	32	39	30	33.4	4.6
						10	296	229	363	296	67	34	36	32	34.2	2.3
						5	221	183	291	232	55	35	35	33	34.5	1.5
						1	136	105	184	142	40	39	35	37	37.0	2.2
						0.5	106	87	148	114	31	40	35	38	37.8	2.3
						0.1	66	59	96	74	20	41	35	40	38.6	3.5
				130	-4.1030	25	92	95	163	117	40	41	41	32	38.0	4.9
						10	64	67	120	83	31	40	35	35	37.0	3.0
						5	50	52	96	66	26	37	35	34	35.3	1.6
						1	33	36	66	45	18	31	29	32	30.3	1.5
						0.5	29	32	58	40	16	32	27	31	30.1	2.4
						0.1	26	27	50	34	13	66	28	33	42.1	20.4

Parameter	Temp. (°F)	All Data	Average	Rep. #1	Rep. #2	Rep. #3
δ	-	3.854	3.919	4.237	3.256	3.789
α	-	2.955	2.906	2.709	3.506	2.955
β	-	-0.379	-0.395	-0.489	-0.278	-0.380
γ	-	0.929	0.907	0.784	0.983	1.111
Log a(14°F)	14	4.603	4.437	4.067	5.880	3.987
Log a(40°F)	40	2.278	2.271	2.201	2.374	2.296
Log a(70°F)	70	0.000	0.000	0.000	0.000	0.000
Log a(100°F)	100	-2.564	-2.532	-2.440	-2.765	-2.526
Log a(130°F)	130	-4.126	-4.063	-3.730	-4.574	-4.163
	Se/Sy	0.445	0.050	0.056	0.058	0.039
	R^2	0.904	0.999	0.999	0.999	0.999
	Σe2	1.311	0.005	0.008	0.007	0.003

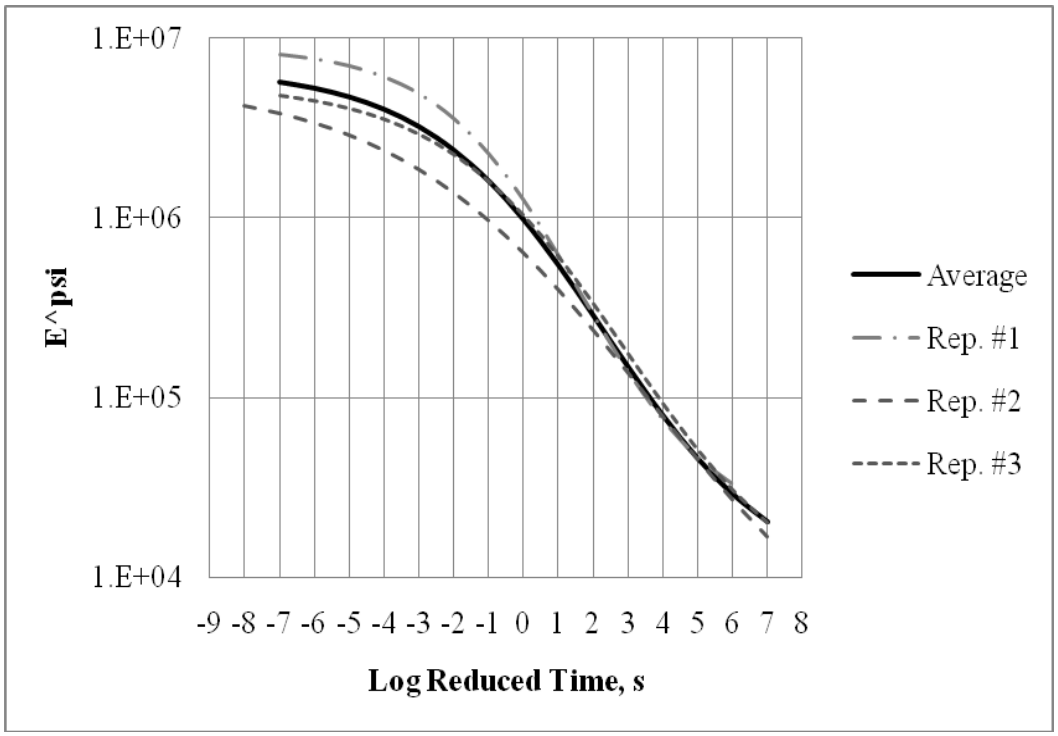

I-17 58-22 7-Year Field																
Air Voids, %Va				Temp.	Shift Factor	Freq.	Dynamic Modulus, |E*| (ksi)					Phase Angle, Φ (degree)				
Rep1	Rep2	Rep3	Avg.	°F		Hz	Rep1	Rep2	Rep3	Avg. |E*|	St. Dev.	Rep1	Rep2	Rep3	Avg. Φ	St. Dev.
7.8384	7.9355	7.7598	7.84	14	2.0499	25	4670	4481	4576	4576	95	10	5	7	7.4	2.6
						10	4491	4247	4369	4369	122	12	6	9	9.1	2.7
						5	4298	4083	4191	4191	108	12	8	10	9.9	2.1
						1	3827	3693	3760	3760	67	11	8	10	9.6	1.8
						0.5	3545	3499	3522	3522	23	12	9	10	10.5	1.9
						0.1	3062	3002	3032	3032	30	13	10	12	11.8	1.4
				40	1.2442	25	3333	3369	3351	3351	18	11	8	10	9.7	1.3
						10	2974	3106	3040	3040	66	13	11	12	12.0	1.0
						5	2755	2906	2831	2831	75	14	11	13	12.6	1.4
						1	2216	2412	2314	2314	98	15	14	15	14.9	0.6
						0.5	2025	2154	2089	2089	65	15	15	15	15.3	0.1
						0.1	1611	1624	1617	1617	7	17	21	19	18.9	1.6
				70	0.0000	25	3440	1748	2594	2594	846	13	17	15	15.0	2.0
						10	2781	1512	2146	2146	635	18	21	19	19.5	1.7
						5	2336	1339	1838	1838	498	20	24	22	21.9	2.0
						1	1636	949	1293	1293	343	21	29	25	25.3	4.2
						0.5	1307	823	1065	1065	242	23	33	28	28.3	5.1
						0.1	816	575	696	696	120	31	43	37	37.0	6.0
				100	-1.5769	25	2161	1689	2150	2000	270	32	28	32	30.9	2.3
						10	1907	1447	1660	1671	230	32	30	32	31.2	0.7
						5	1530	1337	1326	1398	114	33	31	33	32.5	1.3
						1	925	944	785	885	87	40	41	41	40.6	0.4
						0.5	749	776	608	711	90	41	46	43	43.1	2.9
						0.1	460	431	383	425	39	40	53	43	45.2	6.7
				130	-3.4741	25	417	404	482	434	42	29	27	29	28.4	1.1
						10	328	351	353	344	14	27	31	28	28.9	2.1
						5	272	290	292	285	11	29	31	28	29.2	1.4
						1	202	191	193	195	6	30	39	28	32.5	5.7
						0.5	179	150	172	167	15	29	40	29	32.8	6.5
						0.1	142	98	140	127	25	29	40	28	32.4	6.2

Parameter	Temp. (°F)	All Data	Average	Rep. #1	Rep. #2	Rep. #3
δ	-	3.842	3.870	4.875	2.740	4.647
α	-	3.012	2.987	1.800	4.181	2.076
β	-	-1.272	-1.265	-1.267	-1.471	-1.074
γ	-	0.374	0.379	0.688	0.290	0.578
Log a(14°F)	14	2.118	2.050	1.472	2.575	1.948
Log a(40°F)	40	1.273	1.244	1.003	1.461	1.158
Log a(70°F)	70	0.000	0.000	0.000	0.000	0.000
Log a(100°F)	100	-1.589	-1.576	-1.495	-1.643	-1.417
Log a(130°F)	130	-3.480	-3.472	-3.468	-3.457	-3.083
	Se/Sy	0.329	0.260	0.338	0.267	0.266
	R^2	0.951	0.974	0.956	0.973	0.973
	Σe2	0.773	0.177	0.180	0.310	0.149

I-17 64-16 5% A.V.																
Air Voids, %Va				Temp.	Shift Factor	Freq.	Dynamic Modulus, |E*| (ksi)					Phase Angle, Φ (degree)				
Rep1	Rep2	Rep3	Avg.	°F		Hz	Rep1	Rep2	Rep3	Avg. |E*|	St. Dev.	Rep1	Rep2	Rep3	Avg. Φ	St. Dev.
N/A	N/A	N/A	5.00	14	3.8731	25	4292	2998	5703	4331	1353	7	6	8	7.1	0.7
						10	4228	2940	5536	4235	1298	10	6	10	8.7	2.2
						5	4115	2857	5295	4089	1219	10	7	11	9.3	2.4
						1	3793	2468	4532	3598	1046	10	7	11	9.4	2.0
						0.5	3640	2351	4268	3420	977	10	7	10	9.3	1.7
						0.1	3245	2014	3530	2930	806	10	7	10	9.1	1.8
				40	1.8100	25	3417	1798	3439	2885	941	5	29	12	15.3	12.0
						10	3294	2726	3217	3079	308	7	25	11	14.1	9.5
						5	3068	2639	3026	2911	236	9	22	12	14.4	6.9
						1	2662	2062	2523	2416	314	11	18	12	13.6	3.9
						0.5	2503	1839	2364	2235	350	11	16	13	13.1	2.5
						0.1	2062	1471	1920	1818	308	11	15	14	13.4	1.9
				70	0.0000	25	2011	2101	2228	2114	109	8	11	15	11.5	3.4
						10	1851	1874	1863	1863	11	12	15	17	14.9	2.5
						5	1715	1739	1634	1696	55	12	17	19	15.9	3.6
						1	1360	1345	1203	1303	87	16	20	23	19.6	3.9
						0.5	1230	1206	1032	1156	108	18	21	26	21.7	4.3
						0.1	905	902	685	831	126	22	28	33	27.7	5.7
				100	-2.9793	25	474	738	652	621	135	25	25	31	27.1	3.6
						10	387	576	509	490	96	27	32	33	30.7	2.8
						5	243	459	410	371	114	40	34	35	36.6	3.3
						1	216	314	255	262	49	32	42	42	38.6	6.1
						0.5	175	265	196	212	47	32	45	45	40.9	7.5
						0.1	112	169	126	136	30	33	49	52	44.8	10.1
				130	-4.9244	25	195	253	146	198	54	36	39	41	38.8	2.4
						10	146	176	101	141	38	36	39	41	38.9	2.7
						5	112	133	79	108	27	34	39	36	36.6	2.6
						1	71	86	52	70	17	30	42	37	36.1	6.4
						0.5	62	72	44	59	14	28	39	37	34.4	5.6
						0.1	45	54	33	44	10	28	36	37	33.7	5.1

Parameter	Temp. (°F)	All Data	Average	Rep. #1	Rep. #2	Rep. #3
δ	-	3.707	3.661	3.292	4.050	3.671
α	-	3.006	3.072	3.467	2.488	3.184
β	-	-0.377	-0.368	-0.307	-0.470	-0.376
γ	-	1.391	1.380	1.505	1.648	1.129
Log a(14°F)	14	3.792	3.873	4.512	2.480	4.235
Log a(40°F)	40	1.805	1.810	2.399	1.251	1.813
Log a(70°F)	70	0.000	0.000	0.000	0.000	0.000
Log a(100°F)	100	-3.004	-2.979	-3.835	-2.803	-2.527
Log a(130°F)	130	-4.956	-4.924	-5.436	-4.693	-4.845
	Se/Sy	0.363	0.071	0.024	0.193	0.082
	R^2	0.937	0.998	1.000	0.986	0.997
	Σe2	0.642	0.010	0.017	0.038	0.011

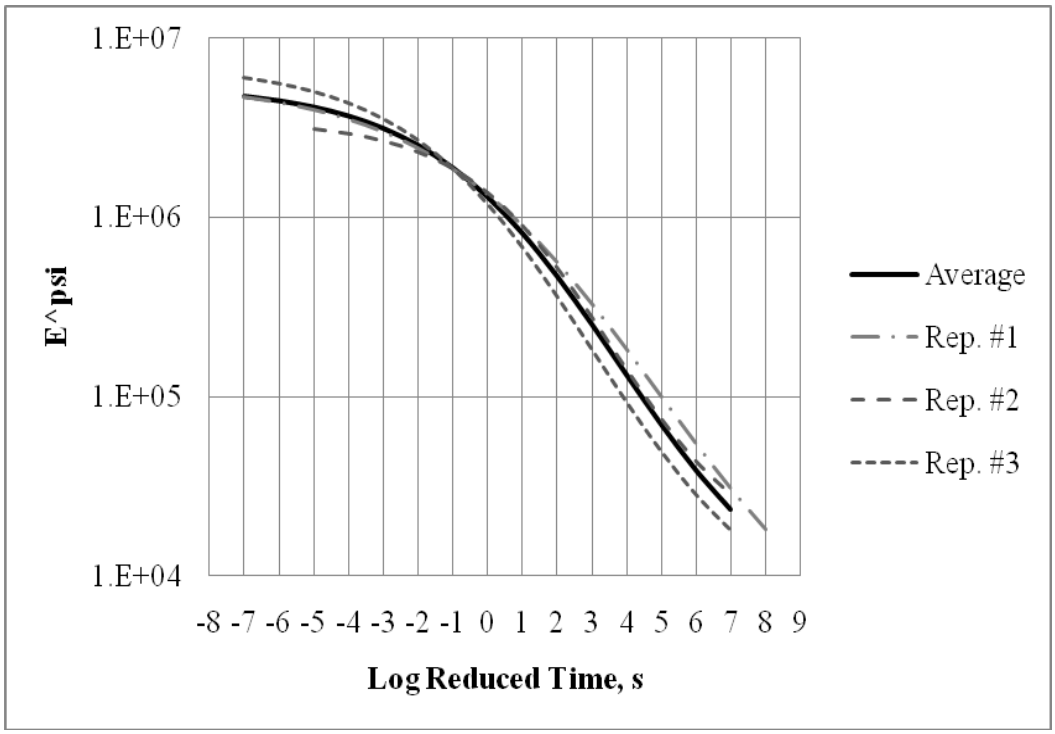

I-17 64-16 8% A.V.																
Air Voids, %Va				Temp.	Shift Factor	Freq.	Dynamic Modulus, |E*| (ksi)					Phase Angle, Φ (degree)				
Rep1	Rep2	Rep3	Avg.	°F		Hz	Rep1	Rep2	Rep3	Avg. |E*|	St. Dev.	Rep1	Rep2	Rep3	Avg. Φ	St. Dev.
N/A	N/A	N/A	8.00	14	4.2039	25	4012	4283	5808	4701	968	6	2	2	3.5	2.4
						10	3829	4086	5501	4472	901	9	5	4	6.1	2.8
						5	3637	3896	5332	4288	913	11	5	4	6.9	3.5
						1	3179	3477	4819	3825	873	13	6	5	8.1	4.6
						0.5	2975	3258	4580	3604	857	13	6	6	8.3	4.4
						0.1	2542	2829	4044	3138	797	15	6	6	9.2	5.2
				40	2.3323	25	3264	2594	4602	3486	1022	7	9	4	6.8	2.7
						10	3081	2374	4308	3254	978	12	11	7	9.9	2.3
						5	2883	2190	4027	3033	927	13	11	7	10.4	2.7
						1	2425	1868	3480	2591	819	15	11	9	11.8	2.9
						0.5	2247	1730	3219	2399	756	15	12	10	12.3	2.6
						0.1	1857	1431	2711	1999	652	16	14	12	13.9	2.2
				70	0.0000	25	1967	1271	2436	1891	586	12	14	13	12.9	1.4
						10	1736	1124	2075	1645	482	17	16	16	16.6	0.6
						5	1536	1005	1808	1450	408	20	18	18	18.8	0.9
						1	1125	739	1298	1054	286	24	23	26	24.1	1.5
						0.5	958	632	1140	910	257	26	26	28	26.7	1.3
						0.1	632	435	732	600	151	32	31	35	32.7	2.1
				100	-2.5871	25	662	441	513	539	113	23	27	32	27.2	4.5
						10	485	336	387	403	75	31	32	32	31.7	0.8
						5	377	272	304	318	54	33	32	33	32.7	0.7
						1	219	170	189	193	25	39	35	38	37.4	1.7
						0.5	178	137	152	156	21	41	38	40	39.9	1.6
						0.1	98	89	92	93	5	47	44	45	45.4	1.5
				130	-4.3658	25	227	133	122	160	58	32	39	38	36.2	3.8
						10	158	92	85	112	40	35	41	40	38.6	3.1
						5	114	70	64	83	27	39	40	38	38.8	0.9
						1	63	44	41	49	12	37	37	34	36.2	1.6
						0.5	50	38	36	41	8	37	37	34	36.0	1.9
						0.1	34	28	29	31	3	39	37	35	36.9	1.6

Parameter	Temp. (°F)	All Data	Average	Rep. #1	Rep. #2	Rep. #3
δ	-	3.579	3.562	3.569	3.221	3.821
α	-	3.163	3.184	3.107	3.514	3.012
β	-	-0.402	-0.406	-0.462	-0.329	-0.420
γ	-	1.198	1.221	1.375	1.105	1.165
Log a(14°F)	14	4.237	4.204	3.197	5.265	4.275
Log a(40°F)	40	2.311	2.332	2.012	2.386	2.586
Log a(70°F)	70	0.000	0.000	0.000	0.000	0.000
Log a(100°F)	100	-2.576	-2.587	-2.337	-2.443	-2.940
Log a(130°F)	130	-4.407	-4.366	-3.804	-4.402	-5.076
	Se/Sy	0.338	0.046	0.047	0.058	0.030
	R^2	0.946	0.999	0.999	0.999	1.000
	Σe2	0.760	0.008	0.007	0.011	0.007

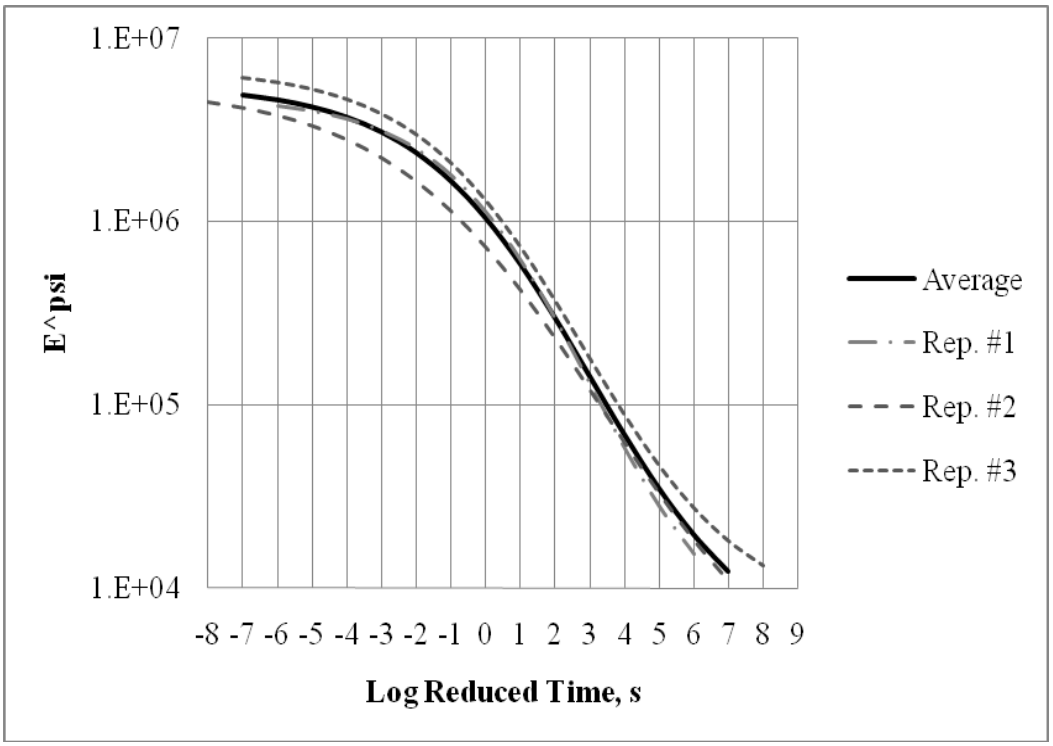

I-17 64-16 Long Term Storage																
Air Voids, %Va				Temp.	Shift Factor	Freq.	Dynamic Modulus, |E*| (ksi)					Phase Angle, Φ (degree)				
Rep1	Rep2	Rep3	Avg.	°F		Hz	Rep1	Rep2	Rep3	Avg. |E*|	St. Dev.	Rep1	Rep2	Rep3	Avg. Φ	St. Dev.
6.11	6.21	6.03	6.12	14	3.4479	25	5970	3316	5845	5044	1498	6	3	10	6.1	3.5
						10	5786	3152	5443	4794	1432	9	4	13	8.8	4.3
						5	5482	3057	5087	4542	1301	10	5	13	9.5	4.0
						1	4860	2827	4268	3985	1046	11	6	15	10.4	4.5
						0.5	4618	2725	3950	3764	960	11	6	13	10.4	3.8
						0.1	4046	2496	3357	3300	776	11	7	13	10.5	3.0
				40	2.0830	25	4132	2309	3502	3314	926	8	9	9	8.8	0.8
						10	3885	2261	3339	3162	827	10	11	10	10.0	0.5
						5	3632	2205	3154	2997	726	10	11	9	10.2	0.8
						1	3068	1940	2736	2581	579	12	12	10	11.4	1.2
						0.5	2812	1872	2557	2414	486	13	13	11	12.3	1.1
						0.1	2187	1623	2100	1970	303	16	15	13	14.6	1.7
				70	0.0000	25	3145	1620	2084	2283	782	11	12	15	12.6	2.0
						10	2704	1429	1760	1965	661	15	15	17	15.7	1.4
						5	2355	1281	1541	1726	561	16	16	18	16.5	1.1
						1	1775	970	1161	1302	421	19	20	20	19.8	0.3
						0.5	1517	848	1008	1124	350	20	22	22	21.4	0.8
						0.1	1048	593	699	780	238	28	27	27	27.4	0.9
				100	-2.6202	25	1234	870	851	985	216	21	28	25	24.6	3.3
						10	1084	759	688	844	211	26	27	25	25.9	0.9
						5	946	668	598	737	184	27	29	27	27.5	1.0
						1	627	436	427	497	113	35	36	31	34.1	2.7
						0.5	527	376	363	422	91	38	38	33	36.3	2.5
						0.1	352	262	238	284	60	45	45	41	43.9	2.4
				130	-5.7570	25	187	147	198	177	27	33	24	22	26.5	6.2
						10	159	129	163	150	19	26	22	21	23.1	2.7
						5	142	118	143	135	14	29	20	20	23.1	5.5
						1	105	92	105	101	7	30	22	22	24.7	4.7
						0.5	91	85	94	90	4	29	22	23	24.4	4.0
						0.1	75	73	75	74	1	34	25	26	28.2	4.7

Parameter	Temp. (°F)	All Data	Average	Rep. #1	Rep. #2	Rep. #3
δ	-	3.521	3.683	3.746	3.662	3.659
α	-	3.485	3.310	3.284	3.084	3.457
β	-	-1.089	-1.061	-1.191	-1.221	-0.854
γ	-	0.238	0.253	0.276	0.248	0.242
Log a(14°F)	14	3.557	3.448	3.029	3.745	3.939
Log a(40°F)	40	2.131	2.083	1.930	2.245	2.231
Log a(70°F)	70	0.000	0.000	0.000	0.000	0.000
Log a(100°F)	100	-2.643	-2.620	-2.634	-2.788	-2.501
Log a(130°F)	130	-5.779	-5.757	-5.950	-6.097	-5.254
	Se/Sy	0.530	0.124	0.170	0.139	0.079
	R^2	0.868	0.994	0.989	0.993	0.998
	Σe2	0.825	0.043	0.056	0.084	0.020

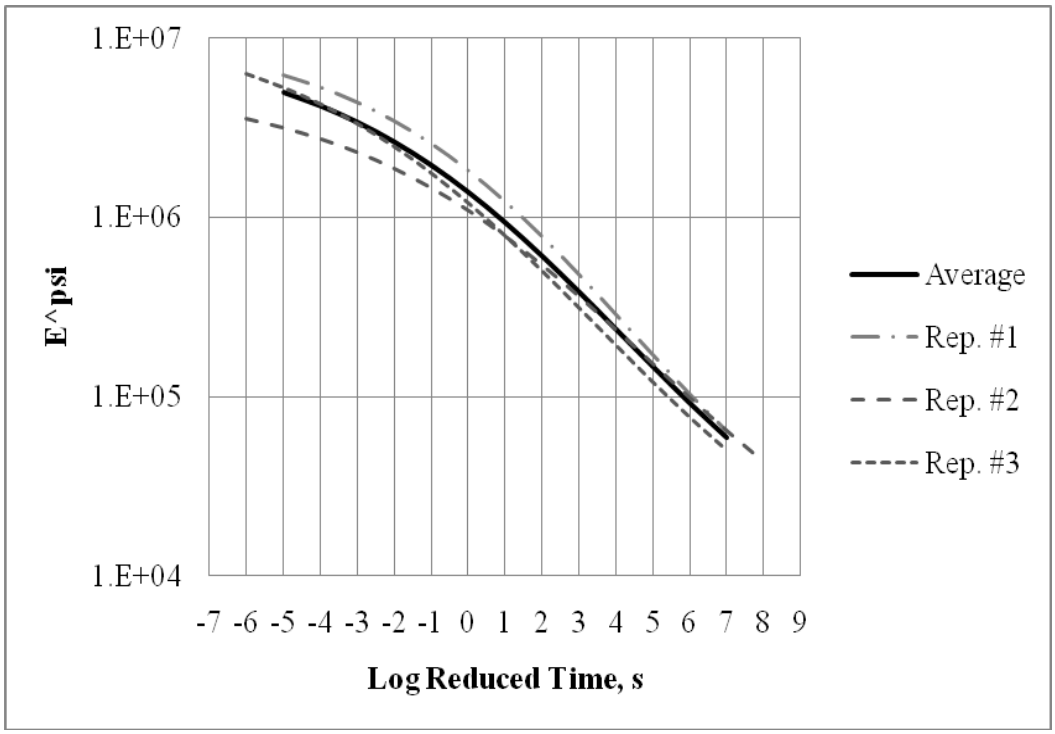

I-17 64-16 7-Year Field																
Air Voids, %Va				Temp.	Shift Factor	Freq.	Dynamic Modulus, |E*| (ksi)					Phase Angle, Φ (degree)				
Rep1	Rep2	Rep3	Avg.	°F		Hz	Rep1	Rep2	Rep3	Avg. |E*|	St. Dev.	Rep1	Rep2	Rep3	Avg. Φ	St. Dev.
3.4767	3.5997	3.1827	3.42	14	3.2249	25	7772	7972	7872	7872	100	11	7	9	8.6	2.0
						10	7427	6920	7174	7174	253	10	8	9	9.3	1.1
						5	7173	6422	6797	6797	376	11	7	9	9.0	2.2
						1	6204	5574	5889	5889	315	11	8	10	9.7	1.7
						0.5	5860	5074	5467	5467	393	12	8	10	10.1	1.8
						0.1	5018	4226	4622	4622	396	13	13	13	12.9	0.0
				40	1.8262	25	4989	2367	3678	3678	1311	10	10	10	10.0	0.2
						10	4370	2092	3231	3231	1139	13	12	12	12.5	0.8
						5	3946	1919	2932	2932	1013	14	12	13	13.2	0.8
						1	3245	1561	2403	2403	842	17	16	16	16.1	0.5
						0.5	2930	1422	2176	2176	754	18	18	18	17.9	0.3
						0.1	2221	1057	1639	1639	582	23	22	22	22.4	0.2
				70	0.0000	25	3095	1546	2321	2321	774	17	17	17	16.9	0.1
						10	2923	1345	2134	2134	789	25	21	23	22.9	1.8
						5	2638	1174	1906	1906	732	28	23	25	25.3	2.3
						1	1923	815	1369	1369	554	39	30	35	34.5	4.7
						0.5	1622	677	1149	1149	473	45	33	39	39.0	6.2
						0.1	1067	412	739	739	327	58	37	47	47.2	10.6
				100	-2.0455	25	2704	1446	1407	1853	738	23	27	27	25.4	2.4
						10	2250	1163	1136	1516	636	22	27	28	25.6	3.4
						5	1973	999	965	1312	573	20	27	30	25.8	4.9
						1	1540	671	636	949	512	26	29	37	30.6	5.7
						0.5	1417	585	515	839	502	27	29	39	31.5	6.5
						0.1	1127	420	349	632	430	42	29	49	39.7	10.2
				130	-4.2959	25	405	398	402	402	3	29	28	28	28.5	0.5
						10	326	307	317	317	9	29	27	28	28.1	1.1
						5	281	258	270	270	11	29	26	28	27.7	1.5
						1	187	164	175	175	11	26	25	26	25.8	0.5
						0.5	163	139	151	151	12	24	25	24	24.4	0.6
						0.1	144	105	125	125	19	20	24	22	22.2	1.9

Parameter	Temp. (°F)	All Data	Average	Rep. #1	Rep. #2	Rep. #3
δ	-	-8.655	-6.434	-7.581	-0.889	-2.610
α	-	16.575	14.181	14.813	9.485	10.479
β	-	-2.139	-2.106	-2.834	-0.963	-1.616
γ	-	0.112	0.122	0.153	0.106	0.129
Log a(14°F)	14	3.287	3.225	2.968	3.528	3.544
Log a(40°F)	40	1.822	1.826	1.902	1.808	1.903
Log a(70°F)	70	0.000	0.000	0.000	0.000	0.000
Log a(100°F)	100	-1.955	-2.045	-2.618	-1.609	-1.902
Log a(130°F)	130	-4.029	-4.296	-5.929	-3.010	-3.791
	Se/Sy	0.406	0.344	0.400	0.356	0.235
	R^2	0.924	0.954	0.937	0.951	0.979
	Σe2	2.258	0.354	0.428	0.556	0.129